Copyright Warning & Restrictions

The copyright law of the United States (Title 17, United States Code) governs the making of photocopies or other reproductions of copyrighted material.

Under certain conditions specified in the law, libraries and archives are authorized to furnish a photocopy or other reproduction. One of these specified conditions is that the photocopy or reproduction is not to be "used for any purpose other than private study, scholarship, or research." If a, user makes a request for, or later uses, a photocopy or reproduction for purposes in excess of "fair use" that user may be liable for copyright infringement,

This institution reserves the right to refuse to accept a copying order if, in its judgment, fulfillment of the order would involve violation of copyright law.

Please Note: The author retains the copyright while the New Jersey Institute of Technology reserves the right to distribute this thesis or dissertation

Printing note: If you do not wish to print this page, then select "Pages from: first page # to: last page #" on the print dialog screen

NJIT New Jersey's Science & Technology University

The Van Houten library has removed some of the personal information and all signatures from the approval page and biographical sketches of theses and dissertations in order to protect the identity of NJIT graduates and faculty.

INFORMATION TO USERS

This manuscript has been reproduced from the microfilm master. UMI films the text directly from the original or copy submitted. Thus, some thesis and dissertation copies are in typewriter face, while others may be from any type of computer printer.

The quality of this reproduction is dependent upon the quality of the copy submitted. Broken or indistinct print, colored or poor quality illustrations and photographs, print bleedthrough, substandard margins, and improper alignment can adversely affect reproduction.

In the unlikely event that the author did not send UMI a complete manuscript and there are missing pages, these will be noted. Also, if unauthorized copyright material had to be removed, a note will indicate the deletion.

Oversize materials (e.g., maps, drawings, charts) are reproduced by sectioning the original, beginning at the upper left-hand corner and continuing from left to right in equal sections with small overlaps. Each original is also photographed in one exposure and is included in reduced form at the back of the book.

Photographs included in the original manuscript have been reproduced xerographically in this copy. Higher quality 6" x 9" black and white photographic prints are available for any photographs or illustrations appearing in this copy for an additional charge. Contact UMI directly to order.

UMI

A Bell & Howell Information Company
300 North Zeeb Road, Ann Arbor, MI 48106-1346 USA
313/761-4700 800/521-0600

Reproduced with permission of the copyright owner. Further reproduction prohibited without permission.

UMI Number: 9605743

Copyright 1995 by
Ding, Yuan
All rights reserved.

UMI Microform 9605743
Copyright 1995, by UMI Company. All rights reserved.

This microform edition is protected against unauthorized
copying under Title 17, United States Code.

UMI

300 North Zeeb Road
Ann Arbor, MI 48103

Reproduced with permission of the copyright owner. Further reproduction prohibited without permission.

ABSTRACT

A THEORETICAL ANALYSIS OF VOLATILE CONTAMINANT REMOVAL BY THE PNEUMATIC FRACTURING PROCESS

by
Yuan Ding

A mathematical model that simulates the process of contaminant removal from a pneumatically induced fracture within a porous medium is presented. It includes: (1) model development; (2) parameter evaluation; (3) statistical sensitivity analysis; and (4) model validation.

Based on the dual porosity approach, a mathematical model for a fractured porous formation is developed for both two dimensional and axial symmetrical cases. This model constitutes a pair of coupled partial differential equations for the porous medium and discrete fracture, respectively. The initial and boundary conditions have been determined based on field considerations of a soil vapor extraction system. By means of Laplace transforms, analytical solutions of the equations are obtained in explicit forms of exponential and error functions.

The four principal physical parameters used in the model include tortuosity, retardation factor, fracture aperture, and extraction flow rate. Fracture aperture and flow rate are related to the characteristics of geologic formation and operational system, while tortuosity and retardation factor are related to geochemical characteristics. Guidelines for determination of these parameters are provided. In addition, a statistical analysis is performed to evaluate the sensitivity of mass removal to variations in these parameters. A linear

Reproduced with permission of the copyright owner. Further reproduction prohibited without permission.

relationship between the standard deviations of mass removal and tortuosity or retardation factor is obtained. The sensitivity of mass removal to the fracture aperture is found to be minimal; however, aperture affects mass removal indirectly through extraction flow rate. Mass removal is determined to be sensitive to flow rate in low flow ranges only.

Validation of the model was carried out using contaminant removal data from two field projects: AT&T Richmond Works and Tinker AFB. Good correlation was obtained between the model predictions and the field data for both sites. In addition, a comparison of the model was made with experimental data from previous laboratory studies, which yields satisfactory agreement over a range of experimental conditions.

Reproduced with permission of the copyright owner. Further reproduction prohibited without permission.

A THEORETICAL ANALYSIS OF VOLATILE CONTAMINANT REMOVAL BY THE PNEUMATIC FRACTURING PROCESS

by
Yuan Ding

A Dissertation
Submitted to the Faculty of
New Jersey Institute of Technology
in Partial Fulfillment of the Requirements for the Degree of
Doctor of Philosophy

Department of Civil and Environmental Engineering

October 1995

Reproduced with permission of the copyright owner. Further reproduction prohibited without permission.

Copyright © 1995 by Yuan Ding
ALL RIGHTS RESERVED

Reproduced with permission of the copyright owner. Further reproduction prohibited without permission.

APPROVAL PAGE

A THEORETICAL ANALYSIS OF VOLATILE CONTAMINANT REMOVAL BY THE PNEUMATIC FRACTURING PROCESS

Yuan Ding

Dr. Paul C. Chan, Dissertation Adviser — Date
Professor of Civil and Environmental Engineering, NJIT

Dr. John R. Schuring, Dissertation Adviser — Date
Professor of Civil and Environmental Engineering, NJIT

Professor Edward G. Dauenheimer, Committee Member — Date
Professor of Civil and Environmental Engineering and Associate
Chairperson of the Department of Civil and Environmental Engineering, NJIT

Dr. C. T. Thomas Hsu, Committee Member — Date
Professor of Civil and Environmental Engineering, NJIT

Dr. George Y. Lei, Committee Member — Date
Associate Professor of Chemistry, NJIT

Dr. Dorairaja Raghu — Date
Professor of Civil and Environmental Engineering, NJIT

Reproduced with permission of the copyright owner. Further reproduction prohibited without permission.

BIOGRAPHICAL SKETCH

Author: Yuan Ding

Degree: Doctor of Philosophy

Date: October 1995

Undergraduate and Graduate Education:

- Doctor of Philosophy in Civil and Environmental Engineering
  New Jersey Institute of Technology
  Newark, New Jersey, 1995

- Master of Science in Civil and Environmental Engineering
  Massachusetts Institute of Technology
  Cambridge, Massachusetts, 1992

- Master of Science in Water Resources Engineering
  Tsinghua University
  Beijing, China, 1987

- Bachelor of Science in Engineering Mechanics
  Tsinghua University
  Beijing, China, 1984

Major: Civil and Environmental Engineering

Publications:

Ding, Y., Schuring, J. R., and Chan, P. C. (1991). "Simulation of Contaminant Removal in Vadose Zone by Pneumatic Fracturing." Proceedings of the 13th Canadian Congress of Applied Mechanics, University of Manitoba, Winnipeg, Canada.

Dong, Z. and Ding, Y. (1989). "A Study of the Boundary Layer for Fully Developed Turbulent Flow in Open Channels." Scientifica Sinica, Series A, No. 11, Beijing, China, (in Chinese).

Reproduced with permission of the copyright owner. Further reproduction prohibited without permission.

Dong, Z. and Ding, Y. (1988). "An Experimental Study of The Homogeneous Turbulent Flow in Open Channels". Technical Report No. 88057, Tsinghua University, Beijing, China, (in Chinese).

Wang, X., Yie, H., Tang, R, and Ding, Y. (1986). "An Investigation on Discharge Coefficients of Needle-Shape Valves." Valves, 1, 21-23 Shenyong, China, (in Chinese).

Reproduced with permission of the copyright owner. Further reproduction prohibited without permission.

This dissertation is dedicated to my parents

Reproduced with permission of the copyright owner. Further reproduction prohibited without permission.

ACKNOWLEDGMENT

I would like to express my sincere appreciation to my advisors, Professors Paul C. Chan and John R. Schuring, who both have given me guidance, encouragement and help from the very beginning and throughout the development of this dissertation. Dr. Chan introduced me to the field of environmental engineering and gave me confidence in my abilities, while Dr. Schuring stimulated my interest in the physical aspect of problem solving and taught me the world of site remediation technology. They have kept me environmentally "interested" during our "weekly seminar".

I would also like to thank my doctoral committee members, Professors Edward G. Dauenheimer, C. T. Thomas Hsu, George Y. Lei, and Dorairaja Raghu for the time and effort spent in improving my dissertation. They have made innumerable constructive suggestions and have been a constant source of encouragement.

I wish to extend my warmest gratitude to Dr. William R. Spillers, Distinguished Professor and Chairman of Department of Civil and Environmental Engineering, who has constantly shown a keen interest in my work, as this interest lent a strong impetus toward the completion of this program. He has helped me see the importance of simplicity and rigor, as well as preciseness and elegance.

Special thanks to Dr. Robert Hazen of NJDEPE for his constant concern and humorous encouragement by sharing his memory as a former doctoral student. He has been an inspiration to my pursuit of new areas in environmental engineering.

Reproduced with permission of the copyright owner. Further reproduction prohibited without permission.

I wish to express my gratitude to Dr. Mohamed E. Labib for his continued encouragement.

My gratitude must also be extended to Mr. Clint Brockway of HSMRC, for his patience and invaluable assistance in preparing instrumentation for the field demonstrations. Without his skillful contributions, the field task would have been much more difficult.

I wish to register a note of thanks to a number of my colleagues and friends, James S. Haklar, Dr. Prasanna Ratnaweera, Travor King, Conan Fitzgerald, Thomas Boland, Anthony Vandeven, Firoz Ahmed, Deepak Nautiyal, Suresh Puppala, and Heather Hall, for their friendship and constant cooperation.

I gratefully acknowledge the financial support of the Department of Civil and Environmental Engineering during my years at NJIT. The field demonstrations were supported by funding from USGS, USDOE and AT&T.

To my parents and sisters, I owe more than words can describe for their lifelong sacrifices and support. Without their love, this work would have no meaning. Last, but not least, thanks to my husband for his encouragement, understanding, and for relinquishing long hours to me.

Reproduced with permission of the copyright owner. Further reproduction prohibited without permission.

TABLE OF CONTENTS

Reproduced with permission of the copyright owner. Further reproduction prohibited without permission.

TABLE OF CONTENTS
(Continued)

Reproduced with permission of the copyright owner. Further reproduction prohibited without permission.

LIST OF TABLES

Table **Page**

Reproduced with permission of the copyright owner. Further reproduction prohibited without permission.

LIST OF FIGURES

Reproduced with permission of the copyright owner. Further reproduction prohibited without permission.

LIST OF FIGURES
(Continued)

Reproduced with permission of the copyright owner. Further reproduction prohibited without permission.

LIST OF FIGURES
(Continued)

Figure **Page**

Reproduced with permission of the copyright owner. Further reproduction prohibited without permission.

CHAPTER 1

INTRODUCTION

1.1 Background

While industry has advanced at a rapid pace since World War II, waste problems have been neglected both intentionally and unintentionally under the guise of modernization. After decades of negligence and unregulated waste disposal practices, the nation is facing serious challenges from environmental damage caused by past industrial activities.

There are many potential sources of environmental contamination, including the agrochemicals, industrial effluents, storage tank leaks, seepage from disposal sites for toxic substances, and petroleum product spills. It has been estimated that the amount of hazardous waste generated annually was 264 million metric tons, which equates to approximately one ton of hazardous waste for each person per year (Harris, 1987). The enormous amount of hazardous waste that has accumulated over the years makes this figure even more astounding. Another study reported that only ten percent of the waste generated prior to 1980 was disposed of by practices that would be considered adequate according to current standards (USEPA, 1980). Thus, as much as 90 percent of the hazardous waste was disposed of at unregulated facilities. These irresponsible disposal practices have created over 22,000 sites containing unregulated hazardous waste throughout the country. The improper disposal of hazardous waste has caused a number of serious problems that not only result in the destruction of the ecological system and natural resources; but also, present a danger to public health and a major financial burden to the nation.

Reproduced with permission of the copyright owner. Further reproduction prohibited without permission.

Among the numerous contaminant sites in the United States, there exist countless environmental tragedies. The incident in Love Canal (Brown, 1980) at Niagara Falls is only one example: Residents were forced to abandon their homes and community to avoid facing further health risks from exposure to highly toxic chemicals. The chemicals originated from the disposal site at Love Canal where at least 20,000 tons of waste, including many hazardous substances such as Dioxin, PCBs (polychlorinated biphenyl), and radioactive waste, were dumped. By the late 1960's, after three decades of chemical dumping in Love Canal, the impact on the community was enormous. Finally in 1978, a state health study and the long-time fight by the victims resulted in the first evacuation of a contaminated community. By 1989, state and federal governments had spent $140 million to clean up the site and relocate the residents. With its political impact across the Nation, Love Canal has come to symbolize the devastating effects of toxic wastes on families and society.

1.1.1 Pollution Control Policy

Although the seriousness of the hazardous waste problem has been recognized for more than two decades, the present regulations and methods of control are still in an early stage of development due to the complexity and potential enormity of the problem. The first and probably the most important modern environmental law was enacted in January of 1970, namely, the National Environmental Policy Act (NEPA) of 1969. NEPA is a milestone in man's understanding of the relationship between his own survival and the survival of the total ecology that has supported all life on earth. This act dictated that decision makers approach industrial development by balancing the environmental, economic, and technological factors to protect and enhance public health and welfare. In response to NEPA, the

Reproduced with permission of the copyright owner. Further reproduction prohibited without permission.

federal government formally established the U.S. Environmental Protection Agency (USEPA) in 1970, i.e., the first government environmental organization in the world. Through the USEPA, the role of the federal government in environmental management has been significantly expanded. During the 1970's, which came to be called the "environmental decade", many important statutes were enacted to restrict the improper handling of hazardous wastes. The Clean Air Act of 1970 legislated the prevention and control of air pollution to protect and enhance the quality of the air resources of the nation. The Clean Water Act of 1972 established the goal of ending industrial pollution of the nation's rivers, streams, and lakes by 1985. The Resource Conservation and Recovery Act of 1976 (RCRA) was designed to assure proper management of hazardous wastes through "cradle-to-grave" regulatory controls. In 1980 and 1984, RCRA was re-authorized twice for enhancement. Since their enaction, these statutes have played a very important role in preventing the creation of new contaminated sites. However, they have had no effect on the hazardous waste sites already in existence. If a healthy environment is to be established, these long-term dangers cannot be ignored.

1.1.2 Remediation Policy

The cleanup action started from the enactment of the Comprehensive Environmental Response, Compensation and Liability Act of 1980 (CERCLA or Superfund) which is a remedial program on cleaning up the nation's worst hazardous waste sites created by past industrial disposal practices. CERCLA established a hazardous substance Superfund as well as regulations controlling inactive hazardous waste sites. Later, this important act was revised and extended by the Superfund Amendments and Reauthorization Act of 1986 (SARA).

Reproduced with permission of the copyright owner. Further reproduction prohibited without permission.

However, the implementation of Superfund is challenging, both technically and economically, since every site is unique and full of uncertainties. The remedial action is tedious, and millions of dollars and many years can be spent to remediate one site.

Among the various hazardous wastes, it is generally recognized that volatile organic compounds (VOCs), such as trichloroethylene, tetrachloroethylene, as well as petroleum fuels, are the major concerns (Bedient et al., 1994). Although VOCs may enter the vadose zone in many different ways, they eventually enter the groundwater system. Groundwater cleanup is very expensive and extremely difficult, if not impossible. An important and necessary step is removal of contaminants from the vadose zone which serves as a source. In fact, it is safe to say that the groundwater remediation will never be complete so long as mobile contaminants remain in the vadose zone.

1.2 Objective and Scope

The primary objective of this study is to evaluate the removal process of volatile contaminants from an open fracture created by the pneumatic fracturing process, which is a new technology developed to enhance in situ remediation. Once a fracture network is established in a formation, contaminants are more easily accessed since the diffusion distance is shortened. Contaminant transport out of the unfractured geologic network between fractures will continue as long as advective flow is maintained throughout the fracture network. This thesis will utilize a dual porosity approach (Streltsova, 1988) to predict mass transport out of the fractured porous formation. The resulting model will permit determination of the length of time required to remediate a site, as well as the residual VOC concentrations remaining in the formation at any given time.

Reproduced with permission of the copyright owner. Further reproduction prohibited without permission.

In the process of developing the fracture transport model, the following tasks will be performed:

1. A mathematical formulation of the physical conditions and transport processes surrounding a discrete pneumatic fracture in the vadose zone will be developed.

2. An analytical solution of the constitutive equation capable of predicting mass removal rates of VOC's in the vapor phase will be obtained.

3. The range of expected diffusion coefficient and retardation fraction will be established using standard published relationships and data.

4. A statistical analysis of the analytical model will be performed to evaluate sensitivity to the input parameters.

5. The analytical solutions will be verified using data from two different field demonstrations and a series of laboratory experiments.

Reproduced with permission of the copyright owner. Further reproduction prohibited without permission.

CHAPTER 2

THE PNEUMATIC FRACTURING PROCESS

2.1 Review of Current In Situ Remedial Technologies

Currently, there are two basic approaches for decontaminating soil in the vadose zone, namely, "ex situ" and "in situ" techniques. Ex situ remediation requires excavation with on-site or off-site treatment, while the in situ remediation removes (or treats) the contaminants in place thus minimizing disturbance to the site. Since excavation may not be feasible in many situations, the in situ remediation approach, in general, is technically and economically superior. As a result, a number of in situ remedial technologies have been developed to treat contamination in the vadose zone. These remedial actions can be grouped into following general categories based on their characteristics.

2.1.1 Physical Treatment

Physical treatment is a relatively simple and safe approach compared with other treatment methods. Since no foreign materials are introduced into the formation, there is little chance that the contamination situation will be worsened.

The soil vapor extraction (SVE) method, known as soil venting, in-situ volatilization, enhanced volatilization, or soil vacuum extraction, is one of the most popular physical treatment technologies (USEPA, 1995). In this process, a vacuum is applied through extraction wells to create a pressure gradient that induces transport of chemical volatiles through the soil to extraction wells. This technology has been widely used in VOC removal from the vadose zone and it can also be useful in decontaminating groundwater, since the lowered VOC vapor

Reproduced with permission of the copyright owner. Further reproduction prohibited without permission.

pressure in the vadose zone will increase volatilization of contaminants in the groundwater. Principal factors which govern the applicability of SVE include contaminant distribution at the site, site hydrogeology, and contaminant properties. In general, SVE is an effective process for highly permeable formations such as sand, but is ineffective for low permeability formations such as silt and clay, since tight formations restrict the air flow through the porous medium (Travis and Macinnis, 1992).

Pump-and-treat is a physical treatment technology which is used for saturated zone in combination with other technologies. Contaminated groundwater is pumped out of the formation and treated either off-site or on-site. This technology is commonly applied to reduce the rate of plume migration, or to confine the plume to a potentiometric low area (Bedient et al., 1994).

2.1.2 Chemical Treatment

In general, chemical methods for detoxification of VOCs in the unsaturated zone are severely hindered by the difficulties of dispersing chemical amendments in a contaminated zone (Bowman, 1989). As such, most attempts of chemical in situ treatments have been limited to chemical spills or dump sites where near-surface contaminated soil could be treated. Potential chemical reactions of the treatment reagents with the soils and wastes must be considered with any chemical treatments. Since most hazardous waste disposal sites contain a mixture of contaminants, a treatment approach that may neutralize one contaminant could render another more toxic or mobile. In addition, the chemical amendment introduced into the soils may create new pollution. The general chemical treatments include solidification-stabilization, neutralization, and oxidation-reduction (Grasso, 1993).

Reproduced with permission of the copyright owner. Further reproduction prohibited without permission.

The solidification-stabilization method is designed to make contaminants physically bound or enclosed within a stabilized mass. This method includes inducing chemical reactions between the stabilizing agent and contaminants to reduce their mobility. Neutralization involves injecting dilute acids or bases into the ground to adjust the pH range. This pH adjustment can serve as pre-treatment prior to oxidation-reduction or biological remediation. The oxidation-reduction method consists of using oxidation-reduction reactions to alter the oxidation state of a compound through loss or gain of electrons, respectively. Such reactions can detoxify and solubilize metals and organics. This technology is a standard wastewater treatment approach, but its application as in-situ treatment is limited.

2.1.3 Biological Treatment

The ultimate goal of biological treatment is to achieve biodegradation of the organic chemicals. From attempts to utilize bacterial cultures to sophisticated genetic engineering applications, a myriad of biodegradation technologies have been explored (Grasso, 1993). Since a large portion of the hazardous waste contamination in the U.S. stems from petroleum hydrocarbon products that have been discharged or spilled into the soil at petroleum refineries, airports, and military bases, bioremediation has become an accepted, simple and effective cleanup method (Mills, 1995). Basically, there are two approaches: stimulating the growth of "indigenous" microorganism populations and adding new "endigenous" microorganisms. Biological treatments may utilize either one or both of these approaches.

Many toxic organic chemicals can be metabolized or degraded to some degree by indigenous soil microorganisms. This natural process can be accelerated by pumping oxygen and nutrients into the contaminated zone to stimulate the resident

Reproduced with permission of the copyright owner. Further reproduction prohibited without permission.

microorganisms (e.g., Dupont, 1993). However, if the infiltration rate is low, remediation may be a very slow process. The process may be enhanced by introducing "acclimated" populations, which are developed from the indigenous microorganisms, back into the formation to increase the survival possibility of the microorganisms and to expedite the biodegradation process.

In the endigenous approach, genetically endigenous microorganisms are introduced into the formation to clean the contaminants. There are two major difficulties in this approach. First, the dispersal of introduced organisms throughout the contaminated zone is very difficult since microorganisms tend to be sorbed by solid particles and become clustered. Second, the newly introduced organisms may destroy the microbial balance once the porous medium has become decontaminated, which creates new ecological problems. Due to these difficulties and other disadvantages, this approach is presently not recommended by USEPA (1993).

In summary, a significant engineering deficiency with in situ bioremediation is the absence of proven methods to introduce degrading populations of microorganisms, nutrients, and other chemicals into the subsurface environment for efficient mixing with microorganisms and the contaminants of concern. In addition, the infiltration rate is an important governing parameter to the effectiveness of the process.

2.1.4 Thermal Treatment

Thermal treatment involves introducing extra energy into the contaminated zone to increase the formation temperature. Two different temperature ranges have been employed: high temperature treatment is used to destroy chemical structure

Reproduced with permission of the copyright owner. Further reproduction prohibited without permission.

as well as soil constituent to retard chemical movement, while low temperature treatment is used to increase chemical mobility and removal rates.

The in situ vitrification (ISV) technology (USEPA, 1994) is a high temperature treatment designed to treat soils, sludges, sediments, and mine tailings contaminated with organic, inorganic, and radioactive compounds. Joule heating, which is applied via electrodes, is used to melt contaminated soils and sludges, producing a glass and crystalline structure (at about $3000^{o}F$ or $1600^{o}C$) with very low leaching characteristics. The glass and crystalline product will permanently immobilize hazardous substance and retain its physical and chemical integrity for geologic time periods. Since the ISV process is costly, it has mostly been restricted to radioactive or highly toxic wastes. The demand for high energy, specialized equipment, and trained personnel greatly limit the use of this method. A field demonstration of ISV is evaluated by USEPA under the Superfund Innovative Technology Evaluation Program at the Parsons Chemical Site in Grand Ledge, Michigan (USEPA, 1994(a), 1994(b)).

The thermally enhanced soil vapor extraction process uses steam/hot-air injection or electric/radio frequency heating to increase the mobility of vapors and facilitate soil vapor extraction (USEPA, 1993c). The temperature in this process is controlled in a low range so that there is no chemical destruction.

2.1.5 Enhancement Technologies

Hydraulic fracturing, also known as hydrofracturing, is an enhancement technology to increase formation permeability (Murdoch, 1992a, 1992b, 1992c). The fracturing process begins by using a hydraulic jet to cut a disk-shaped notch on the borehole wall. Water (with or without chemicals) is then injected into the notch until a critical pressure is reached and a fracture is formed. A proppant

Reproduced with permission of the copyright owner. Further reproduction prohibited without permission.

composed of a granular material (e.g., sand) and a viscous fluid (e.g., guar gum and water mixture) is then pumped into the fracture. As a result, the mobility through difficult soil conditions can be increased.

A summary of this technology is given in a USEPA Demonstration Bulletin (USEPA, 1993). Thus far, two field demonstrations have been conducted, one in conjunction with a vapor extraction system and the other with bioremediation. Since water or other liquid is used in the process, the moisture content of the formation is increased during hydraulic fracturing. This additional water or liquid may block the pathway for VOC transport, and subsequently reduce the efficiency of the VOC removal from fractured formations.

Pneumatic fracturing is a new enhancement technology developed at Hazardous Substance Management Research Center at New Jersey Institute of Technology. This process involves injection of pressurized air into soil or rock formations to create fractures and increase the permeability. The injection is a quick process (e.g., within 10 to 20 seconds), and clean air is the only ingredient of the injection fluid. Thus, the potential chemical hazard or disturbance to the formation's chemical constituents is minimal. This technology has been applied to a number of contaminated sites, and field results show that the process is effective in enhancing the VOC removal from the vadose zone (Schuring and Chan, 1992; HSMRC, 1994a). A more detailed description of this process is presented in the next section.

2.1.6 Remarks

The success of in situ remediation technologies depends largely upon the transport efficiency of materials in and out of the contaminated zone. Contaminants must be transported out of the formation, while chemical, biological, and other

Reproduced with permission of the copyright owner. Further reproduction prohibited without permission.

amendments must be transported in. Currently, most in situ remediation methods are effective only in relatively permeable formations and are inadequate for fine-grained soils due to the low natural permeability. Improving the transport conditions, thus, becomes an urgent task for the current remediation industry. The pneumatic fracturing process meets this need and has already been integrated with physical, thermal and biological treatment technologies. The pneumatic fracturing process is therefore a breakthrough technology which enhances and extends the application of in situ remediation technologies (Schuring and Chan, 1992; USEPA, 1995a; HSMRC, 1994b).

2.2 Pneumatic Fracturing Process

The pneumatic fracturing process, developed and patented (US Patent, 1991) at New Jersey Institute of Technology (NJIT), is a new technology that enhances the in situ VOC removal from the vadose zone for low permeability formations. It is designed to be integrated with the previously mentioned in situ remediation technologies to increase formation permeability. It has been recognized as an acceptable technology for enhancement of vapor extraction by the USEPA within the Superfund Innovative Technology Evaluation (SITE) Program (USEPA, 1993).

2.2.1 Technology

The concept of the pneumatic fracturing for fine-grained soils (such as silt and clay) and sedimentary rock formations (such as shale) is illustrated in Figures 2.1 and 2.2, respectively. High pressure, clean air is injected into the geological formation at an injection point to create fractures. In soil formations, new fractures are created in the soil matrix, while in sedimentary rock formations the

Reproduced with permission of the copyright owner. Further reproduction prohibited without permission.

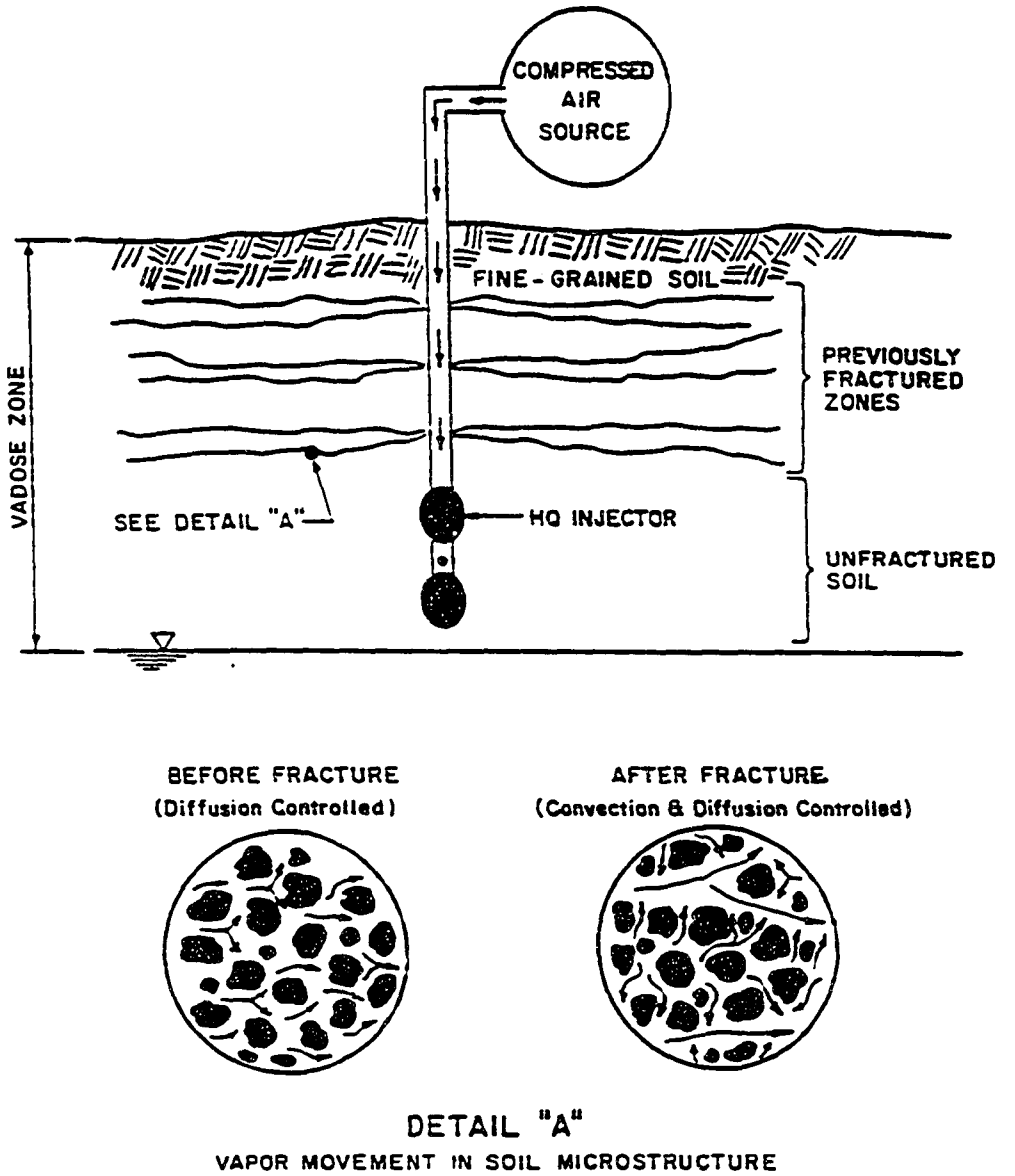

Figure 2.1 Pneumatic Fracturing Concept for Fine-grained Soil Formations (Schuring and Chan, 1992)

Reproduced with permission of the copyright owner. Further reproduction prohibited without permission.

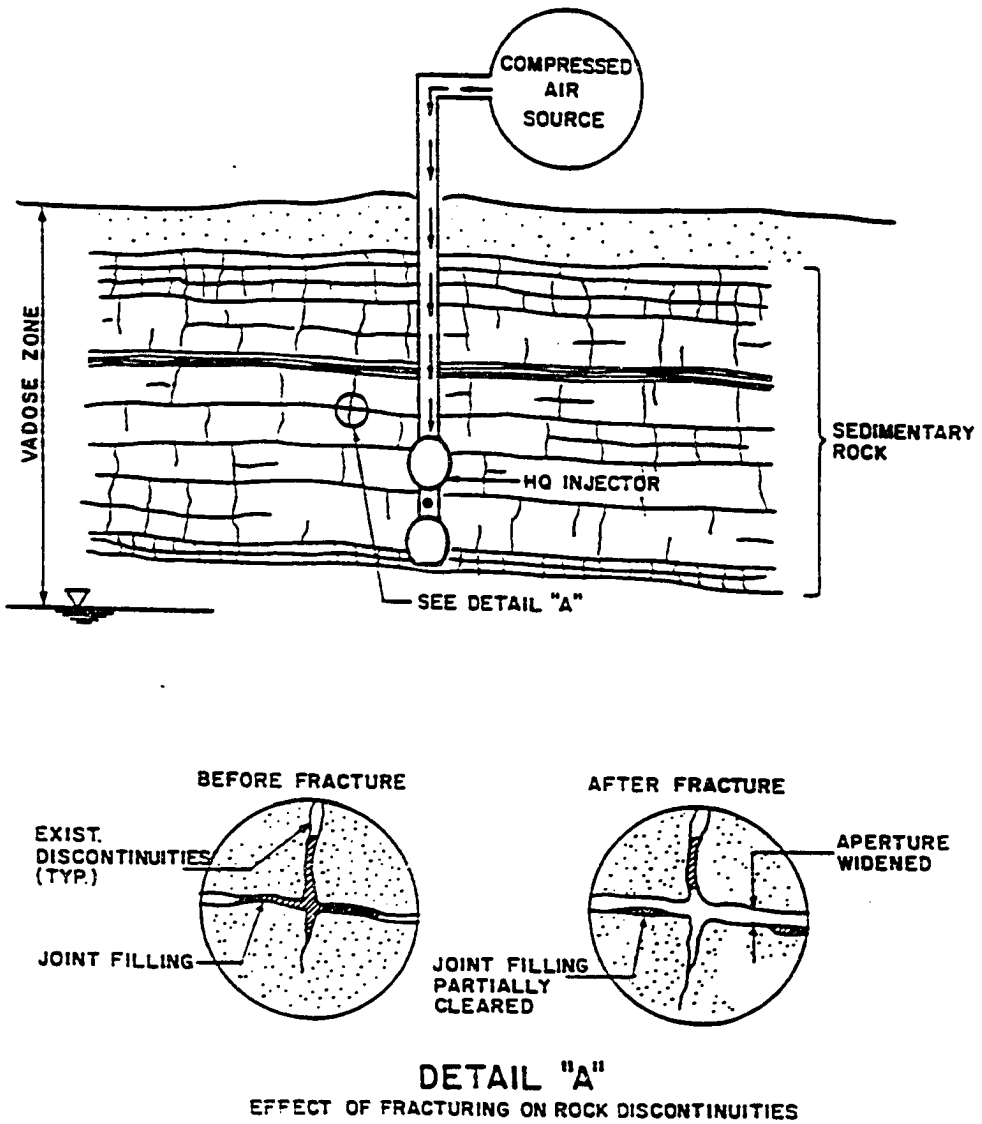

Figure 2.2 Pneumatic Fracturing Concept for Sedimentary Rock Formations (Schuring and Chan, 1992)

Reproduced with permission of the copyright owner. Further reproduction prohibited without permission.

process dilates the existing natural joints and faults. These fractures increase formation permeability and exposed surface area, as well as shorten diffusive pathway lengths. Since the process injections clean air, it does not increase formation moisture content, and should not create new chemical reactions nor worsen the contamination situation.

The operational system for pneumatic fracturing includes a compressed air source, regulators and flow manifolds, pressure release valve, and HQ injector. A pressure transducer (attached to HQ injector) and a series of tilt meters (on the ground surface) are used to measure the fracturing pressure and the movement of the ground surface, respectively. Unlike hydraulic fracturing, pneumatic fracturing is a rapid process and the duration of injection is typically in the range of 10 to 20 seconds, and good field productivity is possible. Based on past field experience, a complete fracturing injection cycle along with process monitoring can be completed within 30 minutes. That translates to about 10 to 15 fractures in a typical production day for a three-person crew.

2.2.2 Development

The development of the pneumatic fracturing process can be divided into two stages, viz., laboratory experiments and field pilot demonstrations.

Laboratory experiments of pneumatic fracturing were begun in 1988 at NJIT (Papanicolaou, 1989; Shah, 1991). Mass removal tests were conducted in three identical vats as shown in Figure 2.3 using a surrogate contaminant. Vat 1 served as the control and was subjected to natural evaporation only. In Vat 2, a traditional soil vapor extraction system was applied. In Vat 3, the same soil vapor extraction system was utilized, except the soil in the tank was also pneumatically fractured. Typical results from these experiments are shown in

Reproduced with permission of the copyright owner. Further reproduction prohibited without permission.

Reproduced with permission of the copyright owner. Further reproduction prohibited without permission.

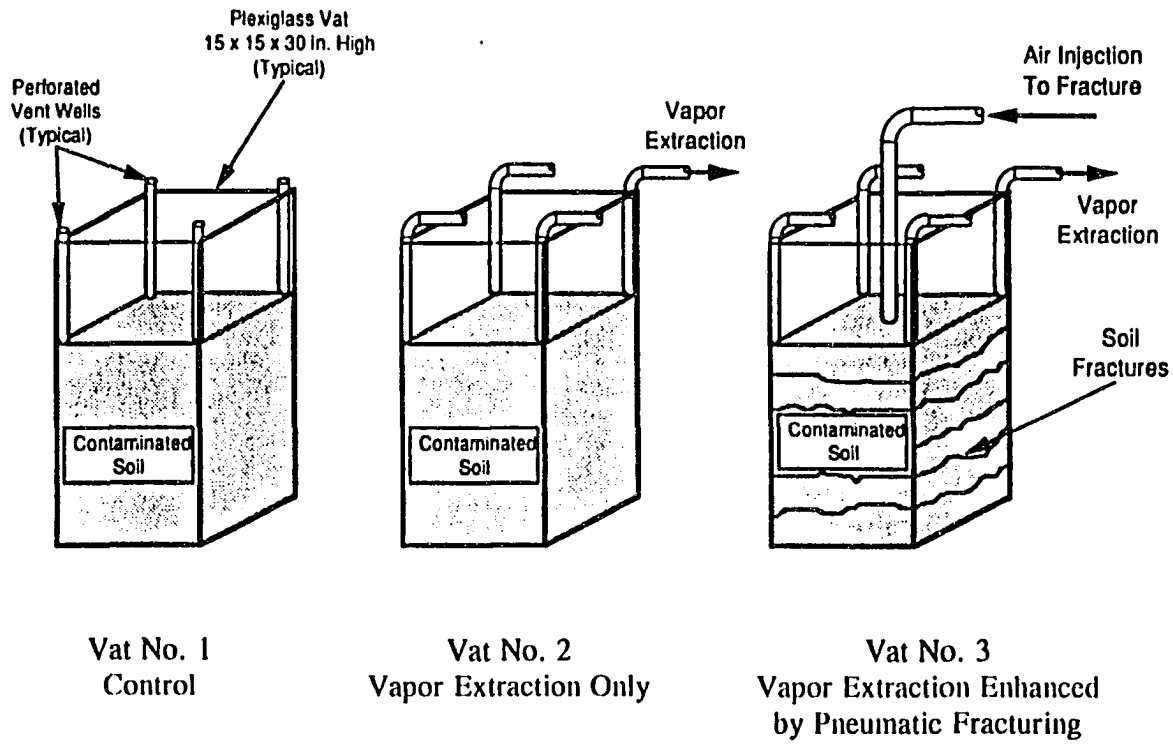

Figure 2.3 Laboratory Experimental Setup (Papanicolaou, 1989)

Figure 2.4, which illustrates that the most efficient mass removal rate was observed in Vat 3, i.e., the tank enhanced with pneumatic fracturing. Similar results were obtained under a variety of soil types and test conditions.

In order to extend the favorable laboratory test results into field application, the prototype pneumatic fracturing system was built and tested in 1989 on a clean site in Frelinghuysen Township, NJ. The objectives of these proving ground demonstrations includes equipment development and evaluation of fracture enhancement. The test site was a glacial lacustrine deposit containing clayey silt and sandy silt, which was ideal since the predominantly fine-grained soils displayed good uniformity. The results of these development tests established the conceptual feasibility of pneumatic fracturing in soil formations. A detailed description is given by Schuring and Chan (1992).

The first field pilot application at a contaminated site was conducted at the AT&T Richmond Works located in Richmond, VA, in 1990 (Schuring et al., 1991). At this site, pneumatic fracturing was combined with soil vacuum extraction to enhance contaminant removal rates. Figure 2.5 illustrates the comparison of effluent concentration between pre- and post- fracturing. The methylene chloride concentration peaked at 17 ppm and reduced to a non-detectable level after thirty-five minutes for pre-fracture period. In contrast, for the post-fracture test, the effluent concentration peaked at 8677 ppm and leveled off at 201 ppm after 150 minutes. Prior to the application of pneumatic fracturing, the vacuum extraction system was essentially ineffective. After fracturing, the efficiency of the mass removal increased up to 1,000 times with respect to the pre-fracture condition.

In addition, the pneumatic fracturing process has been applied in a sedimentary rock formation at an industrial site in Hillsborough, NJ. The site

Reproduced with permission of the copyright owner. Further reproduction prohibited without permission.

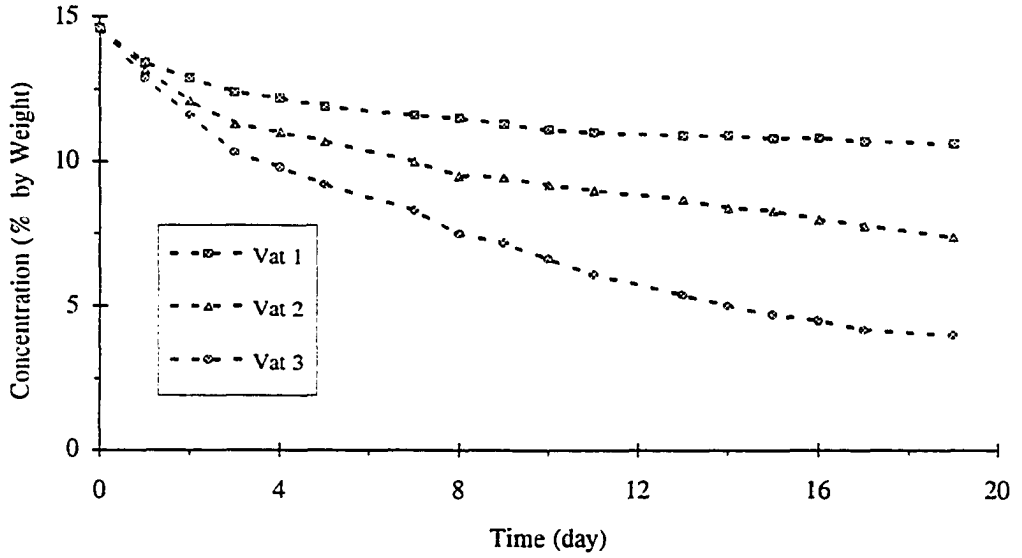

(a) Experiment PF2

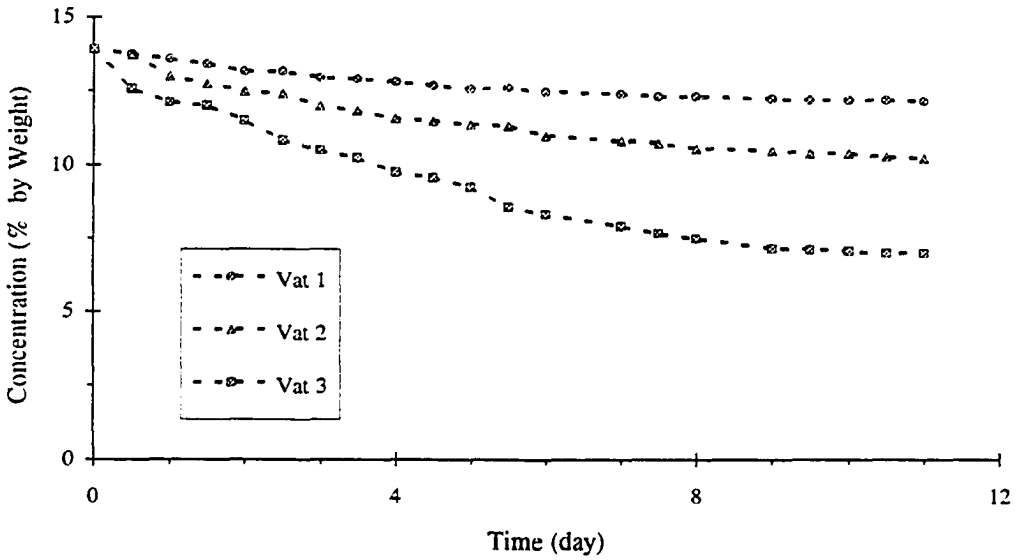

(b) Experiment PF4

Figure 2.4 Laboratory Experimental Results
(Papanicolaou, 1989)

Reproduced with permission of the copyright owner. Further reproduction prohibited without permission.

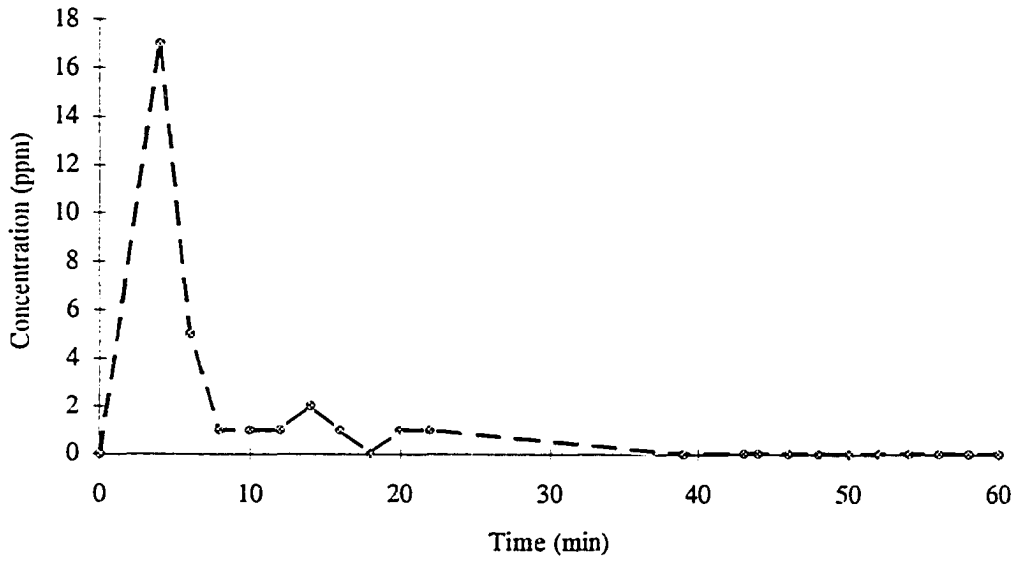

(a) Pre-fracturing

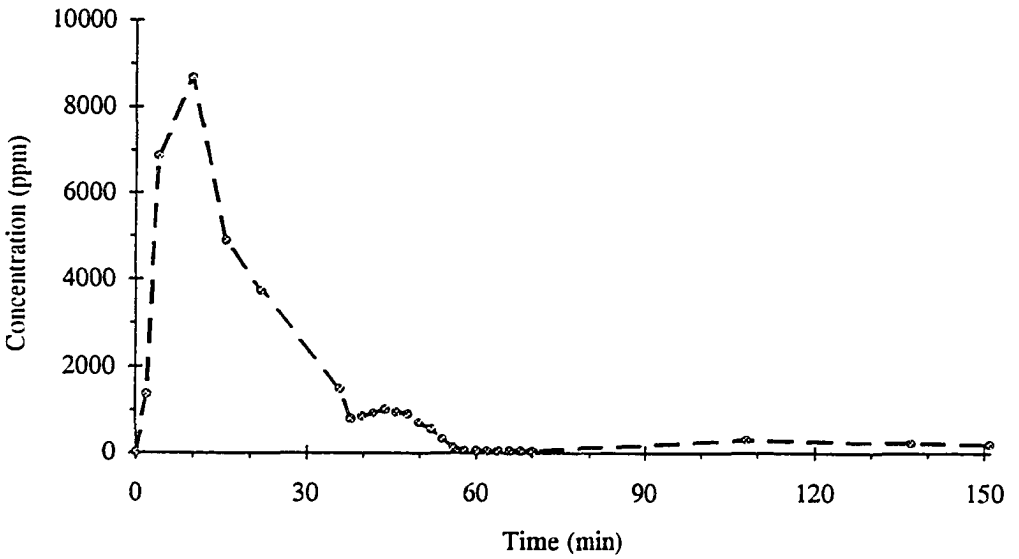

(b) Post-fracturing

Figure 2.5 A Comparison of Effluent Concentrations for Pre- and Post-fracturing (Schuring et al., 1991)

Reproduced with permission of the copyright owner. Further reproduction prohibited without permission.

was underlain by siltstone, which is part of the Brunswick (Passaic) formation. Results from this site showed that the pneumatic fracturing increased the VOC removal rate by 2400% (USEPA 1993c). Moreover, pneumatic fracturing dilated the formation, which extended the influence radius of the vacuum extraction well, and allowed access to new pockets of chemical contamination.

In conclusion, the pneumatic fracturing process has been applied to a number of contaminated sites throughout the country. Thus far, the writer has participated in six contaminated sites and one clean site including: Tinker Air Force Base (OK), AT&T (VA), AT&T (LA), Marcus Hook Refinery (PA), East Orange gas station (NJ), Derelco ECRA site (NJ), and Frelinghuysen Township site (NJ). These field tests have demonstrated that the pneumatic fracturing is very effective in enhancing both soil vacuum extraction and biodegradation for treatment of VOCs in the vadose zone.

Reproduced with permission of the copyright owner. Further reproduction prohibited without permission.

CHAPTER 3

ANALYTICAL SIMULATION

Transport phenomena in porous media have been studied in several disciplines including geology, hydrology, reservoir engineering, and environmental engineering (Bird et al, 1960; Carman, 1956; Greenkorn, 1983; Scheidegger, 1974). Due to the complex nature of porous media, the problems concerning transport in porous media are more difficult than that in pure liquid or gas. Furthermore, transport through fractured porous media is even more complex due to the presence of flow field discontinuities. Although such problems are difficult, they were important initially in the petroleum industry since a number of large oil fields are confined to fractured reservoirs. Later, due to the serious situation of leakage from nuclear waste repositories (e.g., Hoffman and Daniels, 1984), the importance of transport in fractured media was enhanced and raised to a new level: it became an environmental issue. Besides dangers from nuclear waste leakage, disposal of industrial hazardous waste also created enormous environmental problems (USEPA, 1980). Thus, a number of investigations have studied contaminant transport through both non-fractured and fractured porous media (e.g., Fryar and Domenico, 1989; McCarthy and Johnson, 1993)

Generally speaking, there are two approaches for analyzing fractured media: the near field and the far field. The near field approach concentrates on the zone close to the individual fracture, so, usually, a formation with a single fracture is the domain. The far field approach considers large scale formation as the domain. Consequently, there exist many fractures which intersect each other and constitute a fracture network. Studies have been conducted with both approaches and models

Reproduced with permission of the copyright owner. Further reproduction prohibited without permission.

have been developed. Recently, a state-of-the-art report on various aspects of flow and trace-transport in fractured rock was presented by Bear et al. (1993).

A number of studies on fractured porous media were carried out in the 1980's with the primary objective of dealing with radioactive waste disposal problems. Braester and Thunvik (1983) used a single fracture model to analyze gas migration from a radioactive low-level waste repository located in a hard rock formation below the sea bottom. They estimated the capability of the rock formation to convey the gas produced in the repository up to the surface. By using Laplace transfer, Tang and Babu (1979) derived analytical solutions for the convective-dispersive transport of a contaminant from an injection well in a porous medium. Later, Tang (1981) studied the radioactive contaminant transport through a porous medium with a single fracture. Chen (1985) derived analytical and approximate solutions to contaminant transport from an injection well for a confined aquifer and adjacent strata which is mathematically similar to a porous formation with a single fracture. Furthermore, Chen (1986) analyzed radioactive contaminant transport in a porous medium with a single fracture. Parker et al (1994) proposed a model to analyze the diffusive disappearance of immiscible phase organic liquids in fractured media.

On the other hand, with the fracture network approach, Germain and Frind (1989) described a two dimensional model for an orthogonal network in which analytical solutions are incorporated to model matrix diffusion. Sudicky (1989) solved transport along the network numerically in Laplace transform space using the Laplace transform-Galerkin method. Sudicky and Mclaren (1992) presented a new approach to this problem, in which they described an extension of the Laplace transform-Galerkin method for two dimensional, orthogonal networks, which is able to consider advective-dispersive transport in both the fracture network and the

Reproduced with permission of the copyright owner. Further reproduction prohibited without permission.

matrix. Küpper et al. (1995a, 1995b) developed a transfer function approach to model mass transport in a network of fractures. They also applied the transport model subject to advection and dispersion within the fractures, and diffusion within the matrix.

An examination of the nuclear waste transport problem in comparison with the pneumatic fracturing process indicates that there are significant differences between them. The main concerns of the radioactive waste repository are leakage of radionuclide from fracture into the porous matrix and the eventual contact with the biosphere or groundwater system. On the other hand, the principal objective of the pneumatic fracturing process is to provide a high permeability channel for either recovery or delivery as means of site remediation. Thus, the initial and boundary conditions for these two types of problems are different. In addition, the basic feature of the nuclear wastes in unsaturated fractured zone is different from those of pneumatic fracturing process. In the vicinity of the nuclear waste pockets, flow is driven by high temperature (exceeding $100^{o}C$) and large temperature gradients. Thus, isothermal or nearly isothermal flow conditions are not applicable to this situation (Pruess and Wang, 1987).

In addition to migration studies of nuclear waste and industrial waste, a number of other studies have been focused on the removal of hazardous waste from the geological formations, especially since the Superfund program commenced in 1980 (e.g., Hodge and Devinny, 1995; Szatkowski et al., 1994; McCann et al., 1994). Among the various remedial technologies, soil vapor extraction has received the most attention due to its extensive applications (e.g., McWhorter 1990; Beckett and Huntley, 1994). The efficiency of the soil vapor extraction process has been investigated with both theoretical and experimental approaches (Ross and Lu, 1994; Hutzler et al., 1989). However, it appears that

Reproduced with permission of the copyright owner. Further reproduction prohibited without permission.

studies dealing with the problem of contaminant removal by soil vapor extraction from fractured porous media are scarce.

During the last few years, several studies have been carried out on different aspects of the pneumatic fracturing process. Shah (1991) conducted laboratory bench scale tests to study the effects of fracturing on contaminant mass removal rates. King (1993) developed an analytical model for predicting fracture behavior and fracture initiation pressures in geologic formations. Nautiyal (1994) extended the cubic relationship for discrete fracture flow to include compressible gases. Fitzgerald (1993) developed the method and apparatus for integrating pneumatic fracturing with in situ bioremediation.

The purpose of the present study is to address a very important question which remains unanswered on the pneumatic fracturing process: How quick will the contaminant be removed from the formation? This study will provide a rational description of the contaminant removal process, thereby allowing an assessment of the remediation process efficiency and duration.

3.1 Conceptual Model

The current conceptual approaches to the problem of transport through a fractured medium can be classified into three broad categories: (1) the equivalent porous medium approach; (2) the purely discrete fracture medium approach; and (3) the dual porosity approach.

The equivalent porous medium approach is used when the formation of interest contains many inter-connecting fractures. Figure 3.1 illustrates some sample structures of fractured formations. This approach has been applied to large scale field studies where it is appropriate to treat the whole fractured medium as a porous medium equivalent (Zuber and Motyka, 1994). In this porous medium

Reproduced with permission of the copyright owner. Further reproduction prohibited without permission.

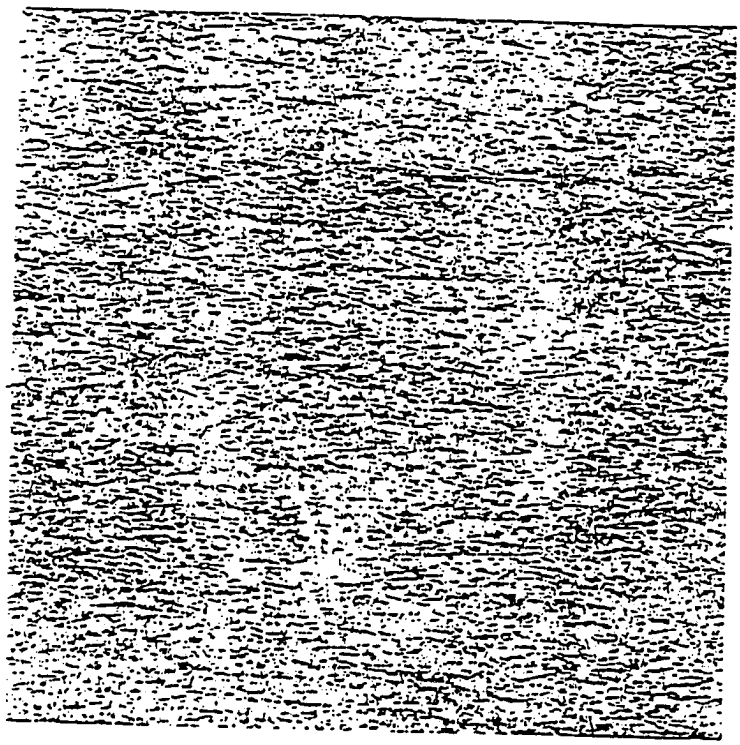

(a) Fractures Generated in a 100m by 100m Region

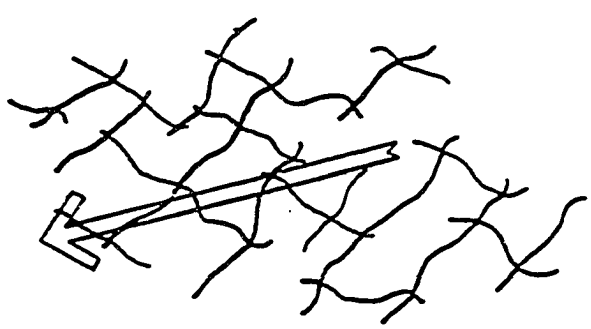

(b) Equivalent Model

Figure 3.1 Equivalent Porous Medium Model
(Murray et al., 1989)

Reproduced with permission of the copyright owner. Further reproduction prohibited without permission.

approximation, the key parameters are the equivalent dispersivity tensor for solute transport (e.g., Gelhar et al., 1979) and the equivalent permeability tensor for the fluid flow (e.g., Hsieh et al., 1985).

The purely discrete fracture approach is used for a tight fractured medium under the conditions when: (1) a formation is made up to blocks of rock with cracks in between; (2) the permeability of blocks is negligible; and (3) there is no fluid exchange between blocks and the cracks. Fissured granite is a typical example. For a formation with these characteristics, it is no longer appropriate to approximate the entire fractured medium with averaged quantities such as the equivalent permeability tensor and the equivalent dispersivity tensor. The purely discrete fracture approach considers each fracture as a pair of parallel plates with a constant aperture, so the flow through the fracture network is similar to a pipe network. Figure 3.2 illustrates the conceptual model for the discrete fracture approach, which has been used in the problems of transport (e.g., Smith and Schwartz, 1984; Schwartz and Smith, 1988) and fluid flow (e.g., Long and Witherspoon, 1985).

The dual porosity approach was first introduced by Barenblatt (1960) to describe the phenomena of liquid transport in fissured rocks. This approach considers two media: a porous medium consisting of relatively large open fissures; and a porous medium consisting of small pores in the adjacent blocks. Thus, there are different porosities for the two porous media. A conceptual scheme of dual porosity approach is illustrated in Figure 3.3. For a fractured porous medium, it is considered that the contaminant is stored in the porous medium and is transported along the discrete fracture (Barenblatt et al. 1990). The dual porosity model has been applied to problems of contaminant transport through fractured porous media (e.g., Streltsova, 1988; Chen 1985).

Reproduced with permission of the copyright owner. Further reproduction prohibited without permission.

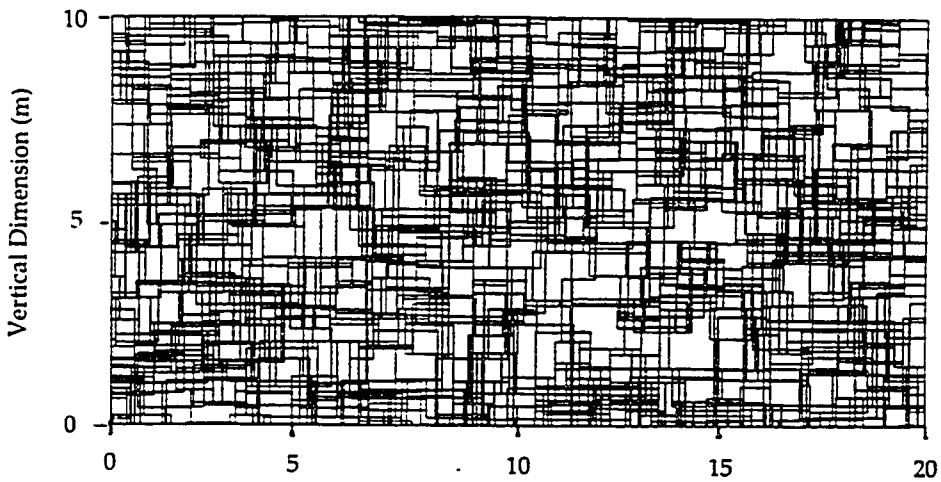

(a) Model 1 (Smith and Schwartz, 1993)

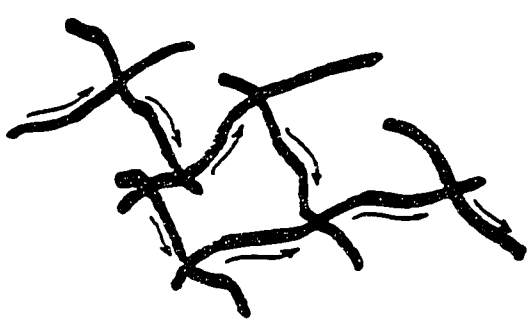

(b) Model 2 (Murray et al., 1989)

Figure 3.2 Purely Discrete Fracture Model

Reproduced with permission of the copyright owner. Further reproduction prohibited without permission.

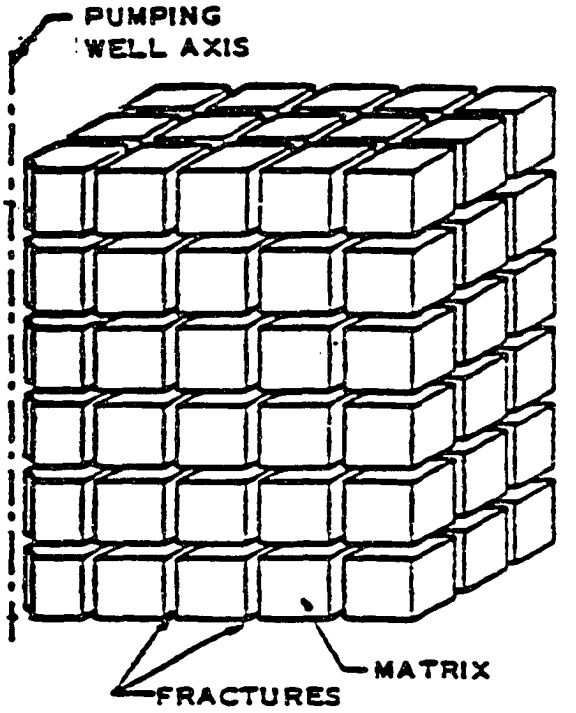

(a) Model 1 (Warren and Root, 1963)

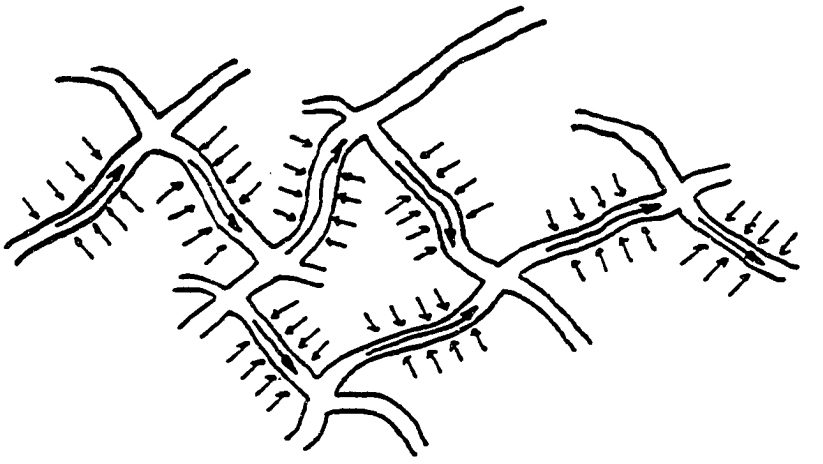

(b) Model 2 (Murray et al., 1989)

Figure 3.3 Dual Porosity Model

Reproduced with permission of the copyright owner. Further reproduction prohibited without permission.

Among the three approaches described above, the dual porosity approach fits the pneumatic fracturing process best for a few reasons. First, the fracture created by the high pressure air injection is quite distinguishable from the soil matrix, resulting in division of the formation into two parts (i.e., the discrete fracture part and the soil matrix part). Second, field evidence to date suggests one fracture injection creates a major fracture plane with only minor secondary network fracturing (Murdoch, 1992a). Third, the soil matrix adjacent to the discrete fracture is porous indeed. Thus, the dual porosity model is most appropriate, and a special case will be studied: a porous medium with a discrete fracture.

Besides characterizing the media, transport mechanisms are of paramount importance in this study. It is well known that the vapor transport processes include three components, namely, convection, diffusion, and dispersion (for example, Dullien, 1991). Convection is the passive movement of chemicals with flowing fluid; diffusion occurs in response to concentration gradients and the Brownian motion of molecules; and dispersion is the result of velocity variations that cause the chemicals to be transported down-gradient.

In the application of the pneumatic fracturing process, the permeability of the soil formation is very low; thus, convection and dispersion in the porous medium adjacent to the fractures can be neglected and diffusion becomes the only remaining transport process (Shackeford, 1991). On the other hand, in a discrete fracture, induced flow carries the contaminant out of the formation. Therefore, diffusion, convection, and dispersion processes may occur simultaneously within the fracture. However, since the fracture opening is quite small compared with the fracture length and it changes rather slowly, velocity variations are assumed to be insignificant and negligible, which means dispersion is negligible.

Figures 3.4 and 3.5 illustrate the conceptual models for two dimensional and

Reproduced with permission of the copyright owner. Further reproduction prohibited without permission.

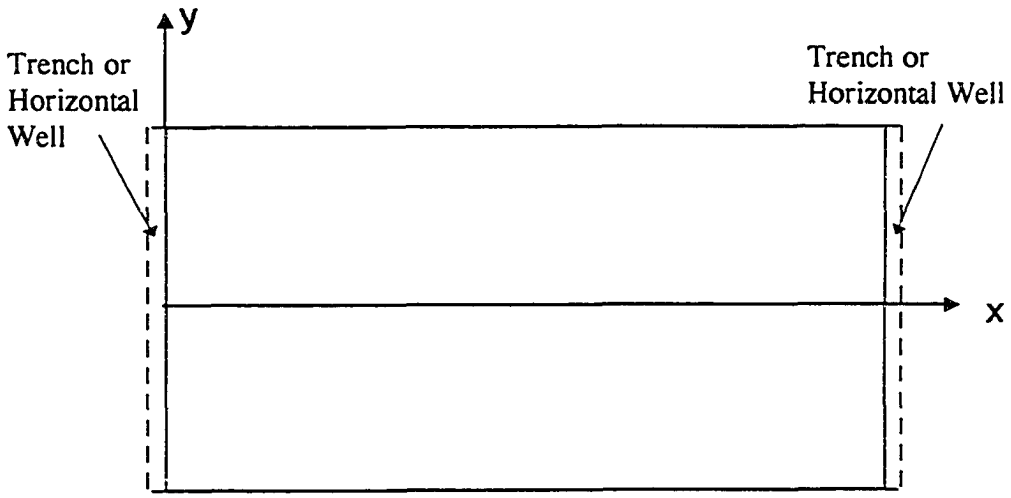

(a) Top View

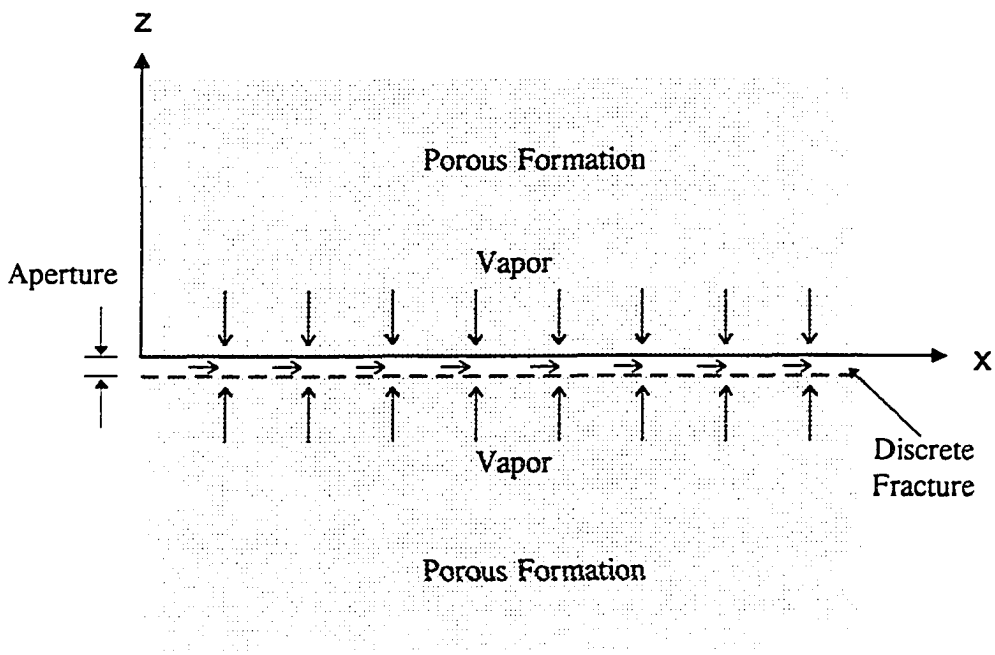

(b) Cross Section

Figure 3.4 Conceptual Model of Chemical Transport for Two Dimensional Analysis

Reproduced with permission of the copyright owner. Further reproduction prohibited without permission.

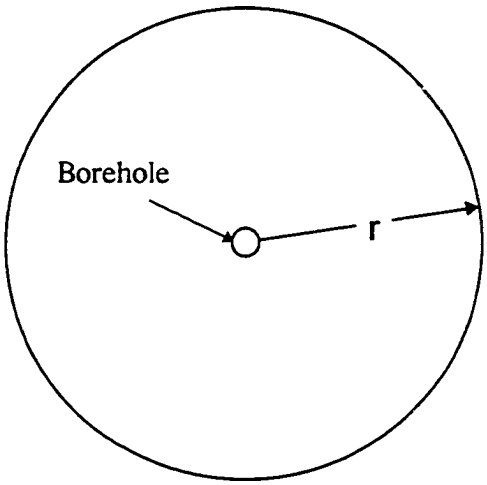

(a) Top View

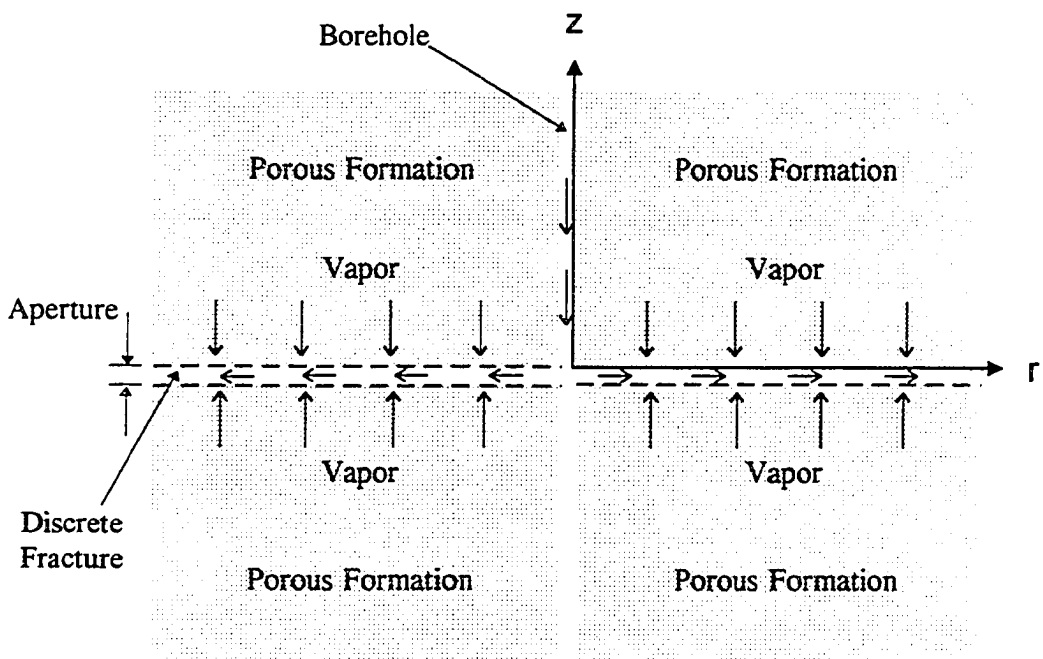

(b) Cross-Section

Figure 3.5 Conceptual Model of Chemical Transport for Axial Symmetrical Analysis

Reproduced with permission of the copyright owner. Further reproduction prohibited without permission.

axial symmetrical cases, respectively. The formation consists of a porous matrix with a single fracture. Although there may be more than one fracture in real field applications, a single fracture is an essential starting point for studies of multi-fractured formations. Since the upper and the lower parts of the porous matrix are considered symmetrical during the process of mass removal, it is only necessary to model the upper part of the porous matrix and the upper half of this discrete fracture. Therefore, the mathematical model will be established based on the finite fracture zone and the semi-infinite (in the z direction) porous zone, in which the porous medium is assumed to be homogenous and isotropic.

The discrete fracture will be assumed to consist of two horizontal parallel planes, i.e., the aperture of the fracture is constant. Furthermore, the aperture is assumed to be stable during the soil vapor extraction, which makes the next condition possible: the flow rate induced by extraction is constant. This assumption is generally consistent with field observations of in situ flow rate measurement.

The moisture content is assumed to be uniformly distributed in the porous matrix and remains as such during the extraction operation. This condition is reasonable when the involved chemicals are much more volatile than water. In addition, it is assumed that there is no chemical reaction during the mass removal process. This is reasonable since no chemicals or any other amendments are introduced into the formation except for the clean air, which will not cause any chemical reactions except for a minor amount of biodegradation.

In summary, the proposed mathematical model is developed based on the following conditions:

1. The formation consists of two zones, i.e., a finite discrete fracture and a semi-infinite porous medium zone.

Reproduced with permission of the copyright owner. Further reproduction prohibited without permission.

2. The porous medium is homogenous and isotropic.
3. The aperture of the fracture is constant.
4. The flow rate induced by vacuum extraction is constant.
5. The water in the soil matrix is immobile.
6. There are no chemical reactions during the process of removal.

3.2 Mathematical Formulation

Following the conceptual model described in the previous section, the mathematical simulation of VOC removal from a fractured porous medium is to be established two dimensionally with Cartesian (x,y,z) coordinates and axial symmetrically with cylindrical (r,φ,z) coordinates. The selection of these two coordinate systems reflects the most commonly encountered field situations. For instance, in the case of a trench or a horizontal well problem, the two dimensional analysis is more convenient and provides a more useful solution; whereas the axial symmetrical analysis provides solutions for problems such as soil vapor extraction from a vertical borehole. The governing equations for concentration distributions of VOCs in the discrete fracture and the porous matrix are derived based on the principle of mass conservation. Once derived, Laplace transforms are used to obtain the analytical solutions. The processes of establishing the governing equations with their initial-boundary conditions and seeking solutions in both coordinate systems are described in the following two sections.

3.2.1 Two Dimensional Analysis

The formation is divided into two zones, the discrete fracture and the porous matrix where different transport mechanisms exist. The characteristics for each individual zone and the relationship between them are derived below.

Reproduced with permission of the copyright owner. Further reproduction prohibited without permission.

1. Governing Equation in a Discrete Fracture

Generally, the aperture of the fracture is very small compared with the length of the fracture; so, the concentration gradient in z direction is neglected. Consequently, the concentration in the discrete fracture is a function of time t and coordinate x without z. Figure 3.6(a) illustrates the chemical flux for an element in the discrete fracture. Applying the principle of mass conservation (Dullien, 1991), the mass balance for this element can be expressed as:

$$F_1 b - \left(F_1 + \frac{\partial F_1}{\partial x} dx \right) b + q_{21} dx = b \frac{\partial C_1}{\partial t} dx \tag{3.1}$$

where

$C_1(t,x)$---chemical concentration in the discrete fracture

$F_1(t,x)$ ---mass flux in the discrete fracture along x direction

$q_{21}(t,x)$ --diffusive flux from the porous matrix into the discrete fracture

b ---------half aperture of the discrete fracture

Mathematically, the above equation can be simplified as:

$$b \frac{\partial C_1}{\partial t} + \frac{\partial F_1}{\partial x} b - q_{21} = 0 \tag{3.2}$$

Since the mass transport in the discrete fracture comprises both convection and diffusion, the mass flux F_1 can be expressed as (Dullien, 1991):

$$F_1 = u_1 C_1 - D_1 \frac{\partial C_1}{\partial x} \tag{3.3}$$

$$u_1 = \frac{Q_1}{2b} \tag{3.4}$$

where

Reproduced with permission of the copyright owner. Further reproduction prohibited without permission.

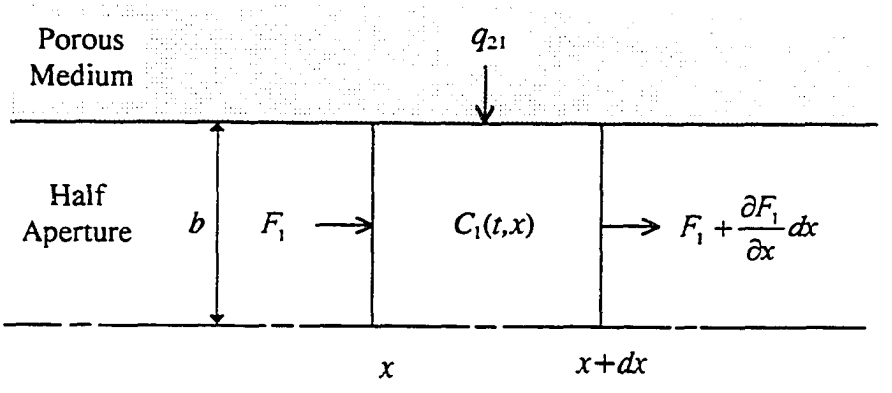

(a) Discrete Fracture

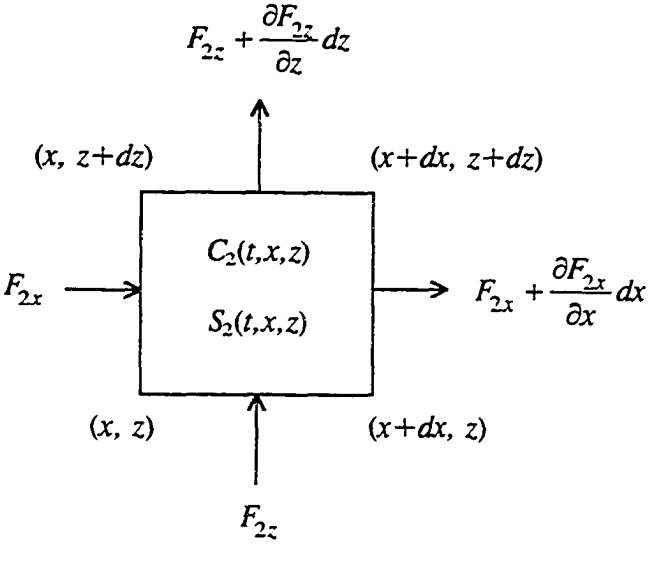

(b) Porous Medium

Figure 3.6 Mass Transport for an Element in Two Dimensional Analysis

Reproduced with permission of the copyright owner. Further reproduction prohibited without permission.

u_1----velocity of air in the fracture

Q_1 ---flow rate per unit width induced by the vacuum extraction

D_1 ---diffusion coefficient in the discrete fracture

In general, the diffusion coefficient in open air (D_1) is dependent on the chemical compound, but independent of chemical concentration for relative low concentration ranges. The range of concentration for the present model is considered to be relative low. Therefore, the diffusion coefficient can be assumed to be a constant chemical parameter. However, for very high concentrations, the diffusion coefficient would have to be related to concentration, which is significantly more complex and beyond the scope of this study.

The diffusive flux from the porous matrix into the discrete fracture, q_{21}, is proportional to the vertical concentration gradient of the porous matrix at the interface of two zones:

$$q_{21} = n_a D_2 \left(\frac{\partial C_2}{\partial z} \right)_{z=0} \tag{3.5}$$

where

$C_2(t,x,z)$ ---chemical concentration in the porous matrix

n_a ----------air filled porosity for the porous medium

D_2----------diffusion coefficient in the porous medium

The diffusion coefficient in the porous medium (D_2) is related to both chemical and soil properties. The evaluation of D_2 will be discussed later in Chapter 4.

Substituting Equations (3.3) and (3.5) into (3.2)

$$\frac{\partial C_1}{\partial t} + u_1 \frac{\partial C_1}{\partial x} - D_1 \frac{\partial^2 C_1}{\partial x^2} - \frac{n_a D_2}{b} \left(\frac{\partial C_2}{\partial z} \right)_{z=0} = 0 \tag{3.6}$$

Reproduced with permission of the copyright owner. Further reproduction prohibited without permission.

For typical cases of pneumatic fracturing, the Peclet number is in the range from 10^4 to 10^5 which means convective transport is much larger than diffusive transport within the discrete fracture. Based on the Peclet number criterion (Bear, 1972), the respective diffusion term can be neglected. The governing equation for the discrete fracture in two dimensional analysis with Cartesian coordinates is, therefore, given by

$$\frac{\partial C_1}{\partial t} + u_1 \frac{\partial C_1}{\partial x} - \frac{n_a D_2}{b}\left(\frac{\partial C_2}{\partial z}\right)_{z=0} = 0 \qquad (3.7)$$

It should be pointed out that both C_1 and C_2 appear in the above equation, which complicates the equation and makes it difficult to solve.

2. Governing Equation for the Porous Medium

Applying the principle of mass conservation, the mass flux for an element in the porous medium, as shown in Figure 3.6(b), can be expressed explicitly as:

$$F_{2x}dz - \left(F_{2x} + \frac{\partial F_{2x}}{\partial x}dx\right)dz + F_{2z}dx - \left(F_{2z} + \frac{\partial F_{2z}}{\partial z}dz\right)dx = \frac{\partial S_2}{\partial t}dxdz + \frac{\partial C_2}{\partial t}n_a dxdz \qquad (3.8)$$

where

$F_{2x}(t,x,z)$ --mass flux in the porous matrix along x direction

$F_{2z}(t,x,z)$ --mass flux in porous matrix along z direction

$S_2(t,x,z)$----chemical adsorbed by the soil water and solid of the porous matrix

n_a ----------air filled porosity of the porous matrix

Mathematically, the above equation can be simplified as

$$\frac{\partial S_2}{\partial t} + n_a \frac{\partial C_2}{\partial t} + \frac{\partial F_{2x}}{\partial x} + \frac{\partial F_{2z}}{\partial z} = 0 \qquad (3.9)$$

Reproduced with permission of the copyright owner. Further reproduction prohibited without permission.

Since there is diffusion in the porous matrix only, the mass transport can be expressed as

$$F_{2x} = -D_{2x} n_a \frac{\partial C_2}{\partial x} \tag{3.10}$$

$$F_{2z} = -D_{2z} n_a \frac{\partial C_2}{\partial z} \tag{3.11}$$

where D_{2x} and D_{2z} are diffusion coefficients in x and z directions, respectively. However, it should be pointed out that the diffusion coefficients in x and z directions are the same since the porous medium is assumed to be homogeneous and isotropic, that is,

$$D_{2x} = D_{2z} = D_2 \tag{3.12}$$

The chemical sorption, $S_2(t,x,z)$, is related to the concentration, $C_2(t,x,z)$. For a linear sorption isotherm, there is

$$S_2 = K_2 C_2 \tag{3.13}$$

$$K_2 = \frac{dS_2}{dC_2} \tag{3.14}$$

where K_2 is the distribution coefficient. Consequently, from Equation (3.13), the following can be obtained

$$\frac{\partial S_2}{\partial t} = K_2 \frac{\partial C_2}{\partial t} \tag{3.15}$$

Substituting Equations (3.10), (3.11) and (3.15) into (3.9), we obtain

$$\left(1 + \frac{K_2}{n_a}\right)\frac{\partial C_2}{\partial t} - D_2\left(\frac{\partial^2 C_2}{\partial x^2} + \frac{\partial^2 C_2}{\partial z^2}\right) = 0 \tag{3.16}$$

Reproduced with permission of the copyright owner. Further reproduction prohibited without permission.

Furthermore, the retardation factor for the porous medium can be introduced as:

$$R_2 = 1 + \frac{K_2}{n_a} \tag{3.17}$$

The retardation factor (R_2) is related to both chemical and soil properties. The determination of R_2 will be discussed in Chapter 4.

Substituting Equations (3.17) into (3.16), we get the governing equation for the porous medium:

$$\frac{\partial C_2}{\partial t} - \frac{D_2}{R_2}\left(\frac{\partial^2 C_2}{\partial x^2} + \frac{\partial^2 C_2}{\partial z^2}\right) = 0 \tag{3.18}$$

Since the movement of chemicals in the porous matrix is predominantly in the z direction toward the fracture, the diffusive transport in horizontal direction is negligible compared with that in the vertical direction. Thus, the above equation can be simplified, and the governing equation for the porous medium in two dimensional analysis with Cartesian coordinate becomes:

$$\frac{\partial C_2}{\partial t} - \frac{D_2}{R_2}\left(\frac{\partial^2 C_2}{\partial z^2}\right) = 0 \tag{3.19}$$

3. Initial and Boundary Conditions

The initial and boundary conditions for Equations (3.7) and (3.19) are set up based on field conditions for a soil vapor extraction system. Initially, the contaminant is assumed to be uniformly distributed in the soil matrix, but absent from the discrete fracture. That is

$$C_1(0,x) = 0, \quad C_2(0,x,z) = C_o \quad \text{at} \quad t = 0$$

where C_o is the initial concentration in the porous medium. The justification for this assumption is based on field observations that contaminated zones are

Reproduced with permission of the copyright owner. Further reproduction prohibited without permission.

relatively large in comparison with the fracture dimension, and clean air is introduced during injection, so the concentration in the fracture can be set as zero for initial condition.

Since clean air is continuously introduced from one end of the fracture (at $x = 0$), the concentration at this point can be set as zero, that is

$$C_1(t,0) = 0 \quad \text{at} \quad x = 0$$

The soil matrix is assumed to extend infinitely, and remain undisturbed. So the concentration in soil matrix at infinity is constant, that is

$$C_2(t,x,\infty) = C_o \quad \text{at} \quad z = \infty$$

At the interface between the discrete fracture and the porous matrix, the concentration of the contaminant should be continuous, that is

$$C_2(t,x,0) = C_1(t,x) \quad \text{at} \quad z = 0$$

Apparently, C_1 and C_2 are linked together not only by the governing Equation (3.7), but also by the above interface boundary condition. As a result, the two partial differential equations have to be solved simultaneously.

4. Solutions

The Laplace transform technique is used to solve the two partial differential equations simultaneously in conjunction with their initial and boundary conditions. The general process includes the following three major steps (Pearson, 1983; Latta, 1983):

1. Transform the partial differential equations to ordinary differential equations by using Laplace transforms.
2. Solve the two simultaneous ordinary differential equations.

Reproduced with permission of the copyright owner. Further reproduction prohibited without permission.

3. Transform the solutions of the ordinary differential equations to solutions of the partial differential equations by using inverse Laplace transforms.

It should be pointed out that ordinary differential equations are not the outcome of the Laplace transforms for this problem. Instead the expressions are still partial differential equations which, however, have one fewer independent variable (time t) than the original equations.

The two governing equations in conjunction with their initial and boundary conditions are summarized as follows

$$\text{For the discrete fracture} \begin{cases} \dfrac{\partial C_1}{\partial t} + \dfrac{Q_1}{2b}\dfrac{\partial C_1}{\partial x} - \dfrac{D_2 n_a}{b}\left(\dfrac{\partial C_2}{\partial z}\right)_{z=0} = 0 \\ C_1(0,x) = 0 \qquad \text{at} \quad t = 0 \\ C_1(t,0) = 0 \qquad \text{at} \quad x = 0 \end{cases} \tag{3.20}$$

$$\text{For the porous medium} \begin{cases} \dfrac{\partial C_2}{\partial t} - \dfrac{D_2}{R_2}\left(\dfrac{\partial^2 C_2}{\partial z^2}\right) = 0 \\ C_2(0,x,z) = C_o \qquad \text{at} \quad t = 0 \\ C_2(t,x,\infty) = C_o \qquad \text{at} \quad z = \infty \\ C_2(t,x,0) = C_1(t,x) \qquad \text{at} \quad z = 0 \end{cases} \tag{3.21}$$

Before taking the Laplace transform, relevant notations should be introduced first.

We define

$$L[C_1(t,x)] = A_1(p,x) \tag{3.22}$$

$$L[C_2(t,x,z)] = A_2(p,x,z) \tag{3.23}$$

Reproduced with permission of the copyright owner. Further reproduction prohibited without permission.

for Laplace transform,

and

$$L^{-1}\left[A_1(p,x)\right] = C_1(t,x) \tag{3.24}$$

$$L^{-1}\left[A_2(p,x,z)\right] = C_2(t,x,z) \tag{3.25}$$

for inverse Laplace transform. Where p is the Laplace transform parameter. Applying Laplace transform to the each term of Equation (3.20) results in

$$L\left(\frac{\partial C_1}{\partial t}\right) = pL(C_1) - (C_1)_{t=0} = pA_1 \tag{3.26}$$

$$L\left(u_1 \frac{\partial C_1}{\partial x}\right) = u_1 \frac{dA_1}{dx} \tag{3.27}$$

$$L\left[\frac{D_2 n_a}{b}\left(\frac{\partial C_2}{\partial z}\right)_{z=0}\right] = \frac{D_2 n_a}{b}\left(\frac{\partial A_2}{\partial z}\right)_{z=0} \tag{3.28}$$

$$L\left[C_1(t,0)\right] = A_1(p,0) = 0 \tag{3.29}$$

Similarly, for each term in Equation (3.21)

$$L\left(\frac{\partial C_2}{\partial t}\right) = pL(C_2) - (C_2)_{t=0} = pA_2 - C_o \tag{3.30}$$

$$L\left[\frac{D_2}{R_2}\left(\frac{\partial^2 C_2}{\partial z^2}\right)\right] = \frac{D_2}{R_2}\left(\frac{\partial^2 A_2}{\partial z^2}\right) \tag{3.31}$$

$$L\left[C_2(t,x,0)\right] = A_2(p,x,0) = L\left[C_1(t,x)\right] = A_1(p,x) \tag{3.32}$$

Reproduced with permission of the copyright owner. Further reproduction prohibited without permission.

$$L[C_2(t,x,\infty)] = A_2(p,x,\infty) = L(C_o) = \frac{C_o}{p} \tag{3.33}$$

Grouping Equations (3.26) through (3.29), and (3.30) through (3.33), respectively, two sets of Laplace transformed equations are obtained as follows:

For the discrete fracture

$$\begin{cases} pA_1 + \dfrac{Q_1}{2b}\dfrac{dA_1}{dx} - \dfrac{D_2 n_a}{b}\left(\dfrac{\partial A_2}{\partial z}\right)_{z=0} = 0 \\ A_1(p,0) = 0 \qquad \text{at} \quad x = 0 \end{cases} \tag{3.34}$$

For the porous matrix

$$\begin{cases} pA_2 - \dfrac{D_2}{R_2}\dfrac{\partial^2 A_2}{\partial z^2} = C_o \\ A_2(p,x,0) = A_1(p,x) \qquad \text{at} \quad z = 0 \\ A_2(p,x,\infty) = \dfrac{C_o}{p} \qquad \text{at} \quad z = \infty \end{cases} \tag{3.35}$$

The above two sets of equations are still linked together and they are not exactly ordinary differential equations since the partial differential terms of A_2 appear in both equations. However, time, t, has disappeared from the equation set with the substitution of p, which is considered to be a parameter rather than a variable. Thus, these two equations are much simpler than the original Equations (3.20) and (3.21).

It can be seen that A_2 in Equation (3.35) can be solved first as a function of A_1. The general solution is in the form

$$A_2 = A_{21}\exp(mz) + A_{22}\exp(-mz) + \frac{C_o}{p} \tag{3.36}$$

Reproduced with permission of the copyright owner. Further reproduction prohibited without permission.

$$m = \sqrt{\frac{R_2 p}{D_2}} \tag{3.37}$$

where A_{21} and A_{22} are undetermined functions.

Applying the boundary conditions at $z = \infty$ and $z = 0$ in Equation (3.35), respectively, it can be shown that

$$A_{21} = 0 \tag{3.38}$$

$$A_{22} = A_1 - \frac{C_o}{p} \tag{3.39}$$

Substituting Equations (3.38) and (3.39) into (3.36), yields the relationship between A_2 and A_1 as:

$$A_2 = \left(A_1 - \frac{C_o}{p} \right) \exp(-mz) + \frac{C_o}{p} \tag{3.40}$$

Considering the form of A_2 in Equation (3.34), it is convenient to express

$$\frac{\partial A_2}{\partial z} = -m \left(A_1 - \frac{C_o}{p} \right) \exp(-mz) \tag{3.41}$$

and furthermore

$$\left(\frac{\partial A_2}{\partial z} \right)_{z=0} = -m \left(A_1 - \frac{C_o}{p} \right) \tag{3.42}$$

Substituting Equation (3.42) into (3.34), the following is obtained

$$pA_1 + \frac{Q_1}{2b} \frac{dA_1}{dx} + \frac{mD_2 n_a}{b} \left(A_1 - \frac{C_o}{p} \right) = 0 \tag{3.43}$$

The above equation can be rewritten as

$$\frac{Q_1}{2b} \frac{dA_1}{dx} + A_1 \left(p + \frac{mD_2 n_a}{b} \right) - \frac{mD_2 n_a C_o}{pb} = 0 \tag{3.44}$$

Reproduced with permission of the copyright owner. Further reproduction prohibited without permission.

This is a first order ordinary differential equation. Along with the boundary condition in Equation (3.34), its solution can be expressed as

$$A_1 = \frac{C_o}{p + \frac{b}{n_a\sqrt{D_2R_2}}p^{3/2}}\left[1 - \exp\left(-\frac{2bx}{Q_1}p - \frac{2n_a\sqrt{D_2R_2}}{Q_1}\sqrt{p}\right)\right] \tag{3.45}$$

Substituting Equation (3.45) into (3.40)

$$A_2 = \frac{C_o}{p} - \frac{C_o}{p}\exp\left(-z\sqrt{\frac{R_2}{D_2}}\sqrt{p}\right) + \frac{C_o}{p + \frac{b}{n_a\sqrt{D_2R_2}}p^{3/2}}\exp\left(-z\sqrt{\frac{R_2}{D_2}}\sqrt{p}\right)$$

$$- \frac{C_o}{p + \frac{b}{n_a\sqrt{D_2R_2}}p^{3/2}}\exp\left(-\frac{2bx}{Q_1}p - \frac{2n_a\sqrt{D_2R_2}}{Q_1}\sqrt{p} - z\sqrt{\frac{R_2}{D_2}}\sqrt{p}\right) \tag{3.46}$$

The above two solutions are for transformed Equations (3.34) and (3.35) but not for the governing Equations (3.20) and (3.21). To obtain the solutions for the original partial differential equations, inverse Laplace transforms are applied to these two solutions. Here, the following shorthand notations are introduced as follows:

$$A_{L1} = \frac{C_o}{p + \frac{b}{n_a\sqrt{D_2R_2}}p^{3/2}} \tag{3.47}$$

$$A_{L2} = \exp\left(-\frac{2xn_a\sqrt{D_2R_2}}{Q_1}\sqrt{p}\right) \tag{3.48}$$

$$A_{L3} = \exp\left(-\frac{2bx}{Q_1}p\right) \tag{3.49}$$

Reproduced with permission of the copyright owner. Further reproduction prohibited without permission.

$$A_{L4} = \exp\left(-z\sqrt{\frac{R_2}{D_2}}\sqrt{p}\right) \tag{3.50}$$

So Equations (3.45) and (3.46) reduce to the shorter forms as

$$A_1 = A_{L1} - A_{L1}A_{L2}A_{L3} \tag{3.51}$$

$$A_2 = \frac{C_o}{p} - \frac{C_o}{p}A_{L4} + A_{L1}A_{L4} - A_{L1}A_{L2}A_{L3}A_{L4} \tag{3.52}$$

Applying inverse Laplace transform to the above two solutions

$$L^{-1}(A_1) = L^{-1}(A_{L1}) - L^{-1}(A_{L1}A_{L2}A_{L3}) \tag{3.53}$$

$$L^{-1}(A_2) = L^{-1}\left(\frac{C_o}{p}\right) - L^{-1}\left(\frac{C_o}{p}A_{L4}\right) + L^{-1}(A_{L1}A_{L4}) - L^{-1}(A_{L1}A_{L2}A_{L3}A_{L4}) \tag{3.54}$$

To apply the inverse Laplace transform, the error function and the complementary error function are needed. They are defined as follows, respectively,

$$\operatorname{erf}(\alpha) = \frac{2}{\sqrt{\pi}}\int_0^{\alpha}\exp(-\zeta^2)d\zeta$$

$$\operatorname{erfc}(\alpha) = 1 - \operatorname{erf}(\alpha)$$

By applying the inverse Laplace transform (Erdelyi, *et al.* 1954), the following is obtained

$$L^{-1}[A_{L1}] = C_o\left[1 - \exp\left(\frac{n_a^2 D_2 R_2}{b^2}t\right)\operatorname{erfc}\left(\frac{n_a\sqrt{D_2R_2}}{b}\sqrt{t}\right)\right] \tag{3.55}$$

$$L^{-1}(A_{L1}A_{L2}) = C_o\operatorname{erfc}\left(\frac{n_a\sqrt{D_2R_2}}{Q_1\sqrt{t}}x\right)$$

Reproduced with permission of the copyright owner. Further reproduction prohibited without permission.

$$-C_o \exp\left[\frac{n_a^2 D_2 R_2}{b}\left(\frac{2x}{Q_1}+\frac{t}{b}\right)\right]\operatorname{erfc}\left(\frac{n_a\sqrt{D_2R_2}}{Q_1\sqrt{t}}x+\frac{n_a\sqrt{D_2R_2}}{b}\sqrt{t}\right) \tag{3.56}$$

Introducing $f_1(t)$ as shorthand notation for the above equation

$$f_1(t,x) = L^{-1}\left[A_{L1}A_{L2}\right] \tag{3.57}$$

To inverse the second term $L^{-1}(A_{L1}A_{L2}A_{L3})$ in Equation (3.53), the following general inverse Laplace transform formula (e.g., Latta, 1983) will be used

$$\begin{cases} \text{if} & L^{-1}\left[A(p)\right] = f(t) \\ \text{then} & L^{-1}\left[A(p)\exp(-ap)\right] = U(t-a)f(t-a) \\ \text{where} & U(t-a) = \begin{cases} 0 & \text{when} \quad t \le a \\ 1 & \text{when} \quad t > a \end{cases} \end{cases} \tag{3.58}$$

Applying the above formula, the following can be obtained

$$L^{-1}(A_{L1}A_{L2}A_{L3}) = U\left(t-\frac{2bx}{Q_1}\right)f_1\left(t-\frac{2bx}{Q_1}\right)$$

$$= C_o U\left(t-\frac{2bx}{Q_1}\right)\left\{\operatorname{erfc}\left[\frac{n_a\sqrt{D_2R_2}}{Q_1}x\left(t-\frac{2bx}{Q_1}\right)^{-\frac{1}{2}}\right]\right.$$

$$\left.-\exp\left(\frac{n_a^2 D_2 R_2}{b^2}t\right)\operatorname{erfc}\left(\frac{n_a\sqrt{D_2R_2}}{Q_1}x\left(t-\frac{2bx}{Q_1}\right)^{-\frac{1}{2}}+\frac{n_a\sqrt{D_2R_2}}{b}\left(t-\frac{2bx}{Q_1}\right)^{\frac{1}{2}}\right)\right\} \tag{3.59}$$

Reproduced with permission of the copyright owner. Further reproduction prohibited without permission.

The first three terms in Equation (3.52) can be obtained from inverse Laplace transform (Erdelyi, *et al.* 1954) as

$$L^{-1}\left(\frac{C_o}{p}\right)=C_o \tag{3.60}$$

$$L^{-1}\left(\frac{C_o}{p}A_{L4}\right)=C_o\operatorname{erfc}\left(\sqrt{\frac{R_2}{D_2}}\frac{z}{2\sqrt{t}}\right) \tag{3.61}$$

$$L^{-1}(A_{L1}A_{L4})=C_o\operatorname{erfc}\left(\sqrt{\frac{R_2}{D_2}}\frac{z}{2\sqrt{t}}\right)$$

$$-C_o\exp\left(\frac{R_2 z}{b}+\frac{n_a^2 D_2 R_2}{b^2}t\right)\operatorname{erfc}\left(\sqrt{\frac{R_2}{D_2}}\frac{z}{2\sqrt{t}}+\frac{n_a\sqrt{D_2R_2}}{b}\sqrt{t}\right) \tag{3.62}$$

To obtain $L^{-1}(A_{L1}A_{L2}A_{L3}A_{L4})$ in Equation (3.52), the following inverse has to be carried out first as the preparation:

$$L^{-1}(A_{L1}A_{L2}A_{L4})=C_o\operatorname{erfc}\left[\left(\frac{n_a^2D_2R_2}{bQ_1}x+\sqrt{\frac{R_2}{D_2}}\frac{z}{2}\right)\frac{1}{\sqrt{t}}\right]$$

$$-C_o\exp\left(\frac{2n_a^2D_2R_2}{bQ_1}x+\frac{n_aR_2}{b}z+\frac{n_a^2D_2R_2}{b^2}t\right)\operatorname{erfc}\left[\left(\frac{n_a^2D_2R_2}{bQ_1}x+\sqrt{\frac{R_2}{D_2}}\frac{z}{2}\right)\frac{1}{\sqrt{t}}+\frac{n_a\sqrt{D_2R_2}}{b}\sqrt{t}\right] \tag{3.63}$$

Applying the inverse Laplace transform formula (3.58)

$$L^{-1}(A_{L1}A_{L2}A_{L3}A_{L4})=C_oU\left(t-\frac{2bx}{Q_1}\right)\left\{\operatorname{erfc}\left[\left(\frac{n_a^2D_2R_2}{Q_1}x+\sqrt{\frac{R_2}{D_2}}\frac{z}{2}\right)\left(t-\frac{2bx}{Q_1}\right)^{-\frac{1}{2}}\right]\right.$$

Reproduced with permission of the copyright owner. Further reproduction prohibited without permission.

$$-\exp\left(\frac{n_a R_2}{b}z+\frac{n_a^2 D_2 R_2}{b^2}t\right)\operatorname{erfc}\left[\left(\frac{n_a^2 D_2 R_2}{Q_1}x+\sqrt{\frac{R_2}{D_2}}\frac{z}{2}\right)\left(t-\frac{2bx}{Q_1}\right)^{-\frac{1}{2}}+\frac{n_a\sqrt{D_2 R_2}}{b}\left(t-\frac{2bx}{Q_1}\right)^{\frac{1}{2}}\right]\Bigg\}$$

(3.64)

Substituting Equations (3.55) and (3.59) into (3.53), and (3.60) - (3.62) and (3.64) into (3.54), respectively, the final solutions of the original sets of partial differential equations (3.20) and (3.21) can be expressed as follows:

for $t \le \frac{2bx}{Q_1}$

$$\frac{C_1}{C_o}=1-\exp\left(\frac{n_a^2 D_2 R_2}{b^2}t\right)\operatorname{erfc}\left(\frac{n_a\sqrt{D_2 R_2}}{b}\sqrt{t}\right) \tag{3.65}$$

$$\frac{C_2}{C_o}=1-\exp\left(\frac{n_a R_2}{b}z+\frac{n_a^2 D_2 R_2}{b^2}t\right)\operatorname{erfc}\left(\frac{1}{2}\sqrt{\frac{R_2}{D_2}}\frac{z}{\sqrt{t}}+\frac{n_a\sqrt{D_2 R_2}}{b}\sqrt{t}\right) \tag{3.66}$$

for $t > \frac{2bx}{Q_1}$

$$\frac{C_1}{C_o}=\operatorname{erf}\left[\frac{n_a\sqrt{D_2 R_2}}{Q_1}x\left(t-\frac{2bx}{Q_1}\right)^{-\frac{1}{2}}\right]+\exp\left(\frac{n_a^2 D_2 R_2}{b^2}t\right)\operatorname{erf}\left(\frac{n_a\sqrt{D_2 R_2}}{b}\sqrt{t}\right)$$

$$-\exp\left(\frac{n_a^2 D_2 R_2}{b^2}t\right)\operatorname{erf}\left[\frac{n_a\sqrt{D_2 R_2}}{Q_1}x\left(t-\frac{2b}{Q_1}x\right)^{-\frac{1}{2}}+\frac{n_a\sqrt{D_2 R_2}}{b}\left(t-\frac{2b}{Q_1}x\right)^{\frac{1}{2}}\right] \tag{3.67}$$

$$\frac{C_2}{C_o}=\operatorname{erf}\left[\left(\frac{n_a\sqrt{D_2 R_2}}{Q_1}x+z\sqrt{\frac{R_2}{D_2}}\right)\left(t-\frac{2bx}{Q_1}\right)^{-\frac{1}{2}}\right]$$

Reproduced with permission of the copyright owner. Further reproduction prohibited without permission.

$$+\exp\left(\frac{n_a R_2}{b}z+\frac{n_a^2 D_2 R_2}{b^2}t\right)\operatorname{erf}\left(\sqrt{\frac{R_2}{D_2}}\frac{z}{\sqrt{t}}+\frac{n_a\sqrt{D_2R_2}}{b}\sqrt{t}\right)$$

$$-\exp\left(\frac{n_a R_2}{b}z+\frac{n_a^2 D_2 R_2}{b^2}t\right)\operatorname{erf}\left[\frac{n_a\sqrt{D_2R_2}}{b}\left(t-\frac{2bx}{Q_1}\right)^{\frac{1}{2}}\right.$$

$$\left.+\left(\frac{n_a\sqrt{D_2R_2}}{Q_1}x+z\sqrt{\frac{R_2}{D_2}}\right)\left(t-\frac{2bx}{Q_1}\right)^{-\frac{1}{2}}\right] \qquad (3.68)$$

or, in combined format as

$$\frac{C_1}{C_o}=1-\exp\left(\frac{n_a^2 D_2 R_2}{b^2}t\right)\operatorname{erfc}\left(\frac{n_a\sqrt{D_2R_2}}{b}\sqrt{t}\right)$$

$$-U\left(t-\frac{2b}{Q_1}x\right)\left\{\operatorname{erfc}\left[\frac{n_a\sqrt{D_2R_2}}{Q_1}x\left(t-\frac{2bx}{Q_1}\right)^{-\frac{1}{2}}\right]\right.$$

$$\left.+\exp\left(\frac{n_a^2 D_2 R_2}{b^2}t\right)\operatorname{erf}\left[\frac{n_a\sqrt{D_2R_2}}{Q_1}x\left(t-\frac{2bx}{Q_1}\right)^{-\frac{1}{2}}+\frac{n_a\sqrt{D_2R_2}}{b}\left(t-\frac{2bx}{Q_1}\right)^{\frac{1}{2}}\right]\right\}$$

(3.69)

$$\frac{C_2}{C_o}=1-\exp\left(\frac{n_a R_2}{b}z+\frac{n_a^2 D_2 R_2}{b^2}t\right)\operatorname{erfc}\left(\sqrt{\frac{R_2}{D_2}}\frac{z}{\sqrt{t}}+\frac{n_a\sqrt{D_2R_2}}{b}\sqrt{t}\right)$$

$$-U\left(t-\frac{2bx}{Q_1}\right)\operatorname{erfc}\left[\left(\frac{n_a\sqrt{D_2R_2}}{Q_1}x+z\sqrt{\frac{R_2}{D_2}}\right)\left(t-\frac{2bx}{Q_1}\right)^{-\frac{1}{2}}\right]$$

Reproduced with permission of the copyright owner. Further reproduction prohibited without permission.

$$-U\left(t-\frac{2bx}{Q_1}\right)\exp\left(\frac{n_a R_2}{b}z+\frac{n_a^2 D_2 R_2}{b^2}t\right)\operatorname{erfc}\left[\frac{n_a\sqrt{D_2R_2}}{b}\left(t-\frac{2bx}{Q_1}\right)^{\frac{1}{2}}\right.$$

$$\left.+\left(\frac{n_a\sqrt{D_2R_2}}{Q_1}+z\sqrt{\frac{R_2}{D_2}}\right)\left(t-\frac{2bx}{Q_1}\right)^{-\frac{1}{2}}\right]$$

(3.70)

As indicated in Equations (3.65) to (3.70), the solutions are of the form in exponential and error functions.

3.2.2 Axial Symmetrical Analysis

In most situations, the in situ soil vacuum extraction process is applied in a vertical borehole rather than in a horizontal trench case. For these cases, the contaminant removal is described better in cylindrical coordinates than in Cartesian coordinates. Since the soil medium is assumed to be homogenous and isotropic in the conceptual model (see Figure 3.5 in Section 3.1), the condition of axial symmetry automatically follows. Consequently, each physical variable of the problem will be independent of coordinate φ. The governing equations for concentration distributions of VOCs in the discrete fracture and the porous matrix will be derived based on the principle of mass conservation, and solved by using the Laplace transform technique.

1. Governing Equation for the Discrete fracture

Figure 3.7(a) illustrates the chemical flux for an element in the discrete fracture for a cylindrical coordinate system. In general, the concentration gradient in the z direction is neglected since the aperture of the fracture is very small compared with the length of the fracture. Consequently, concentration in the discrete fracture is a function of time, t, and coordinate, r, only. Based on the principle

Reproduced with permission of the copyright owner. Further reproduction prohibited without permission.

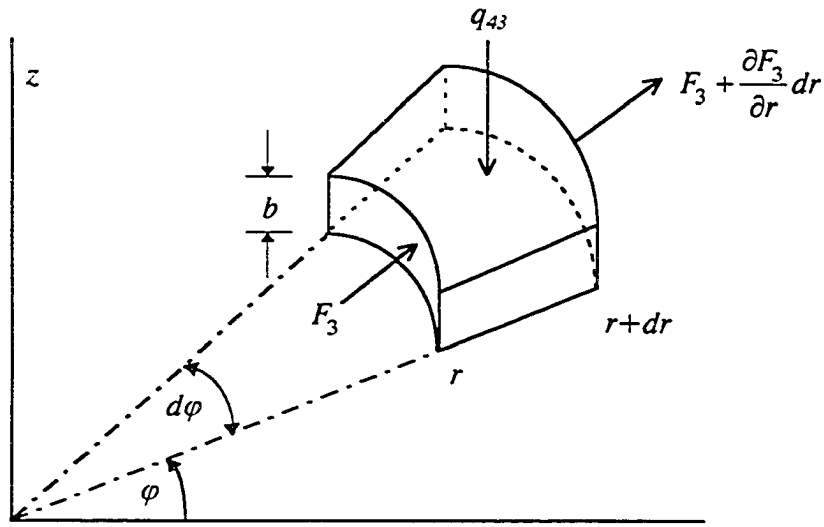

(a) Discrete Fracture

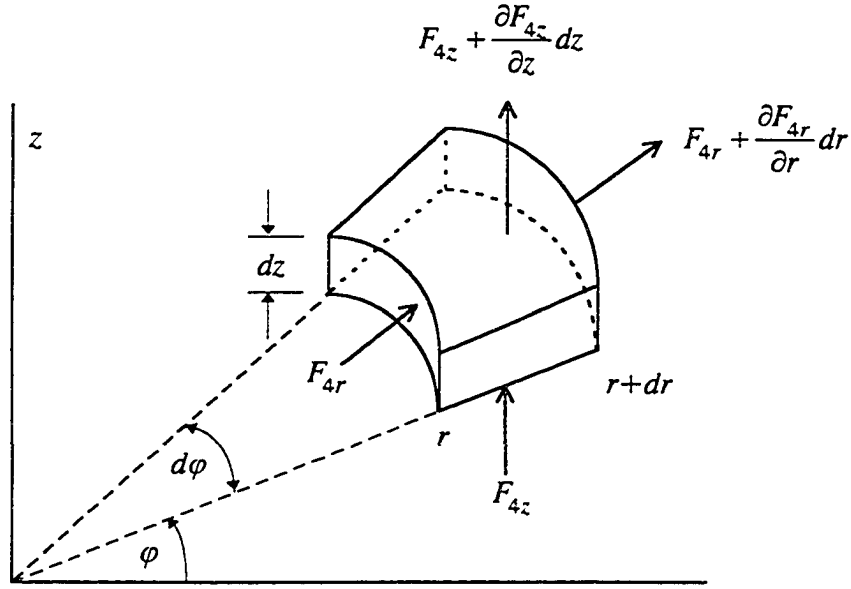

(b) Porous Medium

Figure 3.7 Mass Transport for an Element in Axial Symmetrical Analysis

Reproduced with permission of the copyright owner. Further reproduction prohibited without permission.

of mass conservation, the mass balance for this element can be expressed as:

$$F_3 brd\varphi - \left(F_3 + \frac{\partial F_3}{\partial r}dr\right)b(r+dr)d\varphi + q_{43}rd\varphi dr = \frac{\partial C_3}{\partial t}brd\varphi dr \qquad (3.71)$$

where

$C_3(t,r)$ -- chemical concentration in the discrete fracture

$F_3(t,r)$ -- mass flux in the discrete fracture along r direction

$q_{43}(t,r)$-- diffusive flux from the porous matrix into the discrete fracture

b --------- half aperture of the fracture

The above equation can be simplified as:

$$F_3 + r\frac{\partial F_3}{\partial r} + r\frac{\partial C_3}{\partial t} - \frac{rq_{43}}{b} = 0 \qquad (3.72)$$

where the diffusive flux from the porous matrix into the discrete fracture is proportional to the vertical concentration gradient of the porous matrix at the interface of two zones:

$$q_{43} = D_2 n_a \left(\frac{\partial C_4}{\partial z}\right)_{z=0} \qquad (3.73)$$

where

$C_4(t,r,z)$ ---chemical concentration in the porous medium

Since the mass transport in the discrete fracture consists of both convection and diffusion, $F_3(t,r)$ can be expressed as:

$$F_3(t,r) = u_3 C_3 - D_1 \frac{\partial C_3}{\partial r} \qquad (3.74)$$

$$u_3 = \frac{Q_3}{4\pi br} \qquad (3.75)$$

Reproduced with permission of the copyright owner. Further reproduction prohibited without permission.

where

$u_3(r)$ --- velocity of air in the fracture

Q_3 ------ flow rate induced by the vacuum extraction

D_1 ------ diffusion coefficient for the discrete fracture

Substituting Equations (3.73) and (3.74) into (3.72), the following is obtained

$$\frac{\partial C_3}{\partial t}+\frac{Q_3}{4\pi br}\frac{\partial C_3}{\partial r}-\frac{D_1}{r}\frac{\partial}{\partial r}\left(r\frac{\partial C_3}{\partial r}\right)-\frac{D_2 n_a}{b}\left(\frac{\partial C_4}{\partial z}\right)_{z=0}=0 \qquad (3.76)$$

Again, based on the Peclet number criterion (Bear, 1972), the convective transport is much larger than the diffusive transport within the discrete fracture and the diffusion term can be neglected. Thus the governing equation for a discrete fracture in axial symmetrical analysis with cylindrical coordinates is:

$$\frac{\partial C_3}{\partial t}+\frac{Q_3}{4\pi br}\frac{\partial C_3}{\partial r}-\frac{D_2 n_a}{b}\left(\frac{\partial C_4}{\partial z}\right)_{z=0}=0 \qquad (3.77)$$

2. Governing Equation for the Porous Medium

Figure 3.7(b) shows the chemical transport for an element in the porous medium. The mass balance of the element gives:

$$F_{4r}rd\varphi dz-\left(F_{4r}+\frac{\partial F_{4r}}{\partial r}dr\right)(r+dr)d\varphi dz+\left[F_{4z}-\left(F_{4z}-\frac{\partial F_{4z}}{\partial z}dz\right)\right]rd\varphi dr$$

$$=\frac{\partial S_4}{\partial t}rd\varphi drdz+\frac{\partial C_4}{\partial t}n_a rd\varphi drdz \qquad (3.78)$$

where

$F_{4r}(t,r,z)$ -- mass flux in the porous matrix along r direction

$F_{4z}(t,r,z)$ -- mass flux in the porous matrix along z direction

Reproduced with permission of the copyright owner. Further reproduction prohibited without permission.

$S_4(t,r,z)$ ---chemical adsorbed by the soil water and solid of the porous matrix

n_a ----------air filled porosity

The above equation can be simplified as

$$\frac{\partial S_4}{\partial t} + n_a \frac{\partial C_4}{\partial t} + \frac{\partial F_{4r}}{\partial r} + \frac{F_{4r}}{r} + \frac{\partial F_{4z}}{\partial z} = 0 \tag{3.79}$$

It should be pointed out that the diffusion coefficients are chemical-physical parameters which are not related to the coordinates. Furthermore, the diffusion coefficients in the r and z directions are the same based on homogeneity and isotropy assumptions for the porous medium. That means

$$D_{4r} = D_{4z} = D_2 \tag{3.80}$$

The chemical transport in the porous medium is through diffusion process only. So there are

$$F_{4r} = -D_2 n_a \frac{\partial C_4}{\partial r} \tag{3.81}$$

$$F_{4z} = -D_2 n_a \frac{\partial C_4}{\partial z} \tag{3.82}$$

The linear sorption isotherm is the same for both Cartesian and cylindrical coordinates, so

$$S_4 = K_2 C_4 = (R_2 - 1) n_a C_4 \tag{3.83}$$

where K_2 and R_2 are defined as in the two dimensional analysis [Equations (3.14) and (3.17)], since they are independent of the coordinate system. Based on Equation (3.83), the following is obtained

Reproduced with permission of the copyright owner. Further reproduction prohibited without permission.

$$\frac{\partial S_4}{\partial t} = (R_2 - 1) n_a \frac{\partial C_4}{\partial t} \tag{3.84}$$

Substituting Equations (3.81), (3.82), and (3.84) into (3.79), the governing equation for the porous medium becomes:

$$\frac{\partial C_4}{\partial t} - \frac{D_2}{R_2}\left[\frac{1}{r}\frac{\partial}{\partial r}\left(r\frac{\partial C_4}{\partial r}\right) + \frac{\partial^2 C_4}{\partial z^2}\right] = 0 \tag{3.85}$$

Since the movement of chemicals in the soil matrix is predominantly in the vertical direction toward the fracture, whereas the diffusive transport in radial direction is negligible compared with the vertical direction, the above equation can be simplified. Thus, the governing equation for the porous medium in axial symmetrical analysis with cylindrical coordinate can be expressed as:

$$\frac{\partial C_4}{\partial t} - \frac{D_2}{R_2}\left(\frac{\partial^2 C_4}{\partial z^2}\right) = 0 \tag{3.86}$$

3. Initial and Boundary Conditions

The initial and boundary conditions for Equations (3.77) and (3.86) are set up based on field conditions similar to the analysis in Cartesian coordinates. For a relative large and uniform contaminated area, the initial contaminant is assumed to be uniformly distributed in the soil matrix, but absent from the fracture medium, i.e.,

$$C_3(0,r) = 0, \quad C_4(0,r,z) = C_o \quad \text{at} \quad t = 0$$

where C_o is the initial concentration in the porous matrix.

Since the clean air is induced from the injection point ($r = 0$), the concentration at this point can be set as zero, i.e.,

$$C_3(t,0) = 0 \quad \text{at} \quad r = 0$$

Reproduced with permission of the copyright owner. Further reproduction prohibited without permission.

The concentration in the porous matrix at infinity is assumed to be undisturbed, i.e.,

$$C_4(t,r,\infty) = C_o \quad \text{at} \quad z = \infty$$

At the interface between the discrete fracture and the porous matrix, the concentration of the contaminant must be continuous, i.e.,

$$C_4(t,r,0) = C_3(t,r) \quad \text{at} \quad z = 0$$

4. Solutions

The two governing equations along with their initial and boundary conditions can be summarized as follows:

For the discrete fracture

$$\begin{cases} \dfrac{\partial C_3}{\partial t} + \dfrac{Q}{4\pi br}\dfrac{\partial C_3}{\partial r} - \dfrac{D_2 n_a}{b}\left(\dfrac{\partial C_4}{\partial z}\right)_{z=0} = 0 \\ C_3(0,r) = 0 \qquad \text{at} \quad t = 0 \\ C_3(t,0) = 0 \qquad \text{at} \quad r = 0 \end{cases} \tag{3.87}$$

For the porous medium

$$\begin{cases} \dfrac{\partial C_4}{\partial t} - \dfrac{D_2}{R_2}\left(\dfrac{\partial^2 C_4}{\partial z^2}\right) = 0 \\ C_4(0,r,z) = C_o \qquad \text{at} \quad t = 0 \\ C_4(t,r,0) = C_3(t,r) \qquad \text{at} \quad z = 0 \\ C_4(t,r,\infty) = C_o \qquad \text{at} \quad z = \infty \end{cases} \tag{3.88}$$

It can be seen that C_4 is in Equation (3.87) for C_3 while C_3 is one of the boundary conditions for C_4 in Equation (3.88). As a result, the above two partial

Reproduced with permission of the copyright owner. Further reproduction prohibited without permission.

differential equations are linked together and have to be solved simultaneously.

Introducing the notations for Laplace transform

$$L(C_3) = A_3(p,r) \tag{3.89}$$

$$L(C_4) = A_4(p,r,z) \tag{3.90}$$

and the notations for the inverse Laplace transform

$$L^{-1}[A_3(p,r)] = C_3(t,r) \tag{3.91}$$

$$L^{-1}[A_4(p,r,z)] = C_4(t,r,z) \tag{3.92}$$

where p is the Laplace transform parameter. Applying Laplace transform to each term of Equation (3.87), yields

$$L\left(\frac{\partial C_3}{\partial t}\right) = pL(C_3) - (C_3)_{t=0} = pA_3 \tag{3.93}$$

$$L\left(\frac{Q}{4\pi br}\frac{\partial C_3}{\partial r}\right) = \frac{Q}{4\pi br}\frac{dA_3}{dr} \tag{3.94}$$

$$L\left[\frac{D_2 n_a}{b}\left(\frac{\partial C_4}{\partial z}\right)_{z=0}\right] = \frac{D_2 n_a}{b}\left(\frac{\partial A_4}{\partial z}\right)_{z=0} \tag{3.95}$$

$$L[C_3(t,0)] = A_3(p,0) = 0 \tag{3.96}$$

Similarly, for each term in Equation (3.88)

$$L\left(\frac{\partial C_4}{\partial t}\right) = pL(C_4) - (C_4)_{t=0} = pA_4 - C_o \tag{3.97}$$

Reproduced with permission of the copyright owner. Further reproduction prohibited without permission.

$$L\left[\frac{D_2}{R_2}\left(\frac{\partial^2 C_4}{\partial z^2}\right)\right]=\frac{D_2}{R_2}\left(\frac{\partial^2 A_4}{\partial z^2}\right) \tag{3.98}$$

$$L[C_4(t,r,0)]=A_4(p,r,0)=L[C_3(t,r)]=A_3(p,r) \tag{3.99}$$

$$L[C_4(t,r,\infty)]=A_4(p,r,\infty)=L(C_o)=\frac{C_o}{p} \tag{3.100}$$

Combining Equations (3.93) through (3.96), and (3.97) through (3.100), respectively, yields following two sets of Laplace transformed equations:

For the discrete fracture

$$\begin{cases} pA_3+\dfrac{Q_3}{4\pi br}\dfrac{dA_3}{dr}-\dfrac{D_2 n_a}{b}\left(\dfrac{\partial A_3}{\partial z}\right)_{z=0}=0 \\ A_3(p,0)=0 \qquad \text{at} \quad r=0 \end{cases} \tag{3.101}$$

For the porous matrix

$$\begin{cases} pA_4-\dfrac{D_2}{R_2}\dfrac{\partial^2 A_4}{\partial z^2}=C_o \\ A_4(p,r,0)=A_3(p,r) \qquad \text{at} \quad z=0 \\ A_4(p,r,\infty)=\dfrac{C_o}{p} \qquad \text{at} \quad z=\infty \end{cases} \tag{3.102}$$

It can be seen that A_4 in Equation (3.102) can be solved first as a function of A_3. The general solution can be expressed as

$$A_4=A_{41}\exp(mz)+A_{42}\exp(-mz)+\frac{C_o}{p} \tag{3.103}$$

$$m=\sqrt{\frac{R_2 p}{D_2}} \tag{3.104}$$

Reproduced with permission of the copyright owner. Further reproduction prohibited without permission.

where A_{41} and A_{42} are undetermined functions.

Applying the boundary condition at $z=\infty$ and $z=0$ in Equation (3.102) respectively, A_{41} and A_{42} can be obtained as

$$A_{41}=0 \tag{3.105}$$

$$A_{42}=A_3-\frac{C_o}{p} \tag{3.106}$$

Substituting Equations (3.105) and (3.106) into (3.103), the link equation of A_3 and A_4 is determined as:

$$A_4=\left(A_3-\frac{C_o}{p}\right)\exp(-mz)+\frac{C_o}{p} \tag{3.107}$$

and

$$\frac{\partial A_4}{\partial z}=-m\left(A_3-\frac{C_o}{p}\right)\exp(-mz) \tag{3.108}$$

$$\left(\frac{\partial A_4}{\partial z}\right)_{z=0}=-m\left(A_3-\frac{C_o}{p}\right) \tag{3.109}$$

Substituting Equation (3.109) into Equation (3.101)

$$pA_3+\frac{Q}{4\pi br}\frac{dA_3}{dr}+\frac{mD_2n_a}{b}\left(A_3-\frac{C_o}{p}\right)=0 \tag{3.110}$$

which can be rewritten as

$$\frac{Q}{4\pi b}\frac{dA_3}{dr}+rA_3\left(p+\frac{mD_2n_a}{b}\right)-\frac{mD_2n_aC_o}{pb}=0 \tag{3.111}$$

The solution for the above equation along with its boundary condition in Equation (3.101) is

Reproduced with permission of the copyright owner. Further reproduction prohibited without permission.

$$A_3 = \frac{C_o}{p + \frac{b}{n_a\sqrt{D_2R_2}}p^{3/2}}\left[1 - \exp\left(-\frac{2\pi br^2}{Q_3}p - \frac{2\pi r^2 n_a\sqrt{D_2R_2}}{Q_3}\sqrt{p}\right)\right] \tag{3.112}$$

Substituting Equation (3.112) into Equation (3.107), the following is obtained

$$A_4 = \frac{C_o}{p} - \frac{C_o}{p}\exp\left(-z\sqrt{\frac{R_2}{D_2}}\sqrt{p}\right) + \frac{C_o}{p + \frac{b}{n_a\sqrt{D_2R_2}}p^{3/2}}\exp\left(-z\sqrt{\frac{R_2}{D_2}}\sqrt{p}\right)$$

$$-\frac{C_o}{p + \frac{b}{n_a\sqrt{D_2R_2}}p^{3/2}}\exp\left(-\frac{2\pi br^2}{Q_3}p - \frac{2\pi r^2 n_a\sqrt{D_2R_2}}{Q_3}\sqrt{p} - z\sqrt{\frac{R_2}{D_2}}\sqrt{p}\right) \tag{3.113}$$

The following notations are introduced for convenience,

$$A_{L5} = \exp\left(-\frac{2\pi br^2}{Q_3}p\right) \tag{3.114}$$

$$A_{L6} = \exp\left(-\frac{2\pi r^2 n_a\sqrt{D_2R_2}}{Q_3}\sqrt{p}\right) \tag{3.115}$$

Substituting Equations (3.47), (3.114), and (3.115) into (3.112), (3.47), (3.50), (3.114), and (3.115) into (3.113), respectively, yields

$$A_3 = A_{L1} - A_{L1}A_{L5}A_{L6} \tag{3.116}$$

$$A_4 = \frac{C_o}{p} - \frac{C_o}{p}A_{L4} + A_{L1}A_{L4} - A_{L1}A_{L4}A_{L5}A_{L6} \tag{3.117}$$

Applying the inverse Laplace transform to the above two equations

$$L^{-1}(A_3) = L^{-1}(A_{L1}) - L^{-1}(A_{L1}A_{L5}A_{L6}) \tag{3.118}$$

Reproduced with permission of the copyright owner. Further reproduction prohibited without permission.

$$L^{-1}(A_4) = L^{-1}\left(\frac{C_o}{p}\right) - L^{-1}\left(\frac{C_o}{p}A_{L4}\right) + L^{-1}(A_{L1}A_{L4}) - L^{-1}(A_{L1}A_{L4}A_{L5}A_{L6}) \quad (3.119)$$

Among the terms of the above two equations, $L^{-1}(A_{L1})$, $L^{-1}\left(\frac{C_o}{p}\right)$, $L^{-1}\left(\frac{C_o}{p}A_{L4}\right)$, and $L^{-1}(A_{L1}A_{L4})$ have already been obtained in Section 3.2.1. To obtain the last term in each equation, following two inverse Laplace transform are needed as the preparation:

$$L^{-1}(A_{L1}A_{L6}) = C_o \operatorname{erfc}\left(\frac{r^2\pi n_a\sqrt{D_2R_2}}{Q_3\sqrt{t}}\right)$$

$$-C_o \exp\left(\frac{2\pi n_a^2 D_2 R_2 r^2}{bQ_3} + \frac{n_a^2 D_2 R_2}{b^2}t\right)\operatorname{erfc}\left(\frac{r^2\pi n_a\sqrt{D_2R_2}}{Q_3\sqrt{t}} + \frac{n_a\sqrt{D_2R_2}}{b}\sqrt{t}\right) \quad (3.120)$$

$$L^{-1}(A_{L1}A_{L4}A_{L6}) = C_o \operatorname{erfc}\left[\left(\frac{\pi n_a^2 D_2 R_2 r^2}{Q_3} + \sqrt{\frac{R_2}{D_2}}\frac{z}{2}\right)\frac{1}{\sqrt{t}}\right]$$

$$-C_o \exp\left(\frac{2\pi n_a^2 D_2 R_2 r^2}{bQ_1} + \frac{n_a R_2}{b}z + \frac{n_a^2 D_2 R_2}{b^2}t\right)\operatorname{erfc}\left[\frac{n_a\sqrt{D_2R_2}}{b}\sqrt{t}\right.$$

$$\left. + \left(\frac{\pi n_a^2 D_2 R_2 r^2}{Q_1} + \sqrt{\frac{R_2}{D_2}}\frac{z}{2}\right)\frac{1}{\sqrt{t}}\right] \quad (3.121)$$

Applying the inverse Laplace transform formula (3.58) to the above two equations yields the following

$$L^{-1}(A_{L1}A_{L5}A_{L6}) = C_o U\left(t - \frac{2b\pi r^2}{Q_3}\right)\left\{\operatorname{erfc}\left[\frac{r^2\pi n_a\sqrt{D_2R_2}}{Q_3}\left(t - \frac{2b\pi r^2}{Q_3}\right)^{-\frac{1}{2}}\right]\right.$$

Reproduced with permission of the copyright owner. Further reproduction prohibited without permission.

$$-\exp\left(\frac{n_a^2 D_2 R_2}{b^2}t\right)\operatorname{erfc}\left(\frac{r^2\pi n_a\sqrt{D_2R_2}}{Q_3}\left(t-\frac{2b\pi r^2}{Q_3}\right)^{-\frac{1}{2}}+\frac{n_a\sqrt{D_2R_2}}{b}\left(t-\frac{2b\pi r^2}{Q_3}\right)^{\frac{1}{2}}\right)\Bigg\}$$

(3.122)

$$L^{-1}\left(A_{L1}A_{L4}A_{L5}A_{L6}\right)=C_oU\left(t-\frac{2b\pi r^2}{Q_3}\right)\operatorname{erfc}\left[\left(\frac{r^2\pi n_a\sqrt{D_2R_2}}{Q_3}+\sqrt{\frac{R_2}{D_2}}\frac{z}{2}\right)\left(t-\frac{2b\pi r^2}{Q_3}\right)^{-\frac{1}{2}}\right]$$

$$-C_oU\left(t-\frac{2b\pi r^2}{Q_3}\right)\exp\left(\frac{n_aR_2}{b}z+\frac{n_a^2D_2R_2}{b^2}t\right)\operatorname{erfc}\left[\frac{n_a\sqrt{D_2R_2}}{b}\left(t-\frac{2b\pi r^2}{Q_3}\right)^{\frac{1}{2}}\right.$$

$$\left.+\left(\frac{r^2\pi n_a\sqrt{D_2R_2}}{Q_3}+\sqrt{\frac{R_2}{D_2}}\frac{z}{2}\right)\left(t-\frac{2b\pi r^2}{Q_3}\right)^{-\frac{1}{2}}\right]$$

(3.123)

Substituting Equations (3.55) and (3.122) into (3.118), and (3.60) - (3.62) and (3.123) into (3.119), respectively, the final solutions of Equations (3.87) and (3.88) can be expressed as follows:

For $t \le \dfrac{2\pi br^2}{Q_3}$

$$\frac{C_3}{C_o}=1-\exp\left(\frac{n_a^2D_2R_2}{b^2}t\right)\operatorname{erfc}\left(\frac{n_a\sqrt{D_2R_2}}{b}\sqrt{t}\right) \tag{3.124}$$

$$\frac{C_4}{C_o}=1-\exp\left(\frac{n_aR_2}{b^2}z+\frac{n_a^2D_2R_2}{b}t\right)\operatorname{erfc}\left(\frac{1}{2}\sqrt{\frac{R_2}{D_2}}\frac{z}{\sqrt{t}}+\frac{n_a\sqrt{D_2R_2}}{b}\sqrt{t}\right) \tag{3.125}$$

For $t > \dfrac{2\pi br^2}{Q_3}$

Reproduced with permission of the copyright owner. Further reproduction prohibited without permission.

$$\frac{C_3}{C_o} = \operatorname{erf}\left[\frac{\pi n_a\sqrt{D_2R_2}}{Q_3}r^2\left(t-\frac{2\pi b}{Q_3}r^2\right)^{-\frac{1}{2}}\right]+\exp\left(\frac{n_a^2D_2R_2}{b^2}t\right)\operatorname{erf}\left(\frac{n_a\sqrt{D_2R_2}}{b}\sqrt{t}\right)$$

$$-\exp\left(\frac{n_a^2D_2R_2}{b^2}t\right)\operatorname{erf}\left[\frac{\pi n_a\sqrt{D_2R_2}}{Q_3}r^2\left(t-\frac{2\pi b}{Q_3}r^2\right)^{-\frac{1}{2}}+\frac{n_a\sqrt{D_2R_2}}{b}\left(t-\frac{2\pi b}{Q_3}r^2\right)^{\frac{1}{2}}\right]$$

(3.126)

$$\frac{C_4}{C_o} = \operatorname{erf}\left[\left(\frac{\pi n_a\sqrt{D_2R_2}}{Q_3}r^2+z\sqrt{\frac{R_2}{D_2}}\right)\left(t-\frac{2\pi b}{Q_3}r^2\right)^{-\frac{1}{2}}\right]$$

$$+\exp\left(\frac{n_aR_2}{b}z+\frac{n_a^2D_2R_2}{b^2}t\right)\operatorname{erf}\left(\sqrt{\frac{R_2}{D_2}}\frac{z}{\sqrt{t}}+\frac{n_a\sqrt{D_2R_2}}{b}\sqrt{t}\right)$$

$$-\exp\left(\frac{n_aR_2}{b}z+\frac{n_a^2D_2R_2}{b^2}t\right)\operatorname{erf}\left[\left(\frac{\pi n_a\sqrt{D_2R_2}}{Q_3}r^2+z\sqrt{\frac{R_2}{D_2}}\right)\left(t-\frac{2\pi b}{Q_3}r^2\right)^{-\frac{1}{2}}\right.$$

$$\left.+\frac{n_a\sqrt{D_2R_2}}{b}\left(t-\frac{2\pi b}{Q_3}r^2\right)^{\frac{1}{2}}\right] \qquad (3.127)$$

or, in combined format as

$$\frac{C_3}{C_o} = 1-\exp\left(\frac{n_a^2D_2R_2}{b^2}t\right)\operatorname{erfc}\left(\frac{n_a\sqrt{D_2R_2}}{b}\sqrt{t}\right)$$

$$-U\left(t-\frac{2\pi br^2}{Q_3}\right)\operatorname{erfc}\left[\frac{\pi n_a\sqrt{D_2R_2}}{Q_3}r^2\left(t-\frac{2\pi b}{Q_3}r^2\right)^{-\frac{1}{2}}\right]$$

Reproduced with permission of the copyright owner. Further reproduction prohibited without permission.

$$-U\left(t-\frac{2\pi br^2}{Q_3}\right)\exp\left(\frac{n_a^2 D_2 R_2}{b^2}t\right)\operatorname{erfc}\left[\frac{\pi n_a\sqrt{D_2R_2}}{Q_3}r^2\left(t-\frac{2\pi b}{Q_3}r^2\right)^{-\frac{1}{2}}\right.$$

$$\left.+\frac{n_a\sqrt{D_2R_2}}{b}\left(t-\frac{2\pi b}{Q_3}r^2\right)^{\frac{1}{2}}\right] \qquad (3.128)$$

$$\frac{C_4}{C_o}=1-\exp\left(\frac{n_a R_2}{b^2}z+\frac{n_a^2 D_2 R_2}{b^2}t\right)\operatorname{erfc}\left(\sqrt{\frac{R_2}{D_2}}\frac{z}{\sqrt{t}}+\frac{n_a\sqrt{D_2R_2}}{b}\sqrt{t}\right)$$

$$-\left[U\left(t-\frac{2\pi br^2}{Q_3}\right)\right]\left\{\operatorname{erfc}\left[\left(\frac{\pi n_a\sqrt{D_2R_2}}{Q_3}r^2+z\sqrt{\frac{R_2}{D_2}}\right)\left(t-\frac{2\pi b}{Q_3}r^2\right)^{-\frac{1}{2}}\right]\right.$$

$$-\exp\left(\frac{n_a R_2}{b^2}z+\frac{n_a^2 D_2 R_2}{b^2}t\right)\operatorname{erfc}\left[\left(\frac{\pi n_a\sqrt{D_2R_2}}{Q_3}r^2+z\sqrt{\frac{R_2}{D_2}}\right)\left(t-\frac{2\pi b}{Q_3}r^2\right)^{-\frac{1}{2}}\right.$$

$$\left.\left.+\frac{n_a\sqrt{D_2R_2}}{b}\left(t-\frac{2\pi b}{Q_3}r^2\right)^{\frac{1}{2}}\right]\right\} \qquad (3.129)$$

As with the two dimensional analysis, these solutions contain exponential and error functions as indicated in Equations (3.124) to (3.129).

3.3 Remarks

1. Time Division Function

It can be seen that the concentration expressions given in Equations (3.65) through (3.68) are divided into two different time zones. The time division is not a constant, but rather a characteristic line:

Reproduced with permission of the copyright owner. Further reproduction prohibited without permission.

$$t = \frac{2bx}{Q_1} = \frac{x}{u_1} \qquad \text{or} \qquad x = tu_1 \tag{3.130}$$

The above equation describes the physical location of the introduced air front versus time. In Figure 3.8(a), the first time zone ($t \le x/u_1$) is above the line, while the second time zone ($t > x/u_1$) is below the line. For the two dimensional case, the characteristic line is a first order function since the velocity is constant.

However, for the axial symmetrical condition, it can be seen from Equations (3.124) through (3.126) that the time division is a high order function, since the velocity of the air in the discrete fracture is not constant but a function of the coordinate r. By the basic definition of the velocity

$$\frac{dr}{dt} = u_3 = \frac{Q_3}{4\pi br} \tag{3.131}$$

The above equation can be rewritten as

$$\frac{4\pi br}{Q_3} dr = dt \tag{3.132}$$

Integrating the above equation, yields

$$\int_0^r \frac{4\pi br}{Q_3} dr = \int_0^t dt \tag{3.133}$$

that is

$$t = \frac{2\pi br^2}{Q_3} \tag{3.134}$$

Based on the preceding derivation, it can be seen that the above equation describes the time-location relationship for induced air traveling along the discrete fracture. Although Equations (3.130) and (3.134) are in different forms mathematically, they have the same physical meaning for their respective situations.

Reproduced with permission of the copyright owner. Further reproduction prohibited without permission.

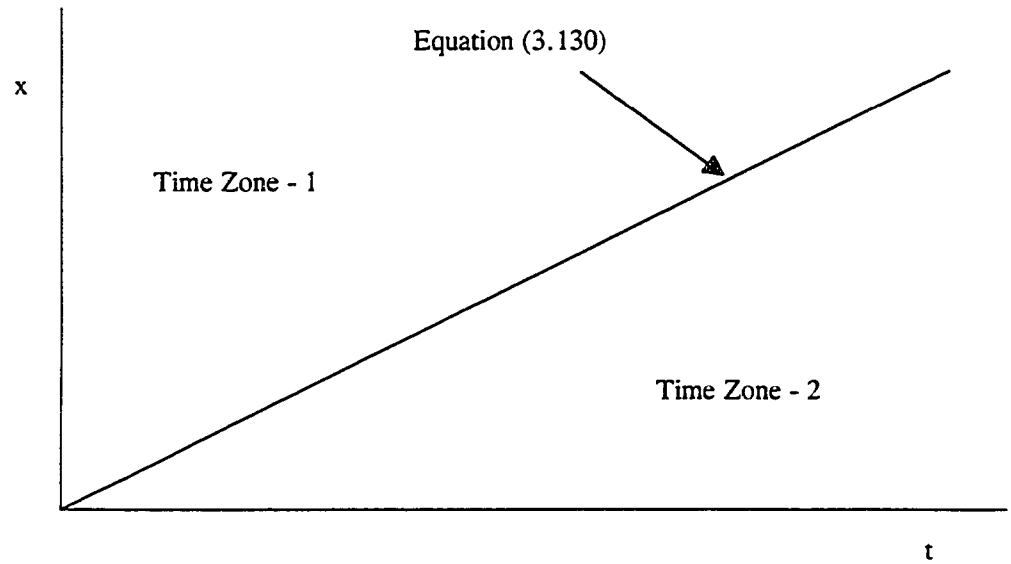

(a) Two Dimensional Analysis in Cartesian Coordinates

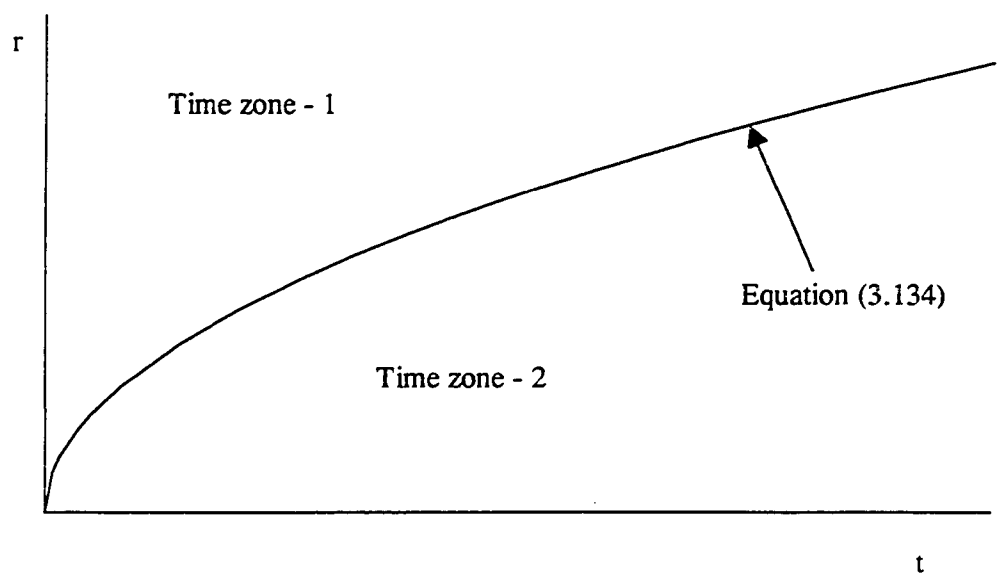

(b) Axial Symmetrical Analysis in Cylindrical Coordinates

Figure 3.8 Time Division Characteristic Line

Reproduced with permission of the copyright owner. Further reproduction prohibited without permission.

Figure 3.8(b) illustrates the frontal location of the introduced air in the axial symmetrical case. As expected, it is not a straight line but a curve. The first time zone ($t \le 2\pi br^2/Q_3$) is above the curve while the second time zone ($t > 2\pi br^2/Q_3$) is below the curve.

2. Mass Removal

Based on the effluent concentration, the total mass removal can be calculated by the following integration:

$$M_1 = Q_1 L_1 \int_0^t C_1 dt \qquad \text{(for two dimensional analysis)} \qquad (3.135)$$

$$M_3 = Q_3 \int_0^t C_3 dt \qquad \text{(for axial symmetrical analysis)} \qquad (3.136)$$

where L_1 is the width of the fracture area, C_1 and C_3 are expressed by Equations (3.69) and (3.127), respectively.

The mass removal results in the next three chapters are based on the above two numerical integrations. The parameters involved in the solutions, and their influence on the solutions, will be presented in Chapters 4 and 5, respectively.

Reproduced with permission of the copyright owner. Further reproduction prohibited without permission.

CHAPTER 4

PARAMETER EVALUATION

In order to apply the model and predict contaminant behavior by the pneumatic fracturing process, key physical and chemical parameters must be known *a priori* including: diffusion coefficient, retardation factor, fracture aperture, and extraction flow rate. In the present study, the aperture of the fracture and the extraction flow rate are measured in the field with monitoring devices. The diffusion coefficient and retardation factor are difficult to measure directly and, thus, the evaluations are based on published information. All four parameters are discussed in this chapter.

4.1 Diffusion Coefficient

Since diffusive transport plays an important role in remedial actions in soils, it is necessary to estimate the diffusion coefficient for contaminant removal analysis. The diffusion coefficient is defined as part of Fick's law which can be expressed as the follows:

$$q = -n_a D \frac{\partial C}{\partial x} \tag{4.1}$$

where

q ----the vapor diffusive flux

C ---concentration of chemical in the soil air

D ---diffusion coefficient in the soil matrix

n_a ---air filled porosity of the soil matrix

Reproduced with permission of the copyright owner. Further reproduction prohibited without permission.

Although the above equation appears to be rather simple, determination of the diffusion coefficient is difficult for porous formations. Since the presence of soil-solid and soil-water affects the diffusion process, the diffusion coefficient for interstitial soil-air should be smaller than that for unobstructed air due to the fact that: (a) diffusion area is decreased by the presence of soil particles; (b) the diffusion distance is increased since the diffusion pathway is not straight but tortuous; and (c) dead pores of the soil structure obstruct the diffusion pathways. The diffusion of gas or vapor through soils has received considerable study beginning with agricultural research. However, in spite of numerous studies, quantitative data on the diffusion coefficient are both limited and diverse. Moreover, the definition of the diffusion coefficient varies among the authors of different disciplines. Thus, an analysis of the diffusion coefficient based on available published data requires careful scrutiny.

There are a significant amount of experimental investigations on diffusion processes through porous media. In the beginning of this century, Buckingham (1904) measured CO_2 movement through four different kinds of soils with different states of compactness and moisture content. He found that porosity was the governing parameter and textures of soils had little influence on diffusion. Penman (1940a, 1940b) conducted an extensive experimental study on gaseous diffusion through various kinds of soils with different tracers. He found that the porosity was important. Currie (1960a, 1960b, 1961), who studied gas diffusion through both dry and wet granular materials, concluded that diffusion coefficients varied for different materials. Lai et al. (1976) conducted both laboratory and field experiments to study gas diffusion behavior. They found that it was difficult, if not impossible, to determine the influence of soil type on diffusion rate. Nielson et al. (1982) and Silker and Kalkwarf (1983) investigated radon

Reproduced with permission of the copyright owner. Further reproduction prohibited without permission.

diffusion experimentally. Their results were similar, and showed that increases in moisture content decreased diffusion rate.

The consensus of laboratory experimental studies on diffusion transport through porous media showed that the diffusion coefficient depends principally on porosity, moisture content, and soil type. However, the mathematical relationships between diffusion coefficient and these parameters differ widely among investigators.

Since natural soil structure is typically disturbed due to the packing efforts in laboratory experiments, a number of field evaluations have been carried out to avoid this artificial effect. Blake and Page (1948) conducted direct in situ measurements of gaseous diffusion in soils. Although their experiments were conducted in the field, the geometric scale was still small (about one foot) for field applications. Two other field scale experiments were conducted by Weeks et al. (1982) and Kreamer et al. (1988). Weeks et al. investigated vertical diffusion to 45m depth of below the ground surface. Kreamer et al. studied horizontal diffusion at a low-level nuclear waste disposal site.

Besides the laboratory and field studies, some investigators analyzed the diffusion problem using a theoretical approach. Marshall (1959) and Millington (1959) obtained different relationships between diffusion and porosity based on the theoretical pore size distribution. Millington and Shearer (1971) developed a mathematical formula to calculate the diffusion of aggregated porous solids. Youngquist (1979) analyzed various pore structure models and predicted diffusive rates through porous media. Nielson et al. (1984) developed a mathematical model for calculating radon diffusion coefficients. Saez et al. (1991) performed a theoretical analysis to predict effective diffusivities in porous media by using spatially periodic models.

Reproduced with permission of the copyright owner. Further reproduction prohibited without permission.

In order to present the influence of the water and solid of the porous medium separately from chemical properties, Carman (1956) first introduced the concept of the tortuosity (τ) which was initially defined as the ratio of straight length and the tortuous diffusive length. Tortuosity, therefore, describes the geometric character of the diffusive path. However, since it is difficult to know the real geometric structure in a soil, tortuosity cannot be determined precisely. On the other hand, the tortuosity corresponding to a geometric condition cannot be determined experimentally since it is very difficult, if not impossible, to distinguish geometric influence from other effects. Thus, it is impossible to determine tortuosity separately. Tortuosity has therefore been redefined in the current literature (e.g., Bear, 1979) to include the overall influence of the soil water and soil solid. The tortuosity used in this thesis is defined by following equation

$$D = \tau D_0 \tag{4.2}$$

where

τ ---- tortuosity

D_0 -- diffusion coefficient in the open air

Figure 4.1 shows the tortuosity data from published literature based on the definition of Equations (4.1) and (4.2). Theoretically, the tortuosity for a porous medium may range from zero to one. The lower and upper limits are for the two extreme boundary cases, i.e., zero air filled space and 100% air filled space, respectively. However, for engineering applications, the tortuosity realistically ranges from 0.1 to 0.7 for typical porosities and moisture contents.

It should be noted that the diffusion coefficient in the open air (D_0) is usually considered to be a chemical parameter which is independent of concentration in low concentration ranges. At high concentrations, however, D_0 is a function of

Reproduced with permission of the copyright owner. Further reproduction prohibited without permission.

concentration. Since most soil remediation situations involve low concentrations, D_0 will be assumed to be a parameter rather than a variable for the purposes of this study. Consequently, the diffusion coefficient in the soil matrix, D, is also a parameter rather than a concentration dependent function.

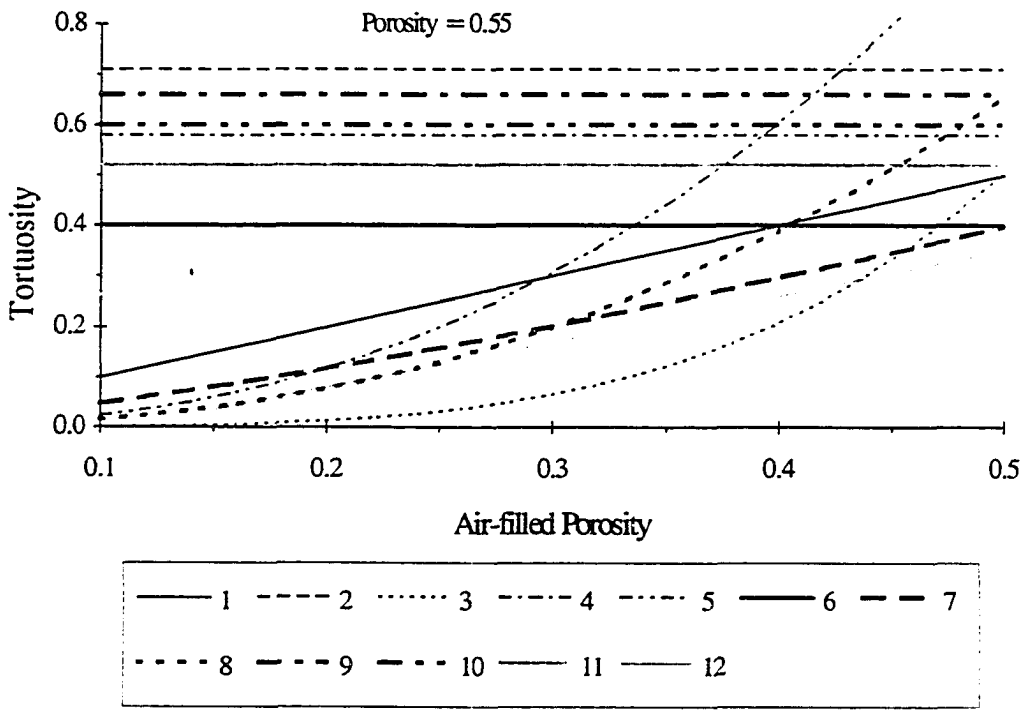

1 --- Buckingham (1904)
2 --- Carman (1956)
3 --- Currie (1960)
4 --- Dullien (1991)
5 --- Grable and Siemer (1968)
6 --- Kreamer et al. (1988)
7 --- Lai et al. (1976)
8 --- Millington (1959)
9 --- Penman (1940)
10 -- Van Bavel (1952)
11 -- Weeks et al. (1982)
12 -- Wesseling (1962)

Figure 4.1 Tortuosity Distribution

Reproduced with permission of the copyright owner. Further reproduction prohibited without permission.

4.2 Retardation Factor

When VOCs are released in a soil formation, they exist not only in a gaseous phase (by mixing with the soil air) but also in a liquid phase (dissolved in the soil water) and solid phase (sorbed by soil solid). For a contaminated site with a long history, the chemicals in the three phases can be considered to be in equilibrium. If the chemicals in gaseous phase are removed as with a vapor extraction system, the equilibrium condition becomes disturbed resulting in chemical transport among the three phases. Continuous vapor extraction will cause conversion of chemicals in liquid and solid phases into the gaseous phase for eventual removal from the formation. Since the amount of chemicals stored in the solid and liquid phases may be much larger than that in the gaseous phase, failure to account for sorption may result in a significant underestimation of the total mass of a contaminant at a site. Consequently, this will lead to underestimation of the time required for remediation. A parameter known as the retardation factor has been introduced to account for these phenomena (e.g., Bear, 1979).

In general, the retardation factor in a liquid-solid system is well defined, but its numerical value falls over a wide range. In unsaturated formations, however, evaluation of a gaseous-liquid-solid, three phase system is necessary. Unfortunately, discussion in the current literature on three phase systems is limited (for instance, Bedient et al., 1994; Dragun, 1988; Freeze and Cherry, 1979; Hemond, 1994), and to the best knowledge of the writer, the retardation factor for such systems has been typically assumed to be either unity, meaning that the retardation effect is not taken into consideration, or an arbitrary number for analytical discussion convenience (Chen, 1988; Tang, 1981). An evaluation of the retardation factor is fundamentally important and will be developed based on both physical and chemical characteristics.

Reproduced with permission of the copyright owner. Further reproduction prohibited without permission.

Since there is no standard definition of retardation factor for a three-phase system, and to avoid the confusion of different coefficients coming from different disciplines (e.g., chemistry, soil mechanics), it seems that the best approach is to start with the basic definition given in Equation (3.17):

$$R_2 = 1 + \frac{K_2}{n_a} \tag{3.17}$$

where

$$K_2 = \frac{dS_2}{dC_2} \tag{3.14}$$

Since R_2 and K_2 are independent of coordinate system, the subscript "2" is removed for general meaning. The following parameters are defined for current discussion purposes:

S----chemical sorbed by the soil water and the soil solid (weight of chemical per volume of soil formation)

C_A --chemical concentration in the soil air (weight of chemical per volume of air)

C_W --chemical concentration in the soil water (weight of chemical per volume of water)

C_S --chemical concentration in the soil solid (weight of chemical per volume of solid)

θ ----volumetric moisture content

n ----porosity

Based on the physical meaning of Equations (3.17) and (3.14), generally, we have

$$R = 1 + \frac{K}{n_a} \tag{4.3}$$

Reproduced with permission of the copyright owner. Further reproduction prohibited without permission.

$$K = \frac{dS}{dC_A} \tag{4.4}$$

Apparently, if the relationship between the sorption and the chemical concentration in the soil air can be established, it will be easy to obtain K, and furthermore, the retardation factor.

Consider a certain soil matrix with volume V. The total chemical stored in the soil water and soil solid of this volume can be calculated in two ways by using the total sorption (S) or the individual sorption $(C_W$ and $C_S)$ for water and solid, respectively. The results should be equal, i.e.,

$$SV = C_W \theta V + C_S (1-n) V \tag{4.5}$$

So the total sorption can be expressed as

$$S = C_W \theta + C_S (1-n) \tag{4.6}$$

Rewriting the above equation,

$$S = C_A \left[\theta \frac{C_W}{C_A} + (1-n) \frac{C_S}{C_A} \right] \tag{4.7}$$

where C_W/C_A is just the reciprocal of the Henry's constant (H), i.e.

$$\frac{C_W}{C_A} = \frac{1}{H} \tag{4.8}$$

It is important to notice that Henry's constant is a dimensional coefficient even though non-dimensional values are sometimes given in the references (e.g., Bedient et al, 1994). Those non-dimensional Henry's constants are not really dimensionless, but actually dimensional quantities with hidden units. The other term in Equation (4.7), C_S/C_A , is the solid-gas partition coefficient for which

Reproduced with permission of the copyright owner. Further reproduction prohibited without permission.

there are no data available in the current literature. Mathematically, this solid-gas partition coefficient can be rewritten as:

$$\frac{C_S}{C_A} = \frac{C_S}{C_W}\frac{C_W}{C_A} = \frac{1}{H}\frac{C_S}{C_W} \tag{4.9}$$

The partitioning of a chemical between liquid and solid phases in a porous medium as determined by laboratory experiments is commonly expressed in a graphical form. The graphical relation of sorption (S_s) versus concentration (C_W) is known as an isotherm. A linear sorption isotherm is described by the following equation

$$K_d = \frac{C_S}{C_W} \tag{4.10}$$

where K_d is the soil partitioning coefficient. Combining Equations (4.8) through (4.10) into (4.7) yields

$$S = C_A\left[\frac{\theta}{H} + (1-n)\frac{K_d}{H}\right] \tag{4.11}$$

Substituting Equation (4.11) into (4.4),

$$K = \frac{dS}{dC_A} = \frac{\theta}{H} + (1-n)\frac{K_d}{H} \tag{4.12}$$

Substituting Equation (4.12) into (4.3), the retardation factor is obtained as

$$R = 1 + \frac{\theta}{n_a}\frac{1}{H} + \frac{1-n}{n_a}\frac{K_d}{H} \tag{4.13}$$

In the above equation, the Henry's constant (H) is available from the standard works (e.g., Bedient et al, 1994). However, as in the case of the diffusion coefficients, the determination of K_d is not so simple since its value depends upon

Reproduced with permission of the copyright owner. Further reproduction prohibited without permission.

the properties of both chemical and soil. Data for K_d from laboratory experiments are scarce and scattered.

In a soil-solute system, the major part of soil sorption of VOCs is contributed by organic matter since the uptake by other soil constituents is considerably lower than that by organic matter. Karickhoff et al. (1979) proposed that the solute sorbed onto a solid is almost exclusively sorbed to the organic carbon fraction. They found a strong correlation between K_d and the organic carbon content of the sediment. The organic carbon partitioning coefficient, K_{oc} , is introduced as the normalization of the K_d

$$K_{oc} = \frac{K_d}{f_{oc}} \tag{4.14}$$

where f_{oc} is the organic carbon fraction. The relationship between the organic carbon fraction and the organic matter fraction (f_{om}) is normally assumed to be fixed as (Dragun, 1988):

$$f_{om} = 1.72 f_{oc} \tag{4.15}$$

K_d can also be normalized by f_{om} , i.e.,

$$K_{om} = \frac{K_d}{f_{om}} \tag{4.16}$$

where K_{om} is the organic partitioning coefficient. From the above three equations, we have

$$K_{oc} = 1.72 K_{om} \tag{4.17}$$

Both K_{oc} and K_{om} are considered to be dependent on chemical properties but independent of the soil organic content. A number of investigations have shown that K_{oc} and K_{om} are functions of solubility (S_o) of the chemical. Other studies

Reproduced with permission of the copyright owner. Further reproduction prohibited without permission.

relate K_{oc} and K_{om} to the octanol-water partition coefficient (K_{ow}). However, as shown in Tables 4.1 and 4.2, the quantitative relationships obtained by various investigators using different methods and chemical groups are different. Since the hidden unit used by different authors may not be the same, some mathematical manipulation is required to compare the results.

Combining Equation (4.13) with (4.14) and (4.16), respectively, we have

$$R = 1 + \frac{\theta}{n_a}\frac{1}{H} + \frac{1-n}{n_a}\frac{K_{oc}}{H} f_{oc} \tag{4.18}$$

and

$$R = 1 + \frac{\theta}{n_a}\frac{1}{H} + \frac{1-n}{n_a}\frac{K_{om}}{H} f_{om} \tag{4.19}$$

Table 4.1 Relationships between Organic Partitioning Coefficient (K_{om}) and Solubility (S_0)

Investigator(s)	Formula	Chemical Group
Chiou et al. (1979)	$\log K_{om} = 4.04 - 0.557 \log S_0$ (S_0 in μmol/L)	Chlorinated hydrocarbons
Karickhoff et al. (1979, 1981)	$\log K_{om} = 0.21 - 0.54 \log S_0$ $\log K_{om} = -0.43 - 0.594 \log S_0$ (S_0 in mol fraction)	Aromatic hydrocarbons and chlorinated hydrocarbons
Kenaga and Goring (1980)	$\log K_{om} = 3.4 - 0.55 \log S_0$ $\log S_0 = 4.78 - 1.28 \log K_{om}$ (S_0 in ppm)	Pesticides
Means et al. (1980)	$\log K_{om} = 3.8 - 0.82 \log S_0$ (S_0 in mg/L)	Polynuclear aromatic hydrocarbons

Reproduced with permission of the copyright owner. Further reproduction prohibited without permission.

Introducing

$$R_W = \frac{\theta}{n_a}\frac{1}{H} \tag{4.20}$$

$$R_S = \frac{1-n}{n_a}\frac{K_d}{H} = \frac{1-n}{n_a}\frac{K_{oc}}{H}f_{oc} = \frac{1-n}{n_a}\frac{K_{om}}{H}f_{om} \tag{4.21}$$

where the water retardation factor (R_W) and solid retardation factor (R_S) represent the retardation effects caused by the soil water and the soil solid sorptions, respectively. The above two equations can be rewritten as

Table 4.2 Relationships between Organic Partitioning Coefficient (K_{om}) and Octanol-Water Partitioning Coefficient (K_{ow})

Investigator(s)	Formula	Chemical Group
Briggs (1981)	$\log K_{om} = 0.52 \log K_{ow} + 0.64$	Pesticides
Brown et al. (1981)	$\log K_{om} = 0.937 \log K_{ow} - 0.22$	Dinitroaniline herbicides
Karickhoff et al. (1979, 1981)	$\log K_{om} = \log K_{ow} - 0.45$ (or $K_{om} = 0.35 K_{ow}$) $\log K_{om} = 0.989 \log K_{ow} - 0.58$	Aromatic or polynuclear aromatics
Kenaga and Goring (1980)	$\log K_{om} = 0.554 \log K_{ow} + 1.14$ $\log K_{ow} = 1.358 \log K_{om} - 0.749$	Pesticides
Means et al. (1980)	$\log K_{om} = \log K_{ow} - 0.55$ (or $K_{om} = 0.28 K_{ow}$)	Polynuclear aromatic hydrocarbons
Rao and Davidson (1980)	$\log K_{om} = 1.03 \log K_{ow} - 0.42$	Insecticides, herbicides, and fungicides
Schwarzenbach and Westall (1981)	$\log K_{om} = 0.72 \log K_{ow} + 0.25$	Non polar organic compounds

Reproduced with permission of the copyright owner. Further reproduction prohibited without permission.

$$R_w = \frac{(\theta/n)}{1-(\theta/n)} \frac{1}{H} \tag{4.22}$$

$$R_S = \frac{(1/n)-1}{1-(\theta/n)} \frac{K_d}{H} \tag{4.23}$$

where (θ/n) is defined as water saturation. The above two equations indicate that solid sorption is more complex than water sorption. From the soil property point of view, water sorption is related to water saturation only, while solid sorption is a function of both water saturation and porosity. From the perspective of chemical property, water sorption is related to Henry's constant only, while the solid sorption depends on both Henry's constant and soil partitioning coefficient.

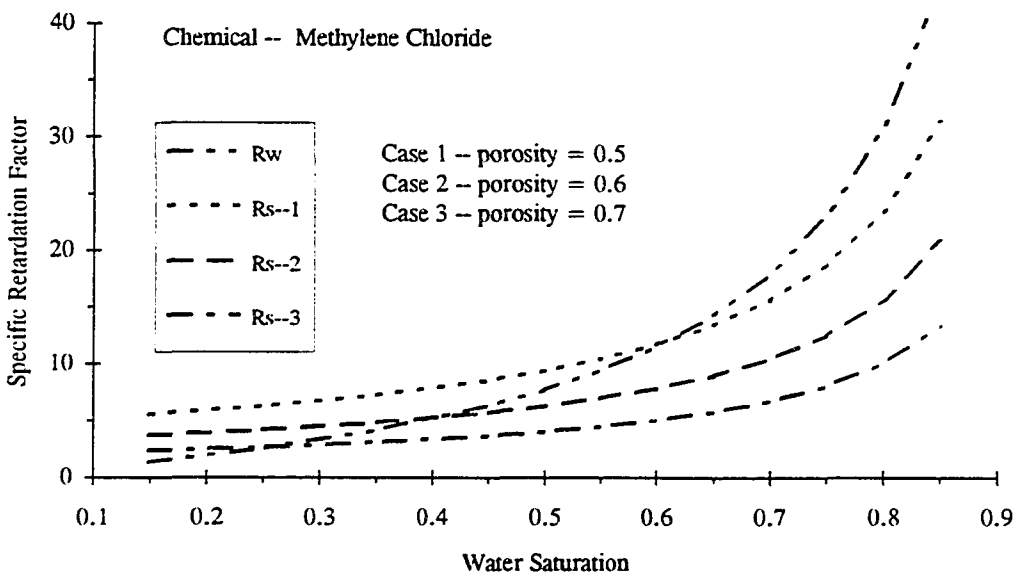

Figure 4.2 Specific Retardation Factors of Soil Water and Solid

Figure 4.2 illustrates the distributions of R_w and R_S versus water saturation for different porosities. Apparently, for the three different cases shown, there is

Reproduced with permission of the copyright owner. Further reproduction prohibited without permission.

only one R_W curve since it is function of water saturation only. Meanwhile, there is a R_S curve for each of the three porosities, since R_S depends on both water saturation and porosity. It can be seen that the specific retardation factors increase with water saturation for both R_W and R_S.

Substituting Equations (4.22) and (4.23) into (4.19), we have

$$R = 1 + R_W + R_S \tag{4.24}$$

Figure 4.3 illustrates the retardation factor distribution versus water saturation for same three porosities. It can be seen that retardation factor increases rapidly when water saturation increases to more than 70%. It should be pointed out that in the case where there is no sorption effect for both the soil water and soil solid (i.e., $R_W = 0$ and $R_S = 0$), the retardation factor is not zero but one.

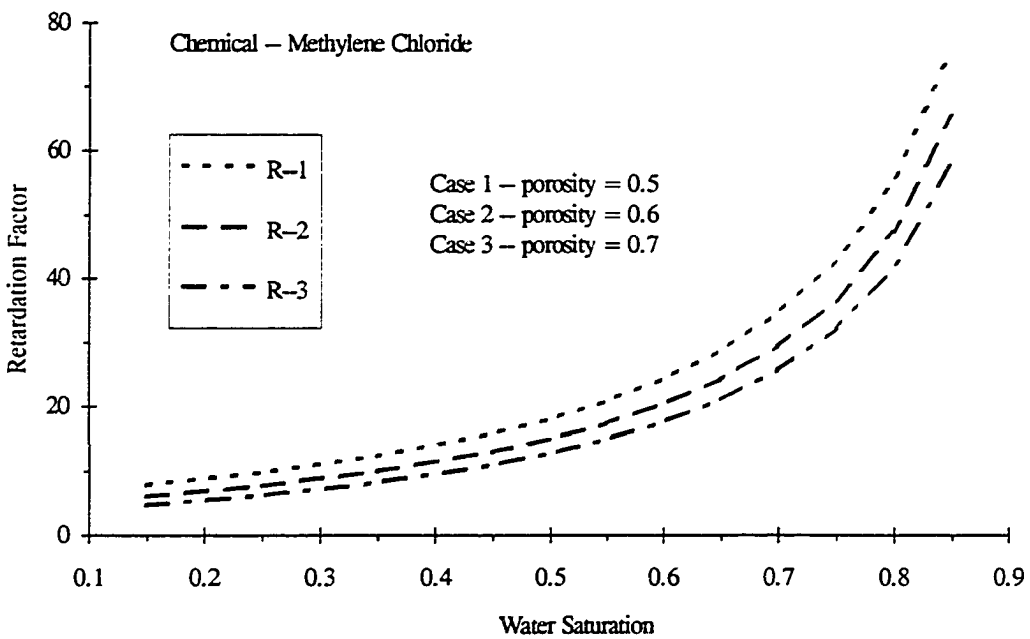

Figure 4.3 Retardation Factor Distribution

Reproduced with permission of the copyright owner. Further reproduction prohibited without permission.

4.3 Aperture of Fracture

The pneumatic fracturing process creates open, self-propped fractures in geologic formations. The aperture of the fracture is defined as the distance between surfaces of fracture. Aperture is determined by a two step procedure. First, the tilt of the ground surface is measured with electronic sensors. Second, the tilt data are converted to the ground surface heave by numerical simulation with a computer. Both of these steps will now be described.

4.3.1 Tilt Measurement

Model 700-series biaxial platform tiltmeters, manufactured by Applied Geomechanics, are used to measure the tilt distribution on the ground surface during and after a fracture injection. The precision electrolytic transducer inside the tiltmeter is capable of detecting minute angular motion. The transducer operates on the fundamental principle that a bubble, suspended in a liquid-filled case, is always bisected by the vertical gravity vector. As the transducer tilts, the case moves around the bubble, linearly changing the electrical resistance measured through the electrolyte. Each tiltmeter can measure two components of a tilt (X and Y). The resolution of the tiltmeters used in this project is 0.1 microradians.

Tiltmeters have been widely used in construction monitoring, structural testing, bridge inspection and maintenance, and ground surface deformation detection (Tofani and Horath, 1990). However, in many previous uses, the goal of measurement was the tilt itself which is the direct output of the tiltmeter. When applying the technique to the pneumatic fracturing process, the tilt data must be converted into vertical displacement or heave. Thus, a large number of tiltmeters (see Figure 4.4) is needed to define ground surface deformation

Reproduced with permission of the copyright owner. Further reproduction prohibited without permission.

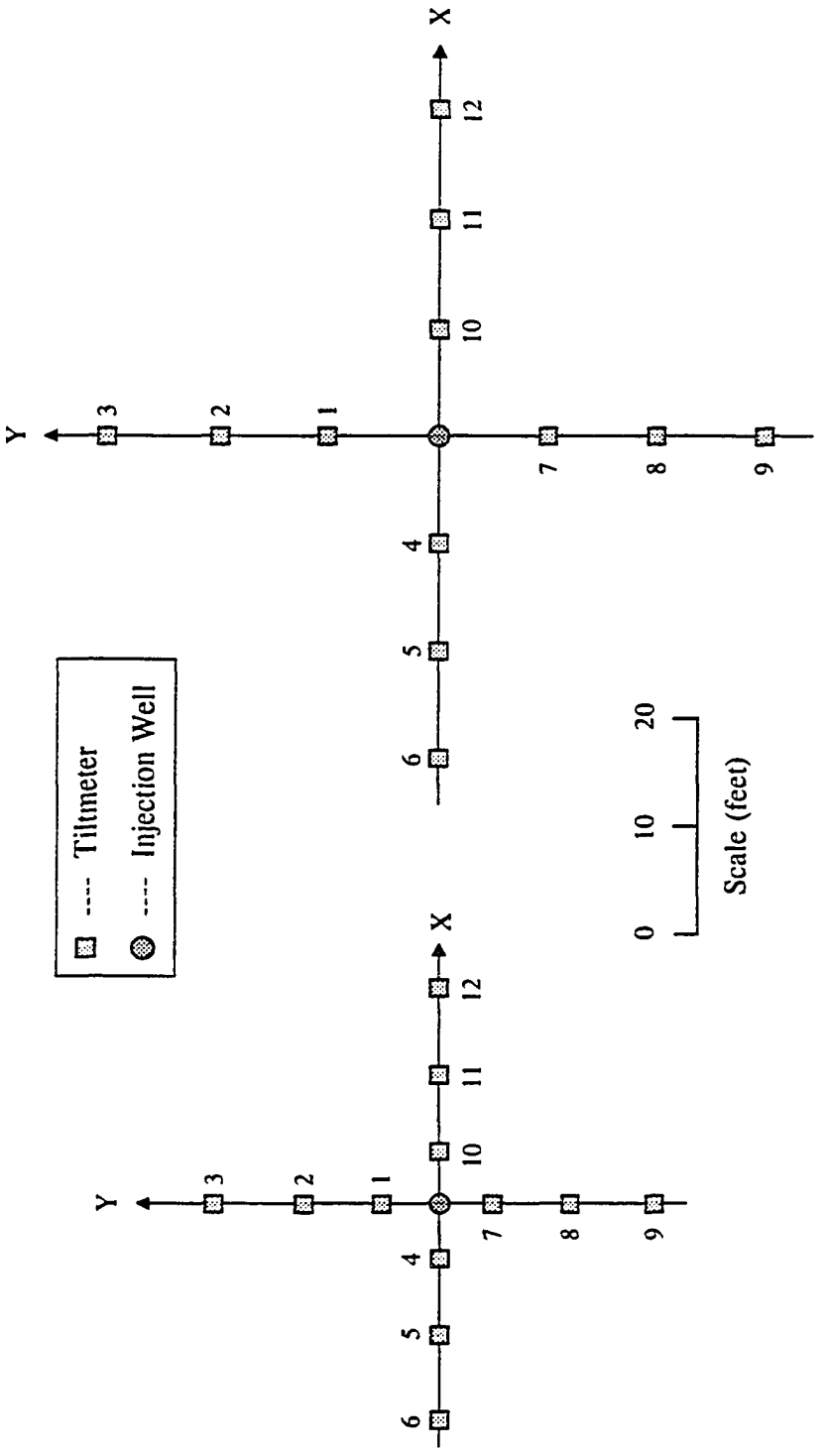

(a) Fracturing Injection at 7 - 9 ft

(b) Fracturing Injection at 18 - 20 ft

Figure 4.4 Tiltmeter Array

Reproduced with permission of the copyright owner. Further reproduction prohibited without permission.

accurately. In reality, purchase cost limits the number of tiltmeters which can be used. Field demonstrations of pneumatic fracturing have utilized 12 tiltmeters positioned at various locations around the fracture injection well.

The spacing between each tiltmeter and the fracturing injection well depends on the formation geology and fracturing depth. In soil formations, the tiltmeters are spaced more closely than in rock formations, since soils are plastic and deform more locally. Also, the influence area of fractures initiated at shallow depths is smaller than deeper fractures, owing to the lower bending stiffness of the formation. Figure 4.4 illustrates the two cases of tiltmeter setup used at the south tank site on Tinker Air Force Base. Layout (a) was for fracture injections made at a depth of 7 to 9 ft, while layout (b) was for a depth of 18 to 20 ft. As indicated, farthest tiltmeter is 20 ft from the injection well for the shallow injections and 30 ft for the deeper injections. Generally speaking, the tiltmeter array could be arranged in any number of ways based on the field conditions and expected directions of fracturing development. However, the X-Y cross array of tiltmeters adopted here has a very convenient feature: the Y components of the tiltmeters along with y axis (tiltmeters No. 1, 2, 3, 7, 8, and 9 in Figure 4.4) and the X components of tiltmeters along with x axis (tiltmeters No. 4, 5, 6, 10, 11, and 12 in Figure 4.4) present the radius tilts, while the X components of tiltmeters along with y axis and the Y components along with x axis present the tangential tilt. With this arrangement of tiltmeters, it is easy to examine the symmetric characteristics of a fracture simply by observing the tilt data, as will be shown later.

24 tilt measurements (each tiltmeter records an X and Y component) are collected for every half second through a computer controlled electronic data acquisition system. Figures 4.5 and 4.6 illustrate the radius and tangential

Reproduced with permission of the copyright owner. Further reproduction prohibited without permission.

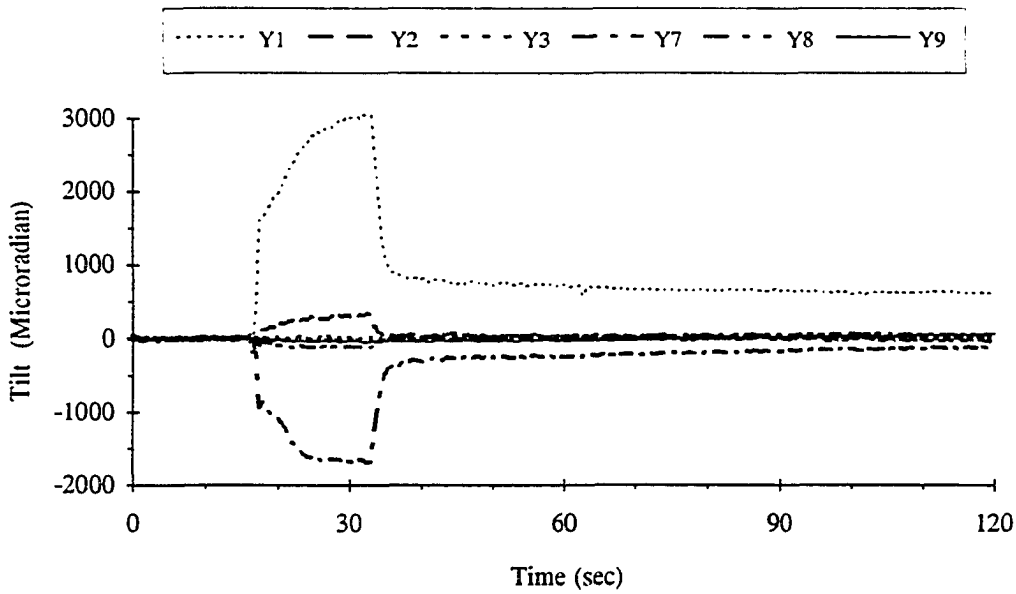

(a) Y Direction

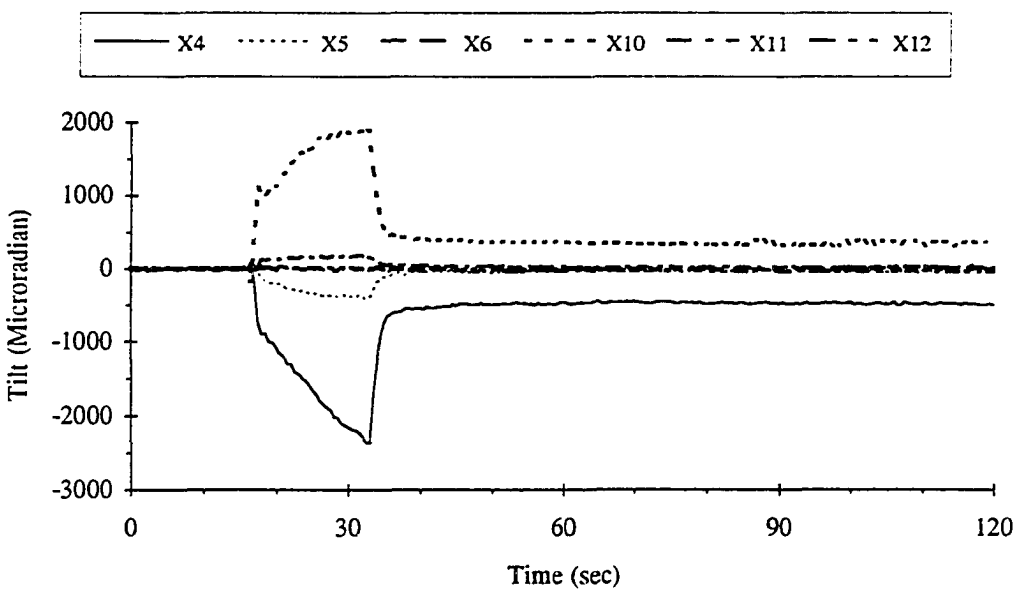

(b) X Direction

Figure 4.5 Radius Components of Tilt Data from Frelinghuysen Township Site, NJ

Reproduced with permission of the copyright owner. Further reproduction prohibited without permission.

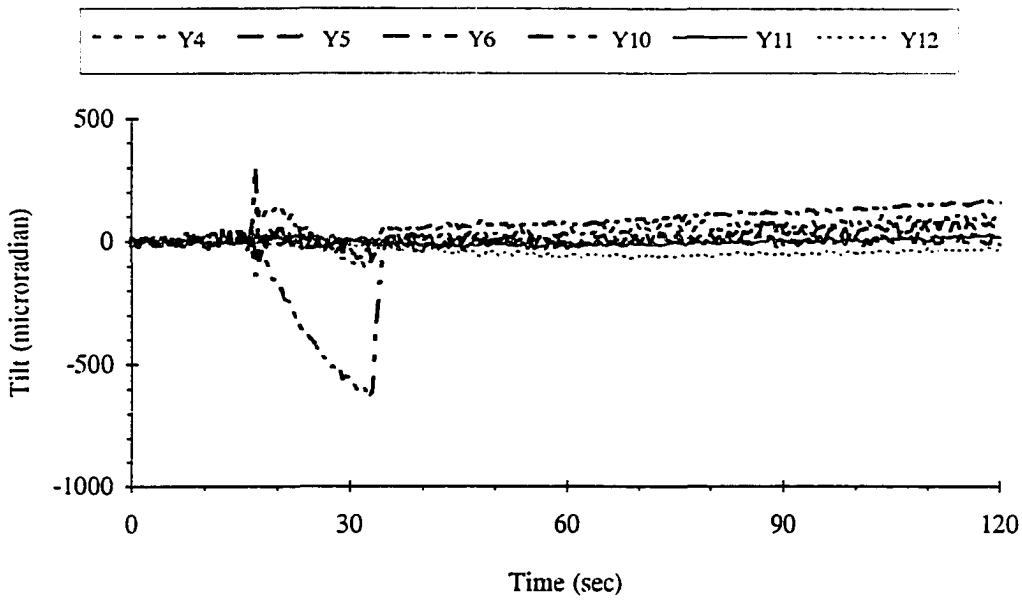

(a) Y Direction

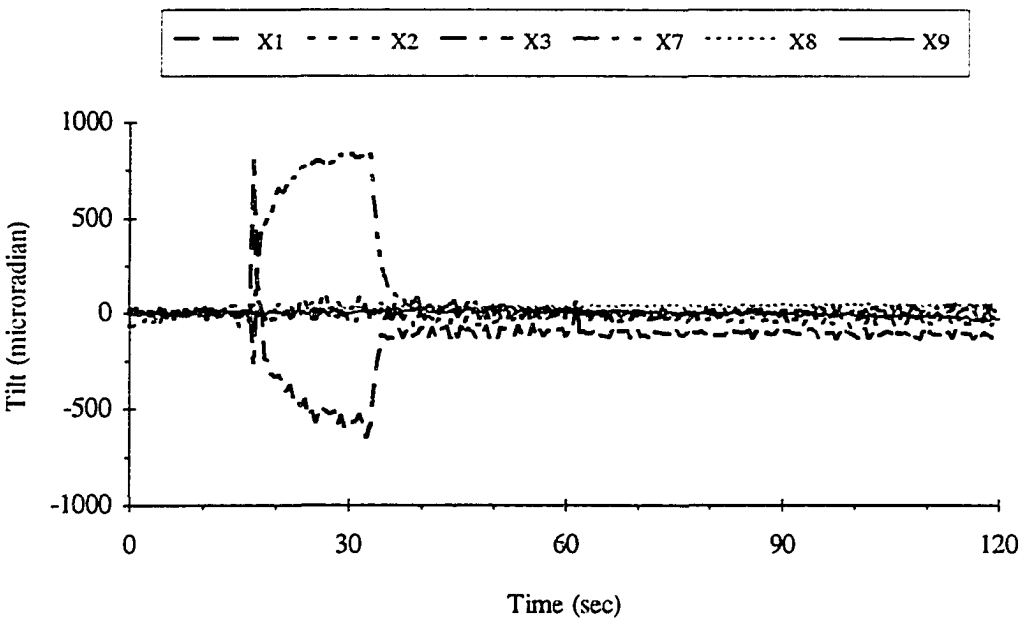

(b) X Direction

Figure 4.6 Tangential Components from Frelinghuysen Township Site, NJ

Reproduced with permission of the copyright owner. Further reproduction prohibited without permission.

components of tilt data from the Frelinghuysen Township site. The tiltmeter array is the same as shown in Figure 4.4(a). It can be seen that the tilt develops rapidly at the beginning of injection and decays towards the end of injection to some steady value which is greater than the initial condition (zero tilt). This confirms that when the fracture injection is shut off, the fracture does not totally close but actually maintains a measurable aperture. Among the 24 tilt components, only 11 sensed tilt and all other components have zero reading. The zero reading for components X2-3, Y4-6, X8-9, and Y11-12 indicate that the tangential tilts at these locations are all zero, which results in a somewhat symmetrical tilt distribution around the fracture injection well. Meanwhile, the zero reading for components X-Y3, X-Y6, X-Y9, and X-Y12 show that the farthest tiltmeter location was not disturbed, i.e., the fracturing radius for this injection was smaller than 20 ft. In general, the responding tiltmeters showed axial symmetric behavior which was expected since the geologic formation was quite uniform. Non-symmetric tilt behavior is observed in non-uniform formations or when fracturing is conducted in the vicinity of structure foundations.

4.3.2 Ground Surface Heave

Using data from the 12 tiltmeters for a selected time, a surface heave contour can be generated through a computer simulation known as "invert". By choosing a series of consecutive times, a time history of the ground surface heave may be obtained. Figures 4.7 through 4.9 shows the time development of the surface heave contours during the injection, as well as the residual heave after termination of the injection. It is noted that these results represent ground surface heave and are not a direct measurement for the fracture aperture under the ground.

Reproduced with permission of the copyright owner. Further reproduction prohibited without permission.

Heave Unit: Inches
Coordinates of Fracture Well: (20,20)
Site: Frelinghuysen Township, NJ

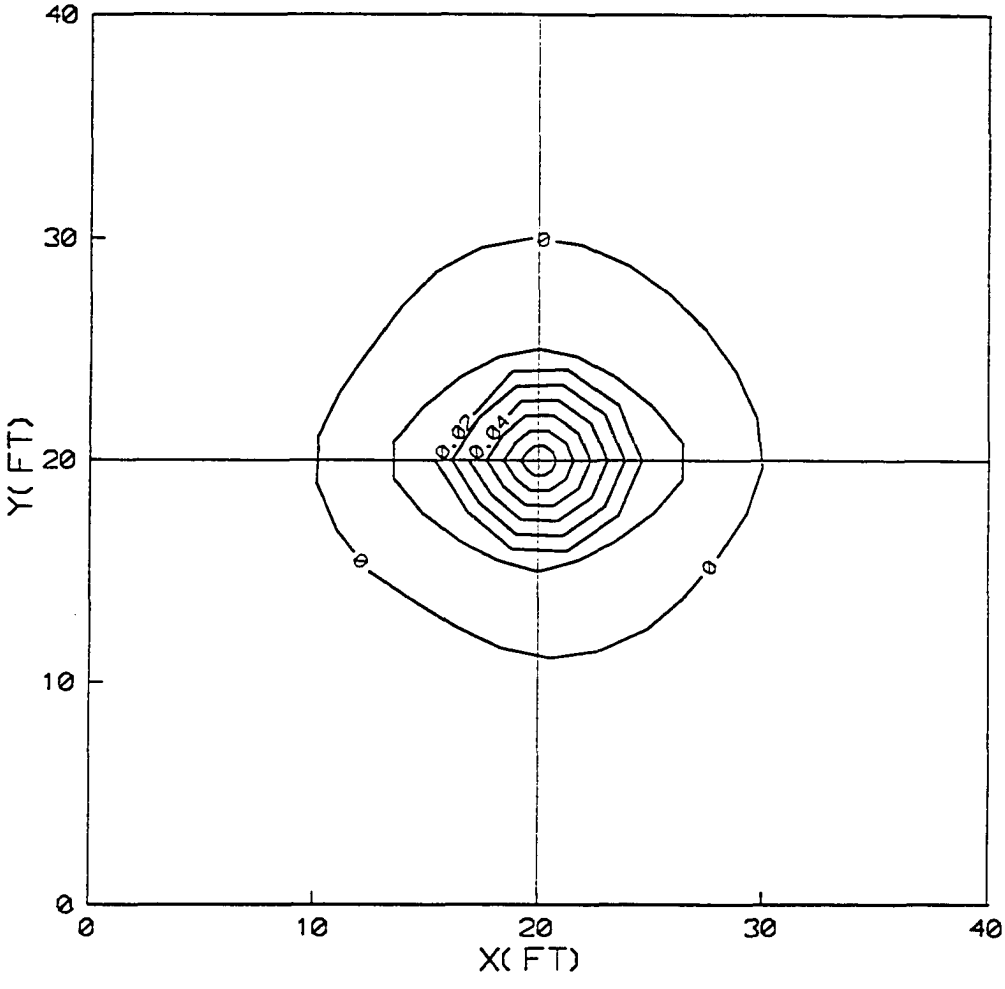

Figure 4.7 Heave Contour for Ground Surface
(Time = 2 sec)

Reproduced with permission of the copyright owner. Further reproduction prohibited without permission.

Heave Unit: Inches
Coordinates of Fracture Well: (20,20)
Site: Frelinghuysen Township, NJ

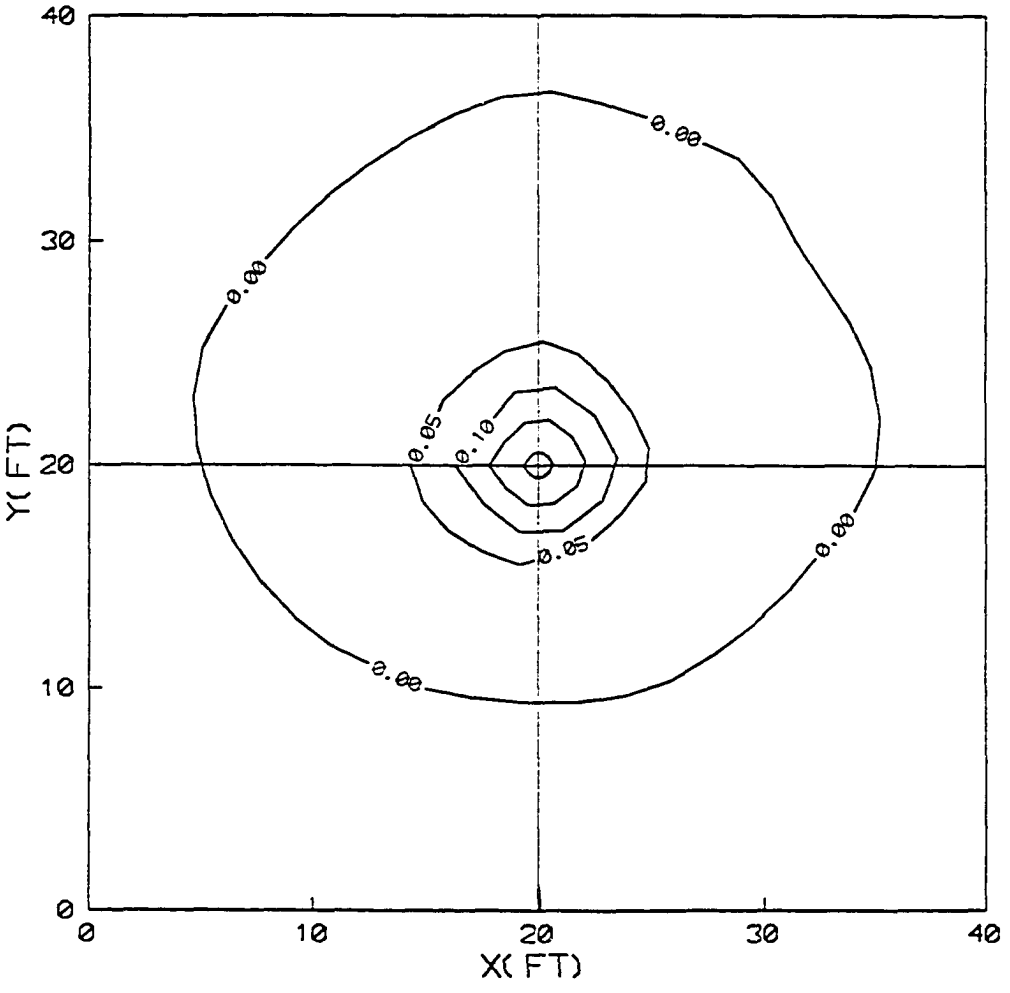

Figure 4.8 Heave Contour for Ground Surface
(Time = 16 sec)

Reproduced with permission of the copyright owner. Further reproduction prohibited without permission.

Heave Unit: Inches
Coordinates of Fracture Well: (20,20)
Site: Frelinghuysen Township, NJ

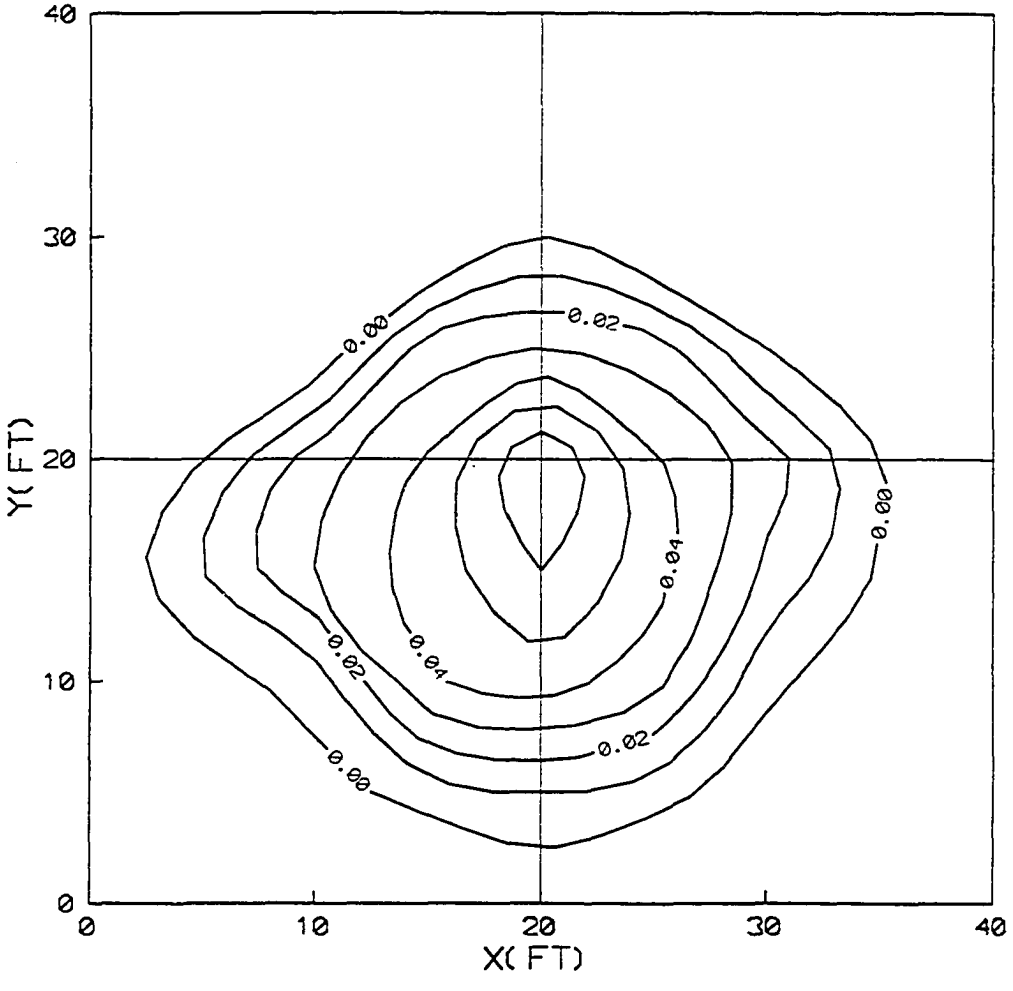

Figure 4.9 Heave Contour for Ground Surface
(Time = 5 min)

Reproduced with permission of the copyright owner. Further reproduction prohibited without permission.

However, heave data obtained from tiltmeters are conservative estimations of aperture, since the real aperture will be equal to or greater than the observed ground surface heave. As indicated in Figures 4.8 and 4.9, the typical maximum heave during a fracture injection is about 0.5 inches, while the residual heave is around 0.1 inches. The aperture used in the present model analysis is the residual heave.

4.4 Flow Rate of Extraction

Since the primary objective of pneumatic fracturing process is to increase the permeability of the geologic formation, the flow rate, induced by soil vapor extraction, becomes an important indicator of process effectiveness. It is important to measure the flow rates both before and after a fracture injection to evaluate the effects of fracturing. Generally speaking, the larger the post-fracture flow rate, the more effective the fracturing. Typical flow increases have ranged from a few times to more than 1000 times at various sites. Since the flow rates for pre- and post-fracture are often in different magnitudes, a versatile measuring system is required. The flow measurement system shown in Figure 4.10 has been custom fabricated for the pneumatic fracturing project. It includes pitot tubes, magnehelics, manometers and an electronic flow meter. The system is capable of measurements over four orders of magnitude, and all ranges are measured redundantly by more than one device.

Reproduced with permission of the copyright owner. Further reproduction prohibited without permission.

Reproduced with permission of the copyright owner. Further reproduction prohibited without permission.

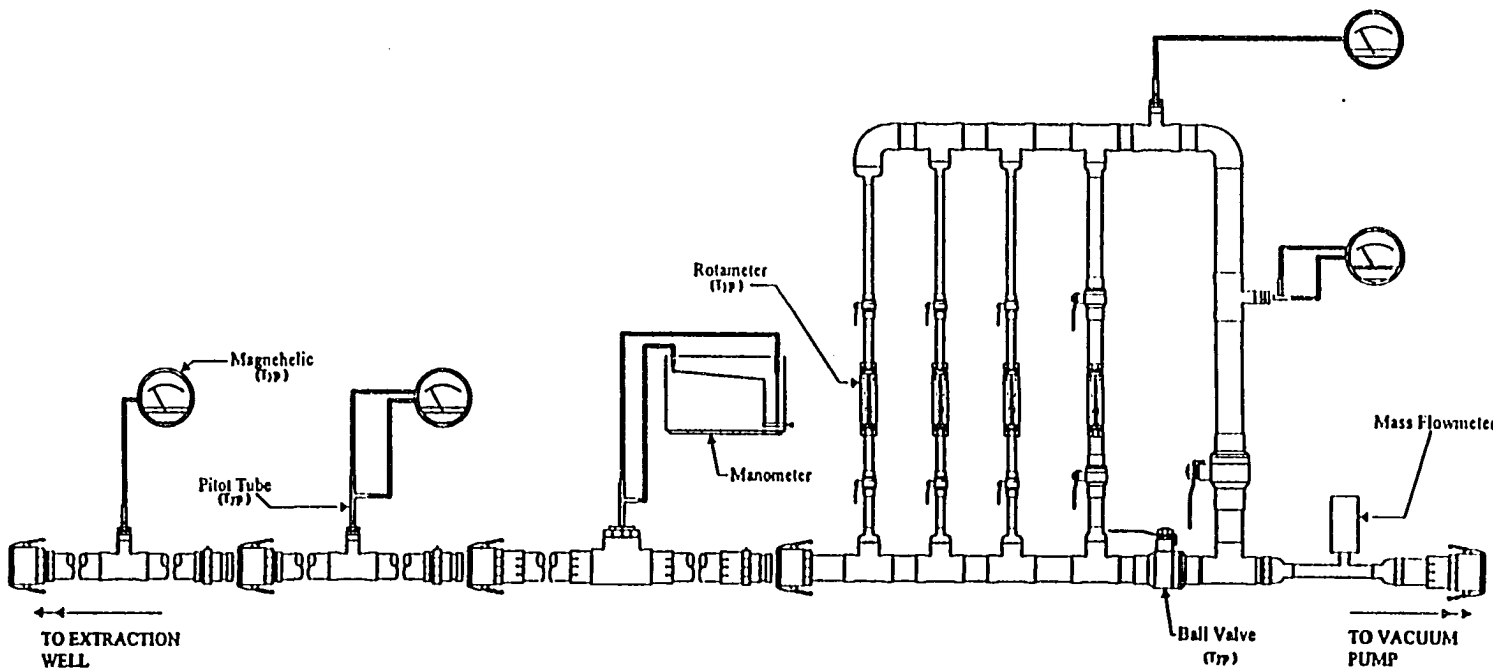

Figure 4.10 Flow Measurement System

CHAPTER 5

A STATISTICAL EVALUATION OF MASS REMOVAL

In general, a contaminated geologic medium is a very complex system, and description of its exact behavior requires many physical and chemical parameters. In addition, soil formations are not spatially homogeneous and field conditions change with time. These variations introduce a degree of uncertainty in contaminant removal predictions, and raise questions such as: What is the statistical reliability of the input parameters from either measurements or previous published data? How sensitive is the solution for a different set of input parameters? Since some of the parameters required for solution of the model are either highly variable or difficult to determine exactly, a statistical evaluation of the influence of the input data on the mass removal is essential to answer these questions.

The direct input parameters for Equations (3.128) and (3.135) include diffusion coefficient, retardation factor, fracture aperture, and extraction flow rate. In this chapter, the influence of these four parameters on this model solution will be analyzed individually. The end objective is to evaluate the behavior of the mean and standard deviation of mass removal for a probabilistic set of input parameters.

5.1 Diffusion Coefficient

It can be seen from Equation (4.2) that the uncertainty of the diffusion coefficient (D) of a chemical in a porous matrix may come from two sources: the diffusion coefficient (D_0) for open air and the tortuosity (τ) of the porous formation.

Reproduced with permission of the copyright owner. Further reproduction prohibited without permission.

Usually, the numerical value for diffusion coefficient of open air is relatively stable and can be determined accurately, while the tortuosity may change frequently due to the soil heterogeneity. Therefore, the statistical evaluation for diffusion coefficient will focus on the statistical behavior of tortuosity. Since the in situ measurement of tortuosity for each site is very difficult to perform, the determination of tortuosity is based on the published data which may not exactly reflect the particular field condition. Given this situation, a statistical evaluation will help to assess the uncertainty introduced by tortuosity variations.

To evaluate the statistical response of mass removal to tortuosity, five sets of tortuosity data with normal probability distributions were chosen. Figure 5.1 illustrates one sample set with a normalized standard deviation of 50%.

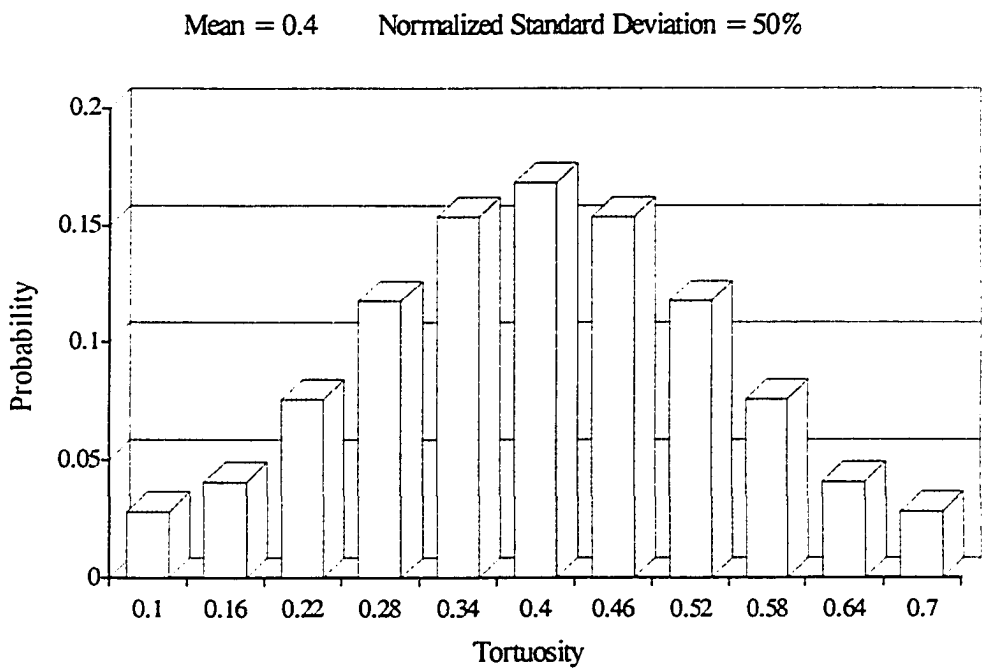

Figure 5.1 Probability Distribution of Tortuosity

Reproduced with permission of the copyright owner. Further reproduction prohibited without permission.

Tortuosity values were chosen in the range from 0.1 to 0.7 based on the discussion in Section 4.1. The mean values of tortuosity remain constant at 0.4 for each set analyzed, although the probability distribution changes for each value of standard deviation which range from 0.04 to 0.2. The normalized standard deviations, defined as the ratio of standard deviation and mean value, are 10%, 20%, 30%, 40%, and 50% for the five cases, respectively.

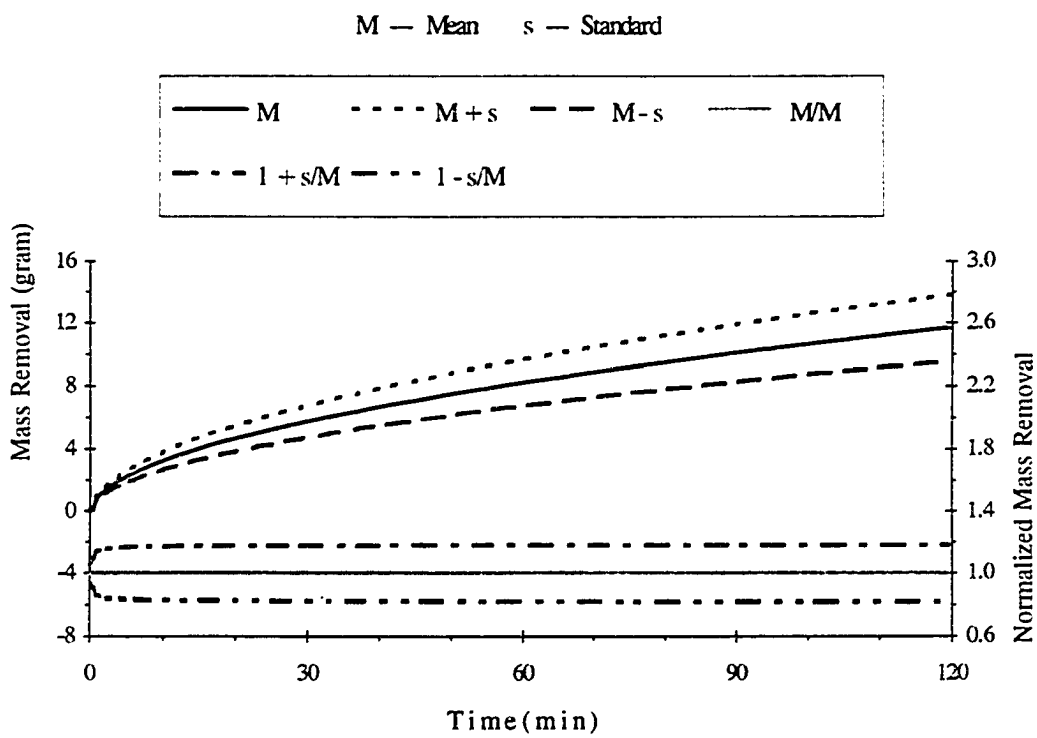

Figure 5.2 Statistical Behavior of Mass Removal with Respect to Tortuosity

Based on these tortuosity distributions, the mass removal is calculated for each individual tortuosity value. The statistical behavior of mass removal including mean and standard deviation are obtained for all five cases. Figure 5.2

Reproduced with permission of the copyright owner. Further reproduction prohibited without permission.

shows the results based on the tortuosity distribution with 50% normalized standard deviation. Double vertical axes are used to illustrate properties of both standard deviation and normalized standard deviation simultaneously, since they are in two different scales. The upper three curves are based on the left vertical axis. The solid curve represents the mean value for mass removal, while the dot and dash curves define the first confidence range extending from [mean - standard deviation] to [mean + standard deviation]. It can be seen that the standard deviation increases when the mass removal itself increases with time.

However, the normalized standard deviation, characterized by the lower three curves based on the right vertical axis, is almost constant except for the initial period (less than 20 minutes). The heavy line at unity represents the mass removal normalized by itself. The single dash and double dash curves define the normalized first confidence range extending from [1 - normalized standard deviation] to [1 + normalized standard deviation]. It can be seen that the normalized standard deviation is stabilized to 18% in this case. The fact that the normalized standard deviation of mass removal is smaller than that of tortuosity means the mass removal data have less uncertainty than tortuosity. This phenomenon may also be observed directly from Figure 5.3, which compares the normalized distributions of tortuosity and mass removal directly. As indicated, normalized distribution of mass removal is narrower than that of tortuosity.

To illustrate the behavior of mass removal subject to different tortuosities more explicitly, Figure 5.4 presents four mass removal distributions along with their normalization by mean value for four tortuosities ranging from 0.18 to 0.57. It can be seen that the mass removal values increase and become more diverse with increasing time, while the normalized mass removal curves tend towards a steady state and become parallel to one another. A comparison of Figure 5.2 with

Reproduced with permission of the copyright owner. Further reproduction prohibited without permission.

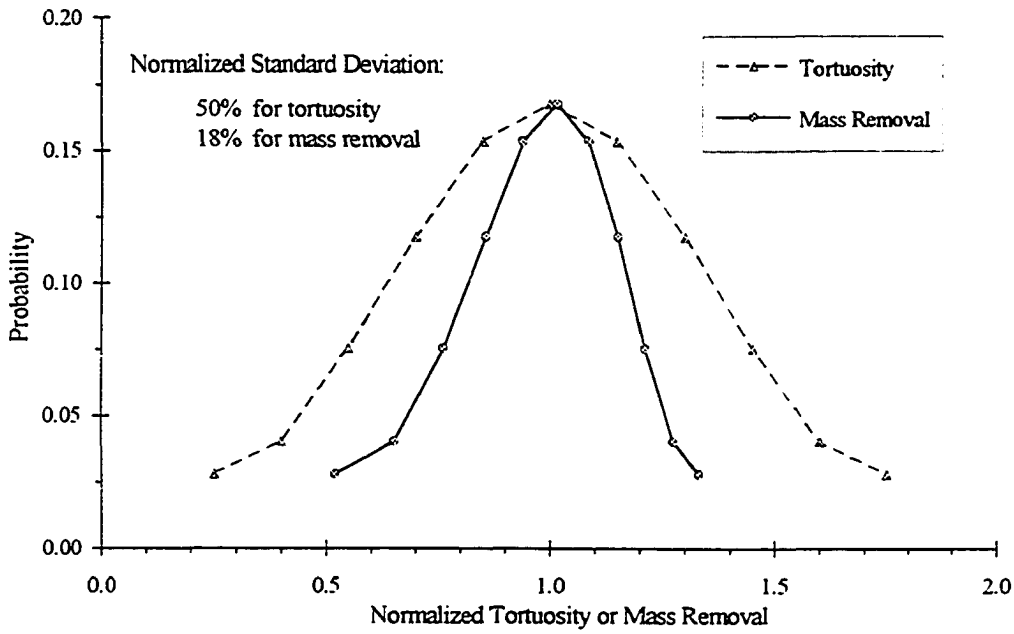

Figure 5.3 A Comparison of Tortuosity and Mass Removal Distributions

5.4 actually illustrates the reason why the standard deviation of mass removal increases with mass removal, while the normalized standard deviation does not. The larger the tortuosity, the larger diffusion coefficient which means the faster diffusive transport. Therefore, larger tortuosity values will result in larger mass removal rates and faster remediation. It should be noted that the removal rate for various chemicals may be different when multiple compounds are present. Under these conditions, the chemical with the smallest diffusion coefficient will likely control the remedial time.

The summary of the relationship of normalized standard deviations between tortuosity and mass removal is illustrated in Table 5.1 and Figure 5.5. A linear regression is obtained for the five numerical samples with a correlation of 0.999. The slope of the regression equation is 0.35 which means that the normalized

Reproduced with permission of the copyright owner. Further reproduction prohibited without permission.

standard deviation for mass removal is 35% of that for tortuosity based on the given tortuosity values.

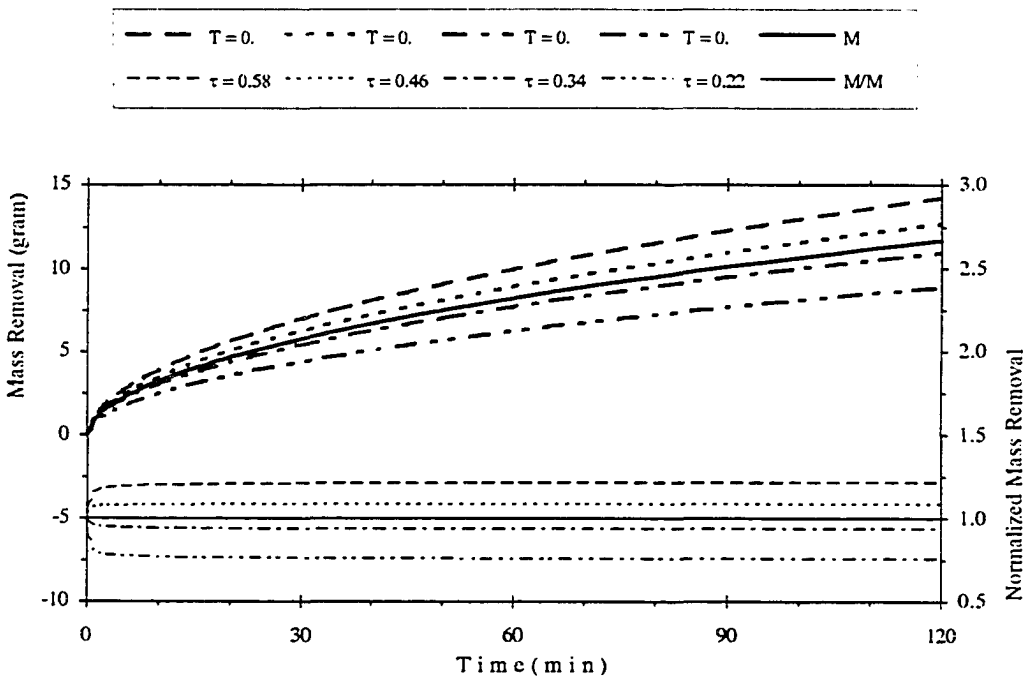

Figure 5.4 Mass Removal Distributions with Respect to Four Tortuosities

Table 5.1 Relationship of Normalized Standard Deviations between Tortuosity and Mass Removal

Normalized Standard Deviation of Tortuosity	Normalized Standard Deviation of Mass Removal
0.1	0.04
0.2	0.07
0.3	0.11
0.4	0.15
0.5	0.18

Reproduced with permission of the copyright owner. Further reproduction prohibited without permission.

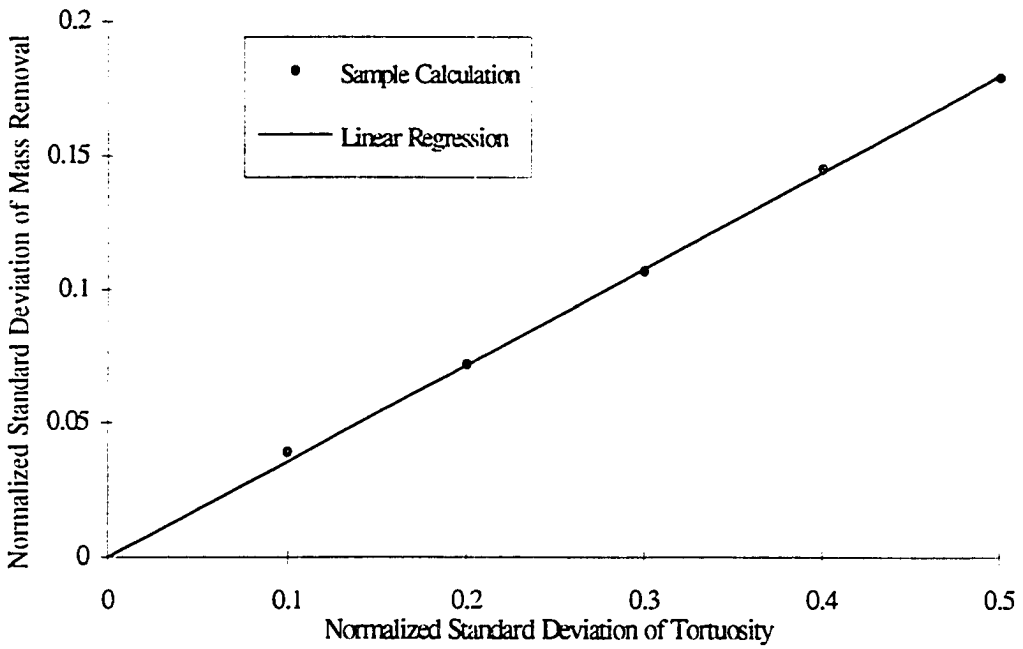

Figure 5.5 Relationship of Normalized Standard Deviations between Tortuosity and Mass Removal

5.2 Retardation Factor

It can be seen from Figure 4.3 that the retardation factors range from 10 to 30 for the most commonly encountered range of water saturations (30% to 70%). A similar approach used for tortuosity has been applied to evaluating retardation factor. Five sets of retardation factors with normal probability distributions were used. Figure 5.6 illustrates one distribution set for retardation factors from 10 to 30. For each set of retardation factors, the mean value remains at 20, while the standard deviation varies from 1.0 to 5.0 which gives 5%, 10%, 15%, 20%, and 25% as the normalized standard deviations, respectively. For each retardation factor, mass removal is calculated. The statistical properties of mass removal

Reproduced with permission of the copyright owner. Further reproduction prohibited without permission.

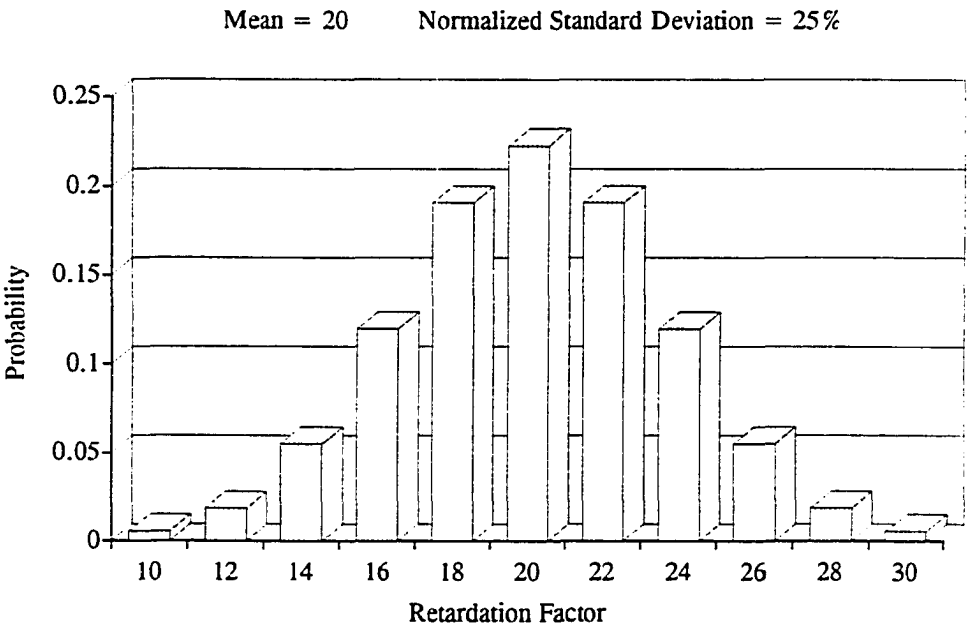

Figure 5.6 Probability Distribution of Retardation Factor

with respect to each retardation factor distribution are obtained. Figure 5.7 shows the results for a 25% normalized standard deviation. The upper three curves, based on the left vertical axis, present the mean value (solid line) of mass removal and the first confidence range (between the dot and dash curves), while the lower three curves, based on the right vertical axis, present the first normalized confidence range. In a manner similar to the tortuosity analysis, the standard deviation increases when the mass removal increases with time, while the normalized standard deviation is almost constant (8.7% for this case) except for the initial period of time (less than ten minutes).

Comparisons of retardation factor and mass removal probability distributions are presented in Figure 5.8. It can be seen that the mass removal distribution is narrower than that of retardation factor.

Reproduced with permission of the copyright owner. Further reproduction prohibited without permission.

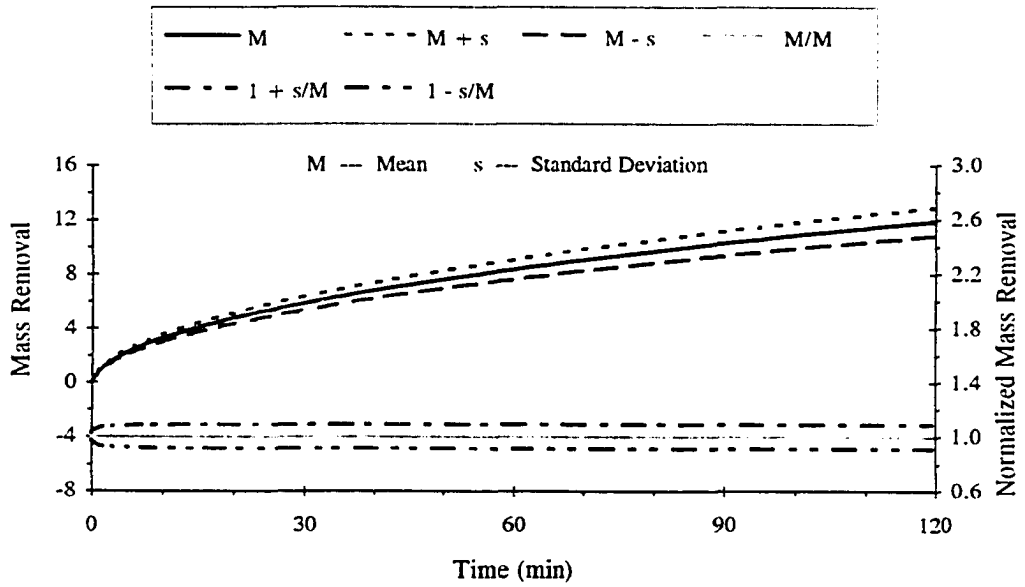

Figure 5.7 Statistical Behavior of Mass Removal with Respect to Retardation Factor

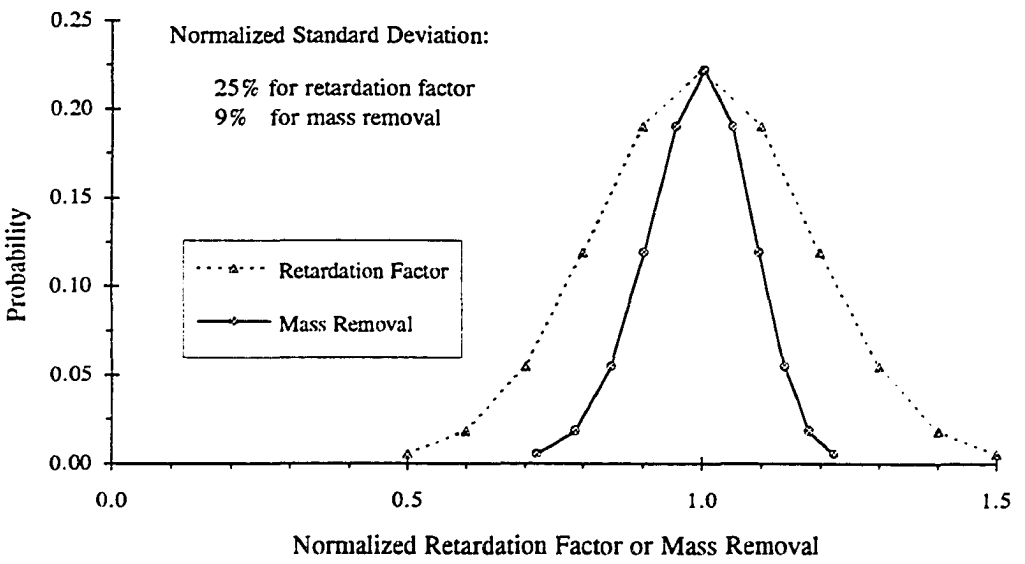

Figure 5.8 A Comparison of Retardation Factor and Mass Removal Distributions

Reproduced with permission of the copyright owner. Further reproduction prohibited without permission.

To illustrate the influence of retardation factor to mass removal more explicitly, Figure 5.9 illustrates the mass removal distribution for various retardation factors from 14 to 26. It can be seen that mass removal increases with retardation factor, which, however, does not mean that the cleanup will be finished sooner. Actually, larger retardation factors correspond to the larger quantities of total initial contaminant stored in the soil water and the soil solid, resulting in longer remedial time.

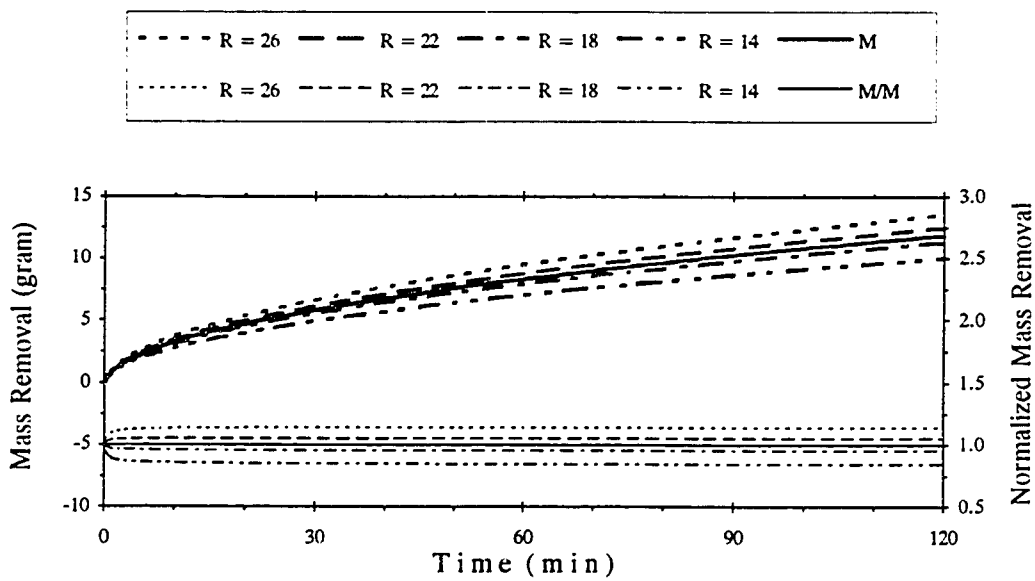

Figure 5.9 Mass Removal Distributions for Four Retardation Factors

Table 5.2 and Figure 5.10 illustrate the relationship of normalized standard deviations between retardation factor and mass removal. The linear regression is made with a correlation coefficient of 0.999. The slope of the regression line is 0.35 which means the uncertainty for mass removal is 35% of that for retardation factor.

Reproduced with permission of the copyright owner. Further reproduction prohibited without permission.

Table 5.2 Relationship of Normalized Standard Deviations between Retardation Factor and Mass Removal

Normalized Standard Deviation of Retardation Factor	Normalized Standard Deviation of Mass Removal
0.05	0.019
0.10	0.037
0.15	0.053
0.20	0.070
0.25	0.087

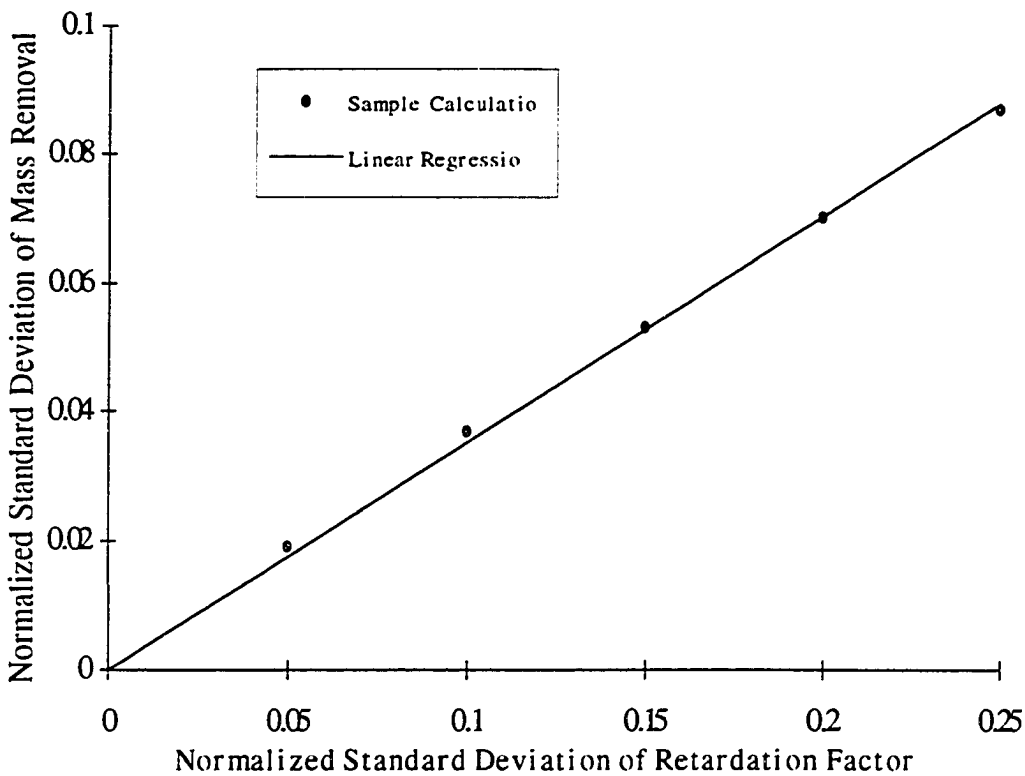

Figure 5.10 Relationship of Normalized Standard Deviations between Retardation Factor and Mass Removal

Reproduced with permission of the copyright owner. Further reproduction prohibited without permission.

A comparison of Figures 5.1 through 5.5 with 5.6 through 5.10 suggests that the influences of tortuosity and retardation factor on mass removal are similar. This behavior becomes apparent if the effluent concentration (C_3) in Equation (3.128) is reexamined. In this solution, diffusion coefficient (related to tortuosity) and retardation factor are exactly symmetrical which means the exchange of their position in the equation will not affect the solution itself. However, situations are different in Equation (3.129) for remaining concentration (C_4) in the soil formation. Diffusion coefficient and retardation factor are not symmetrical in this equation. Therefore the influence of these two parameters will not be similar in determining residual concentrations.

5.3 Aperture of Fracture

Based on field experiments, the aperture of fractures ranges from 10 to 40 mm during fracturing injection and 0.5 to 5 mm during vapor extraction after fracturing injection. Since it will be shown in this section that the direct influence of the aperture to mass removal is very small, a large range of aperture values are chosen for statistical evaluation. Figure 5.11 shows the 11 selected aperture values with a normal probability distribution. The mean value is 3 mm and the standard deviation is 1.5 mm, which gives normalized standard deviation as 50%. For this set of aperture data, the statistical properties of mass removal are presented in Figure 5.12. Instead of using the first confidence range, the tenth confidence range is used to make the three curves distinguishable since the standard deviation for mass removal is very small. It can be seen that the differences caused by different aperture data is almost negligible except for the short initial period of time (less than ten minutes).

Reproduced with permission of the copyright owner. Further reproduction prohibited without permission.

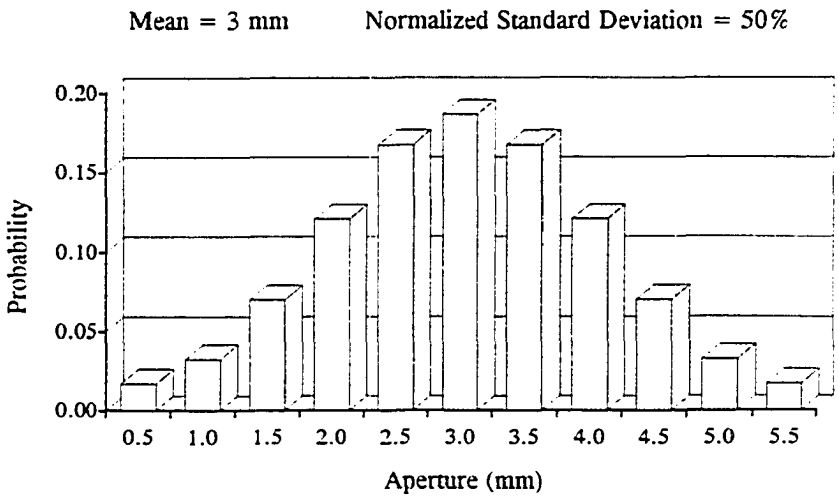

Figure 5.11 Probability Distribution of Aperture

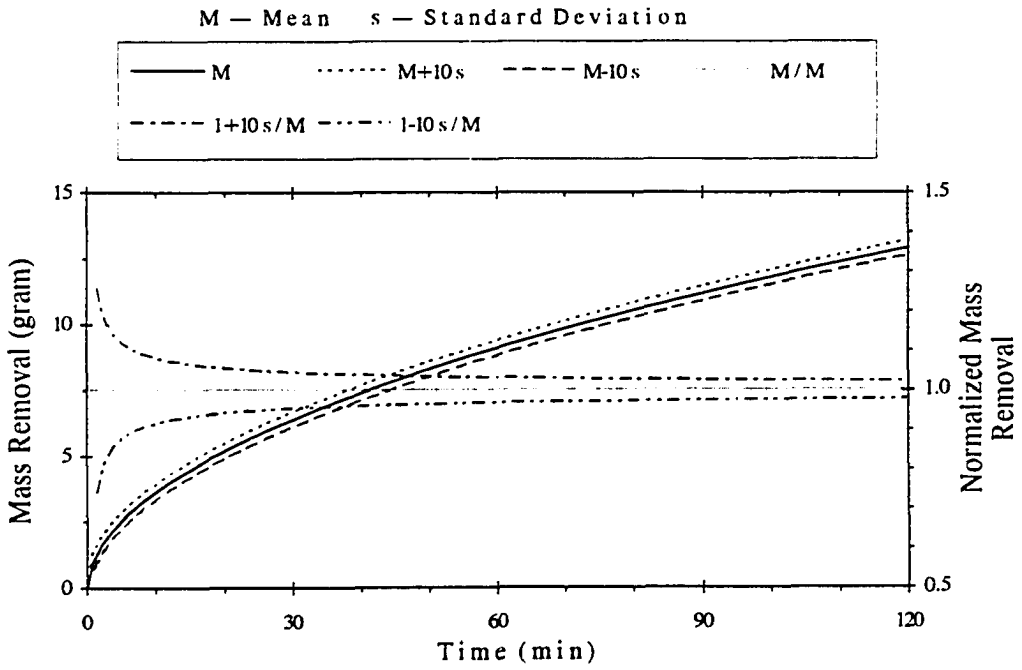

Figure 5.12 Statistical Behavior of Mass Removal with Respect to Aperture

Reproduced with permission of the copyright owner. Further reproduction prohibited without permission.

Figure 5.13 shows the comparison of normalized aperture and mass removal distribution. The normalized standard deviation is only 3% for mass removal with respect to 50% for aperture.

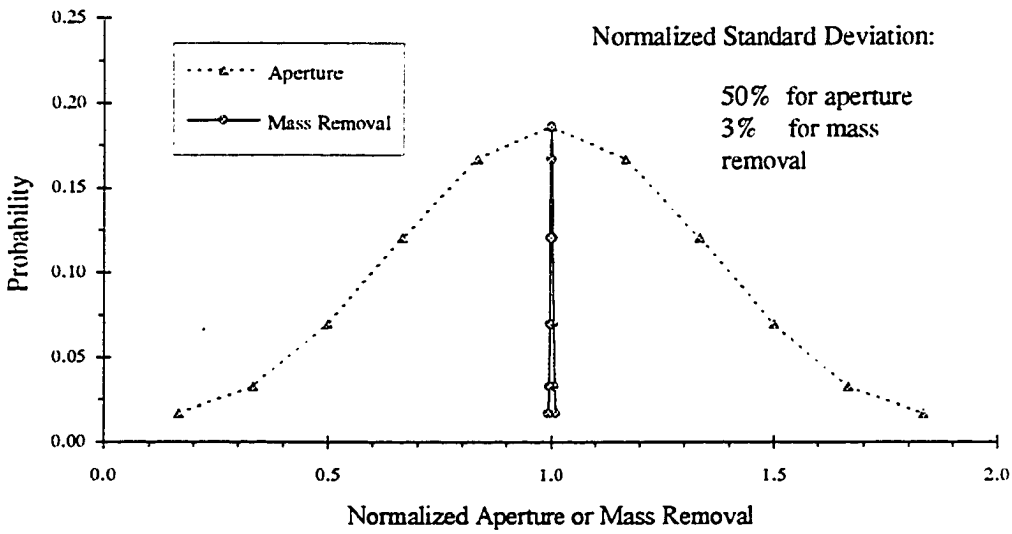

Figure 5.13 A comparison of Aperture and Mass Removal Distributions

These results indicate that the aperture of fracture has little influence on the mass removal, which is fortunate since actual fracture aperture is difficult to measure in the field. However, the relationship between the mass removal and the fracture aperture in this analytical solution does not suggest that fracture aperture is unimportant in remedial actions. On the contrary, achievement of a substantial fracture aperture is key to the pneumatic fracturing process. It is important to note that the preceding statistical evaluation of aperture is made under the assumption that the flow rate is independent of aperture measurement, i.e., constant flow rate is used. Actually, the relationship between fracture aperture and flow rate is governed by the "cubic" law which states that the flow

Reproduced with permission of the copyright owner. Further reproduction prohibited without permission.

rate will increase eight-fold if fracture aperture is doubled. Since the flow rate does have a significant influence on the mass removal, as will be discussed in the next section, aperture is considered important only through its influence on flow rate. In summary, then, this section has demonstrated that the direct influence of aperture to mass removal is insignificant, although it does have an indirect influence through flow rate.

5.4 Flow Rate of Extraction

Although field measurements of flow rates are usually relatively accurate during soil vapor extraction operations, a small change of aperture and vacuum pressure will change flow rate substantially since the flow rate is intimately related to fracture aperture or vacuum pressure. As a result, flow rates typically vary within a relatively large range in field applications. Since the controlling relationship between flow rate and aperture is the cubic law, the flow rate variations have non-linear characteristics. Meanwhile the influence of flow rate on mass removal is also a non-linear phenomenon as will be seen in this section.

Due to the very non-linear characteristics of flow rate, 11 flow rates are chosen as shown in Figure 5.14 with logarithmic uniform distribution from zero to two, resulting in a range of flow rates from 1 to 100 liter/min. Normal probability distribution is used for the logarithm of flow rate, which gives the log-normal distribution of flow rate shown in Figure 5.15. For this set of flow rates, the mean value is 14 liter/min and the standard deviation 13 liter/min, which gives 94% as the normalized standard deviation.

Figure 5.16 illustrates the influence of the 11 flow rates on mass removal. It can be seen that the mass removal only varies slightly for flow rates above 40 liter/min, but significant changes occur for the flow rates smaller than 10

Reproduced with permission of the copyright owner. Further reproduction prohibited without permission.

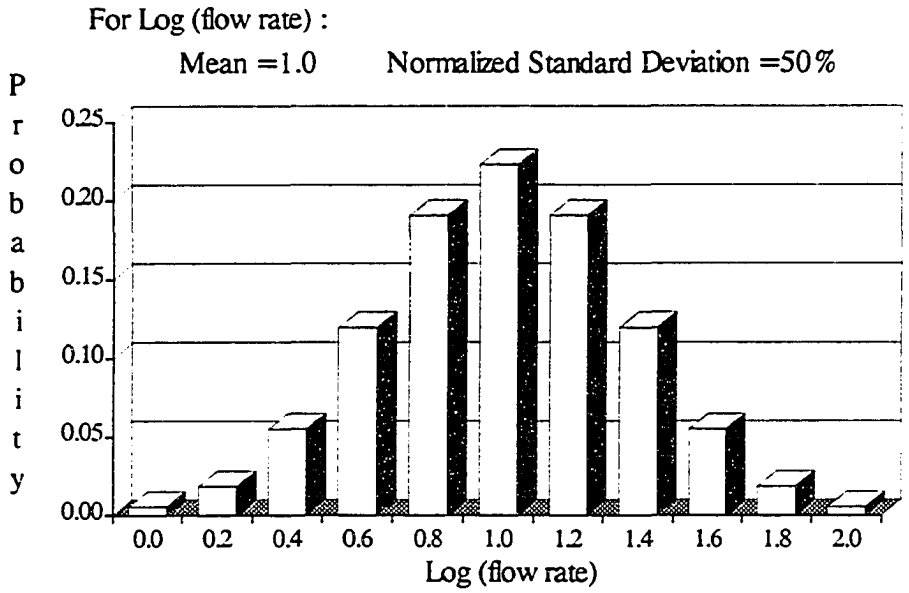

Figure 5.14 Probability Distribution of Logarithm of Flow Rate

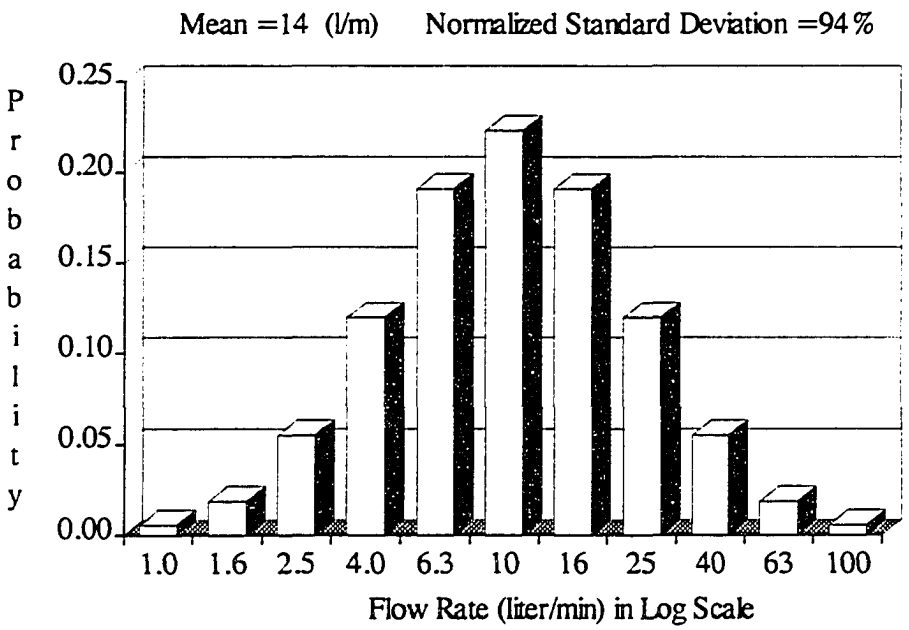

Figure 5.15 Probability Distribution of Flow Rate

Reproduced with permission of the copyright owner. Further reproduction prohibited without permission.

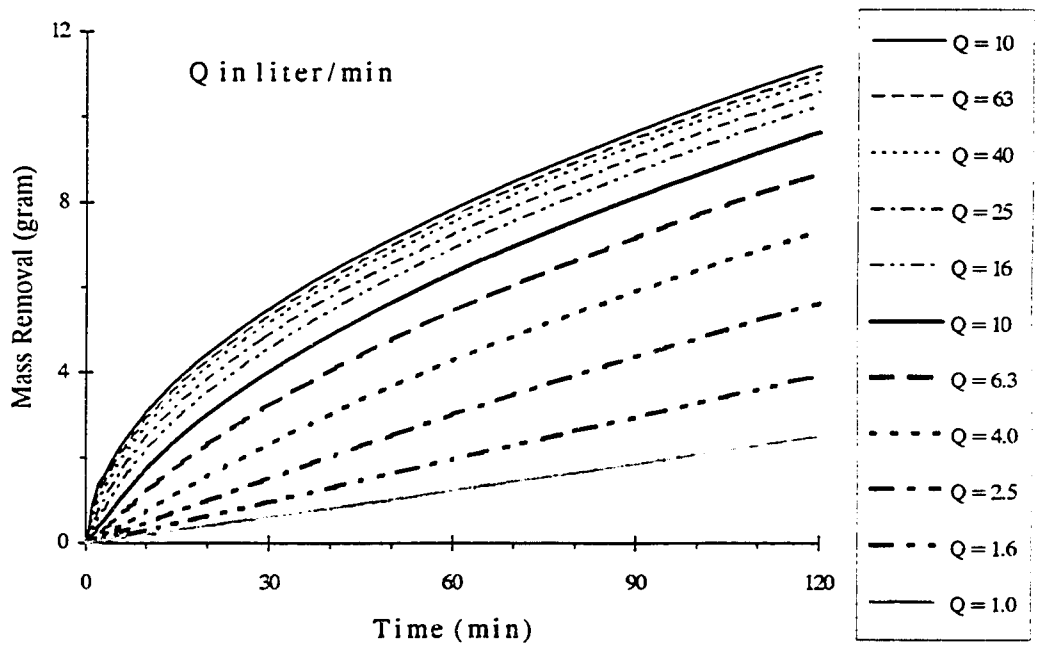

Figure 5.16 Mass Removal Distributions form Various Flow Rates

liter/min. This behavior may be explained by considering the fundamental mechanisms of transport. Flow rate impacts mass removal since: (1) larger flow rates carry away the chemical faster; and (2) larger flow rates result in the lower concentration at the interface boundary, which increases the diffusive transport in the soil matrix, since diffusion rate is controlled by the concentration gradient. These two controlling processes (convection and diffusion) have both a related phase and an independent phase. When flow rate is low, the increase in flow rate will effectively reduce the interface boundary concentration and have a large influence on the diffusive transport. This is also the stage when mass removal is very sensitive subject to flow rate changes. However, when flow rate is large enough to keep a very low interface boundary concentration, an increase in flow

Reproduced with permission of the copyright owner. Further reproduction prohibited without permission.

rate has less influence on the diffusive transport. At this point, diffusion is the "bottle neck" and becomes the dominant controller, so mass removal is not sensitive to flow rate.

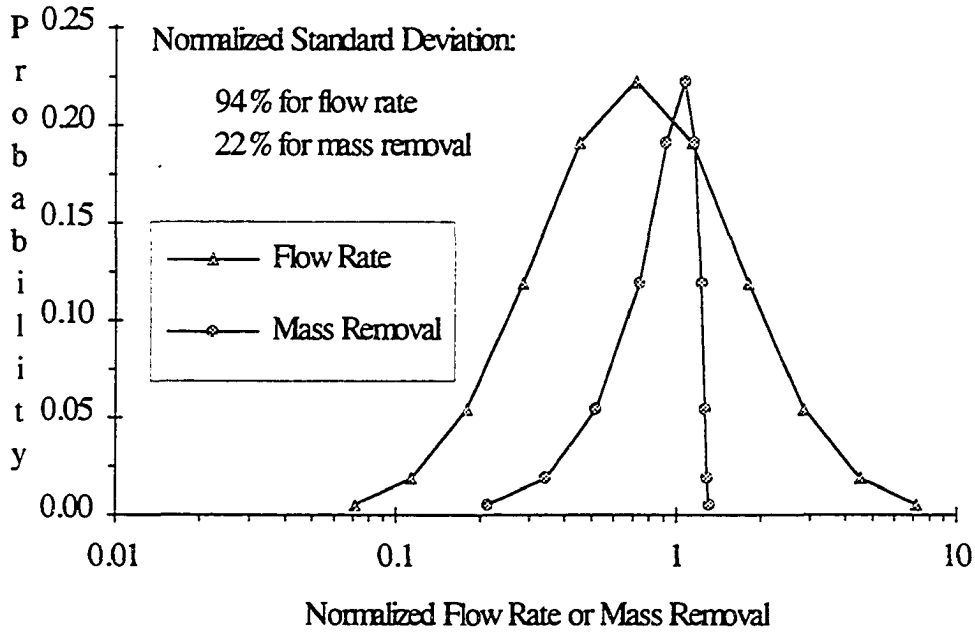

Figure 5.17 A Comparison of Flow Rate and Mass Removal Distributions in Semi-logarithmic Scale

This non-symmetric distribution is explicitly depicted in Figures 5.17 and 5.18. Both Figures show the comparison of probability distributions for flow rate (input) and mass removal (output) but in different scales. Figure 5.17 is in a semi-logarithmic scale in which flow rate has a symmetric distribution with equal increments, while mass removal exhibits a non-symmetric distribution with a high rate of change on the right side of the perk. Figure 5.18 has a linear scale in which the flow rate exhibits a rather long tail on the right side, while mass

Reproduced with permission of the copyright owner. Further reproduction prohibited without permission.

removal again drops rapidly. The shape of the mass removal distribution also indicates that mass removal is more sensitive at low flow rates than at high flow rates. Such information on the mechanism of mass removal are useful in optimizing pumping rate from an economic point of view.

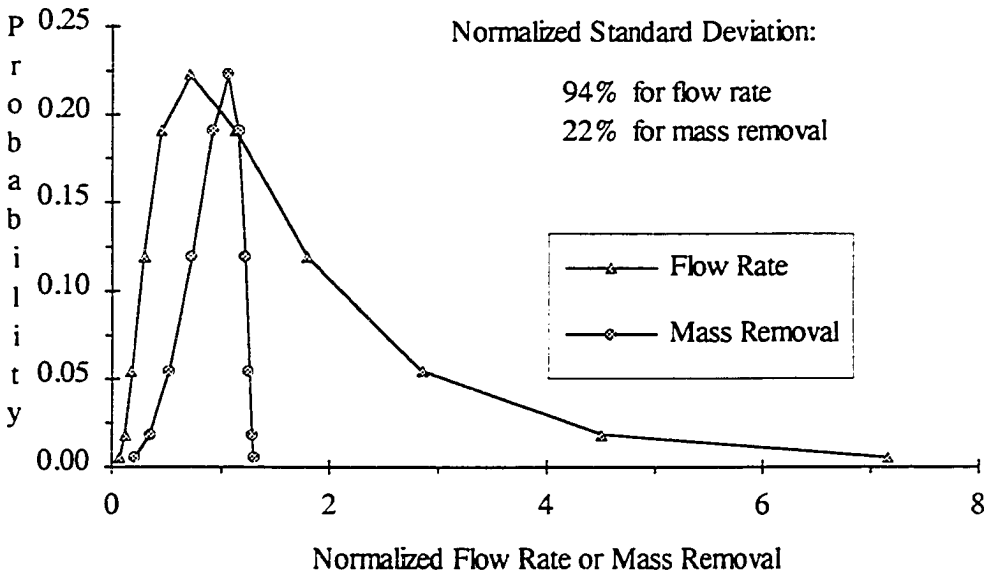

Figure 5.18 A Comparison of Flow Rate and Mass Removal Distributions in Linear Scale

Figure 5.19 shows the behavior of standard deviation of mass removal. Again, the standard deviation increases as mass removal increases, while the normalized standard deviation tends to stabilized at 22%. Since the normalized standard deviations for flow rates is 0.94, the uncertainty for the mass removal is smaller than that for the flow rate. However, the relationship may be different for different flow rate ranges due to its non-linear characteristics.

Reproduced with permission of the copyright owner. Further reproduction prohibited without permission.

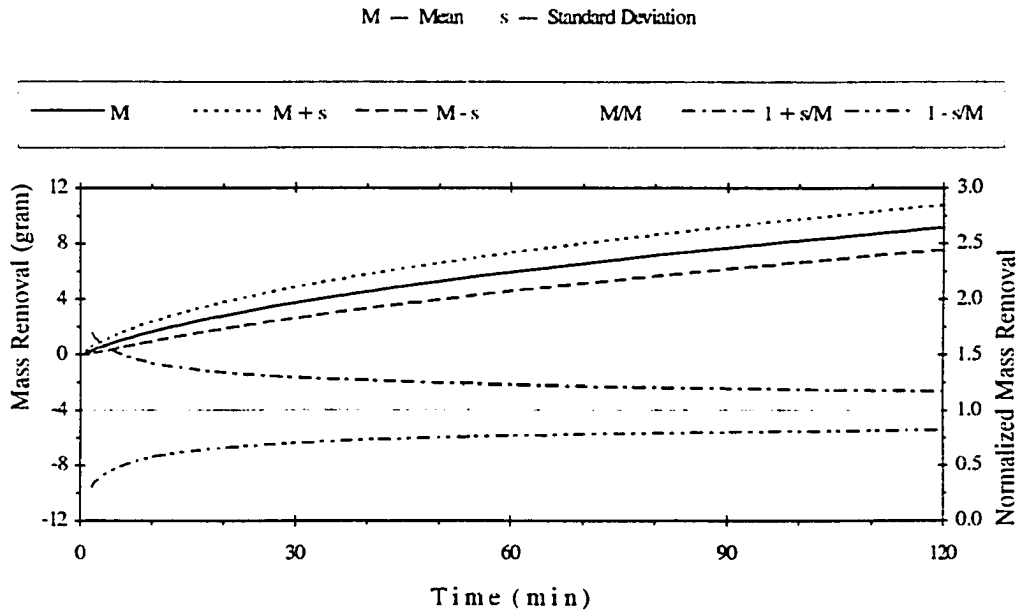

Figure 5.19 Statistical Behavior of mass Removal with Respect to Flow Rate

5.5 Summary

Among the four parameters discussed in this chapter, tortuosity and retardation factor introduce the greatest uncertainty in prediction of mass removal. The normalized standard deviation for mass removal is about 35% of the normalized standard deviation for both tortuosity and retardation factor. Fracture aperture has very limited direct influence on the mass removal; however, it has substantial indirect influence through its impact on flow rate. Mass removal is sensitive to changes in flow rate for relatively low flow ranges (less than 10 liter/min). However, when flow rate is high (greater than 40 liter/min), changes in flow rate have minimal influence on mass removal.

Reproduced with permission of the copyright owner. Further reproduction prohibited without permission.

CHAPTER 6

CASE STUDIES

The principal objective of this chapter is to validate the analytical model using both field and laboratory data. First, post-fracture mass removal rates from two field projects will be compared with model predictions. The sites chosen were AT&T Richmond Works and Tinker Air Force Base, since the field data measured at these two sites had the highest level of quality control and assurance. This chapter will also utilize data from previous laboratory investigations to provide model verification. Specifically, the experimental results from soil test tank experiments performed by Papanicolaou (1989) and Shah (1991) will be compared with the analytical model

6.1 AT&T Richmond Works Site

6.1.1 Site Descriptions

The AT&T Richmond Works site is an excellent case for model comparison studies for two reasons. First, the contaminated zone is a relatively homogenous stratum of stiff silty clay, and thus satisfies the physical conditions required in the model assumptions. Second, it was the only site equipped with a continuous-reading mass spectrometer attached directly to the extraction well, which allowed a high degree of reliability for mass removal measurements.

The site for the pilot demonstration of pneumatic fracturing was an abandoned above-ground tank farm at the AT&T Richmond Works in Richmond, Virginia. The general layout of the site is illustrated in Figure 6.1 and the site is

Reproduced with permission of the copyright owner. Further reproduction prohibited without permission.

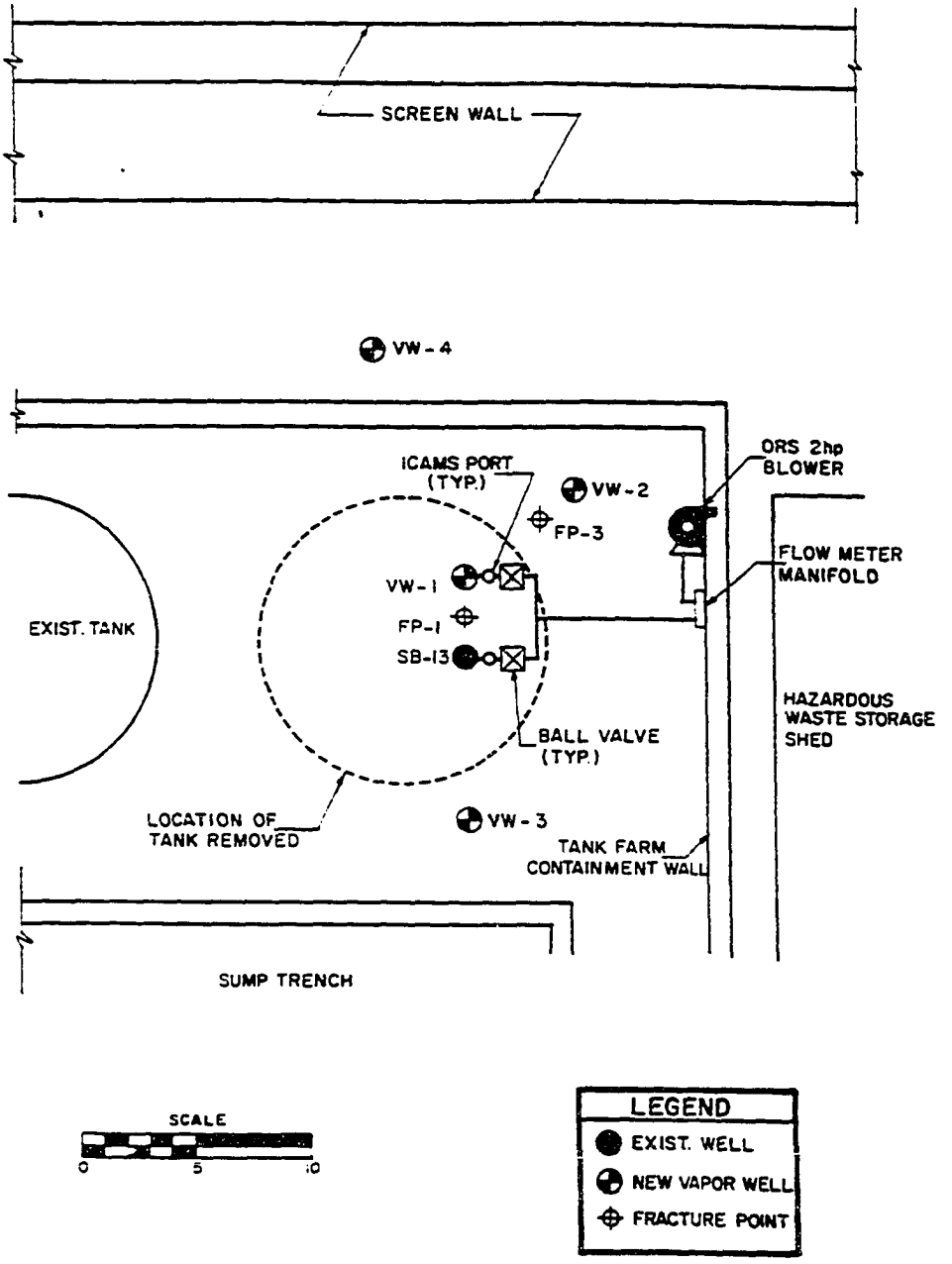

Figure 6.1 AT&T Richmond Works Site Layout

Reproduced with permission of the copyright owner. Further reproduction prohibited without permission.

described in detail by Schuring et al. (1991). This tank farm structure consisted of a six-inch thick, lightly reinforced concrete slab surrounded by a twelve-inch thick perimeter containment wall. A concrete sump trench extended down the middle of the tank farm, and the steel VOC storage tank immediately over the demonstration location had been removed. The soil formation consisted of stratified clay, silt, sand, and gravel. The surficial stratum was a stiff clay that extended to variable depths up to twenty feet. Laboratory tests on the clay indicated that it had a Unified Classification of CH-MH and was highly overconsolidated. The clay stratum was entirely in the vadose zone and was underlain by a more permeable sand and gravel layer, which contained an unconfined water table. Soil samples from the vadose zone showed that the methylene chloride ($MeCl_2$) and 1,1,1-trichloroethane (TCA) were the two principal VOCs in the clay with concentration ranging up to 485 ppm and 250 ppm, respectively.

A vapor extraction system was installed and operated to establish the pre- and post-fracture effluent behavior. VOC concentrations in the soil gas were measured with a Perkin-Elmer ICAMS continuous-reading mass spectrometer. The effluent was sampled at two minute intervals, and were displayed and printed by a microcomputer. The system had a lower detection limit of 1 ppm.

6.1.2 Application of Analytical Solution

In order to model the effluent concentration and mass removal data with respect to time using the analytical solution derived in Chapter 3, it is first necessary to estimate the numerical values of the four transport parameters discussed in Chapters 4 and 5. For methylene chloride, the following values were chosen:

Reproduced with permission of the copyright owner. Further reproduction prohibited without permission.

(1) Tortuosity -- a normal probability distribution in the range from 0.1 to 0.7;

(2) Retardation factor -- a normal probability distribution in the range from 10 to 30;

(3) Aperture of the fracture -- 0.2 inches based on field measurement; and

(4) Extraction flow rate -- 30 liter/min based on field measurement.

For 1,1,1-trichloroethane, the numerical values of four parameters are similar, except the retardation factor was assumed in the range of 5 to 15 due to differing chemical sorption effects.

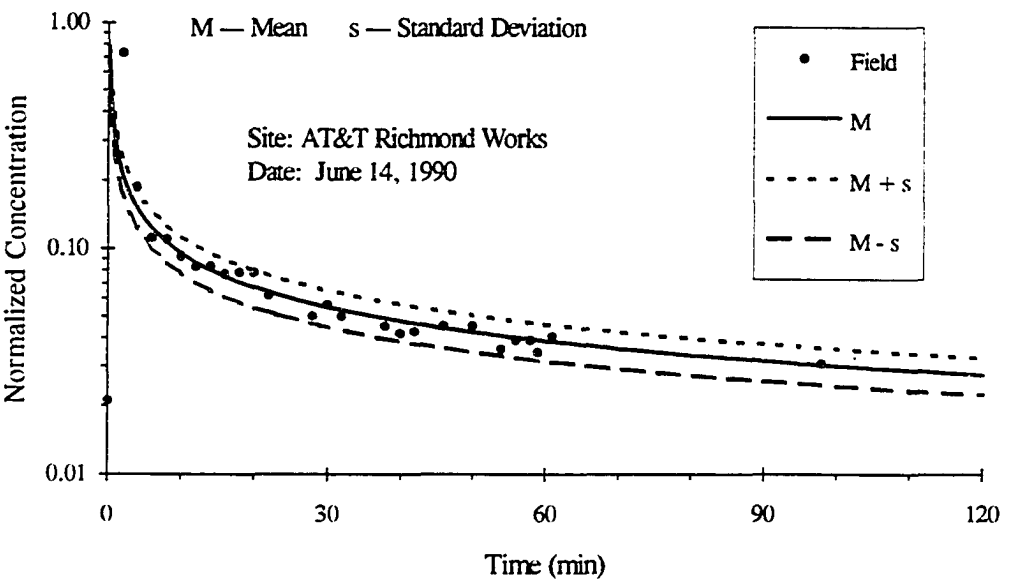

Figure 6.2 A Comparison of Effluent Concentrations between Field Measurement and Analytical Solution (Methylene Chloride)

A comparison of field and model effluent concentrations for $MeCl_2$ is shown in Figure 6.2, In this figure, the points represent field measurements; the solid line is the mean curve of the analytical solution based on statistical input

Reproduced with permission of the copyright owner. Further reproduction prohibited without permission.

parameters; and the dot- and dash-line define the first confidence range of the analytical solution. As indicated, all field effluent concentrations of methylene chloride fall in the first confidence range predicted by the model except for one point at the beginning. It is also noted that the field data are randomly distributed around the mean curve, which demonstrates an excellent match with the model.

A review of the data suggests that the effluent concentration behavior can be approximately divided into three stages. In the first stage, the concentration increases rapidly at the very beginning and reaches the maximum at 80% of initial concentration within 2 minutes. Then, in the second stage, the concentration decreases quickly to 10% of initial concentration within 20 minutes. Later, in the third stage, the concentration still decreases but at a slower rate.

Figure 6.3 compares the effluent concentration of TCA between the field measurements and the analytical solution. It can be seen that there is more spread of the field data around the model predictions than for $MeCl_2$, so the second confidence range is also shown. In general, the initial field data are somewhat higher than concentrations predicted by the model. At later times ($>$ 20 minutes), the field data are below the model predictions, although all data points fall in either the first or second confidence range.

A review of Figures 6.2 and 6.3 demonstrates that the normalized effluent concentration data are in general agreement with model predictions, and compounds exhibit similar behavior in form. The similarity comes from the same field conditions for both compounds. This phenomenon will be seen again in the next case study. The magnitudes of the $MeCl_2$ data show excellent agreement with all field values except one falling within the first confidence range. The greater deviation of the TCA heterogeneity data is attributed to the non-uniformity of the distribution of this compound in the test zone.

Reproduced with permission of the copyright owner. Further reproduction prohibited without permission.

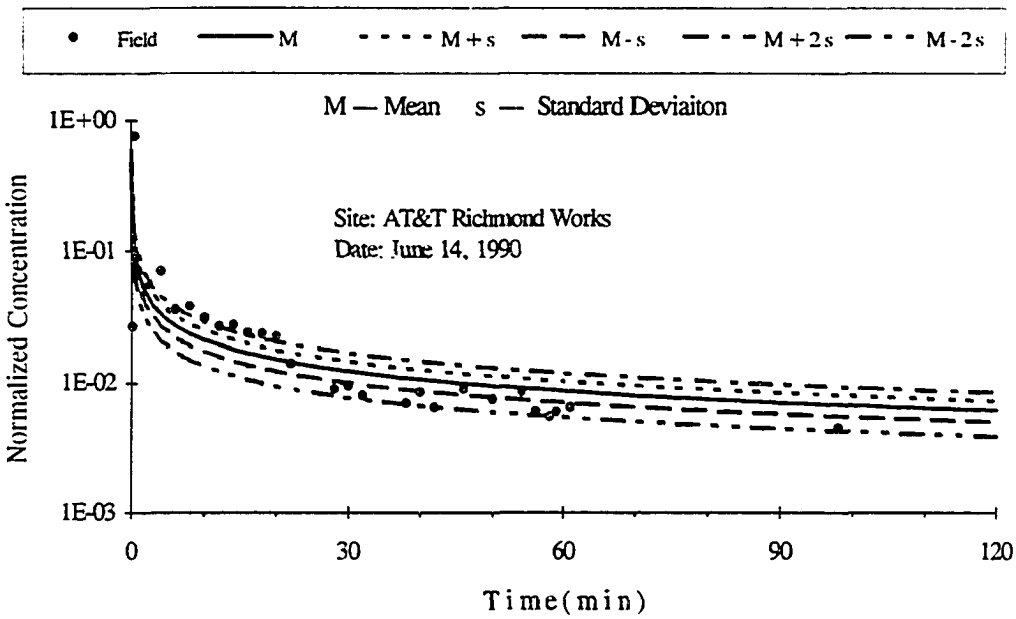

Figure 6.3 A Comparison of Effluent Concentrations between Field Measurement and Analytical Solution (TCA)

Comparisons of total mass removal versus time for the field measurements and the analytical solution are illustrated in Figures 6.4 and 6.5 for $MeCl_2$ and TCA, respectively. As expected, the trends are similar to those previously observed for effluent concentration. For $MeCl_2$, the analytical solution provides an excellent match with the field measurement, since all the field data are located close to the mean curve. For TCA, the model predicts smaller values than the observed field data for the first half hour, and then exceeds the field data for later times, since the effluent concentrations predicted by the model have the same trend.

Reproduced with permission of the copyright owner. Further reproduction prohibited without permission.

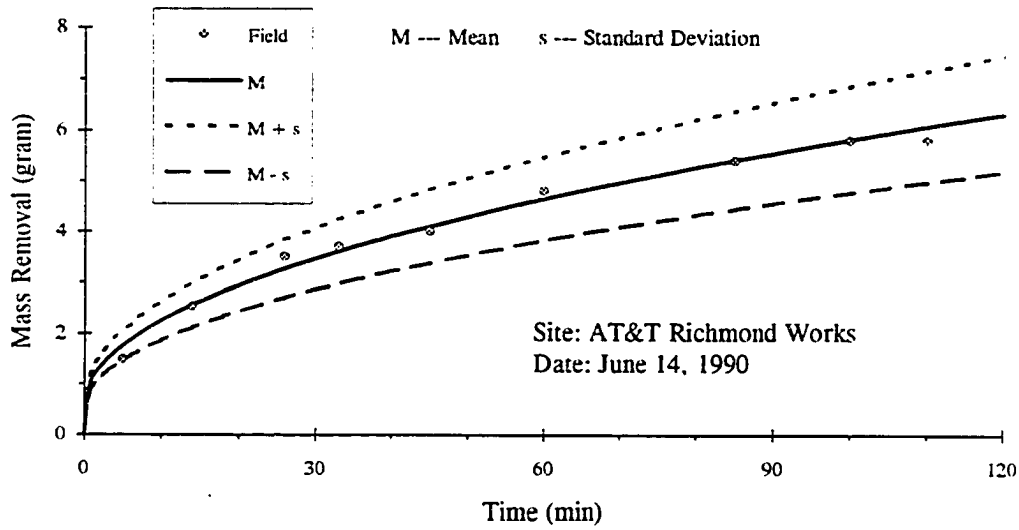

Figure 6.4 A Comparison of Mass Removal between Field Measurement and Analytic Solution (Methylene Chloride)

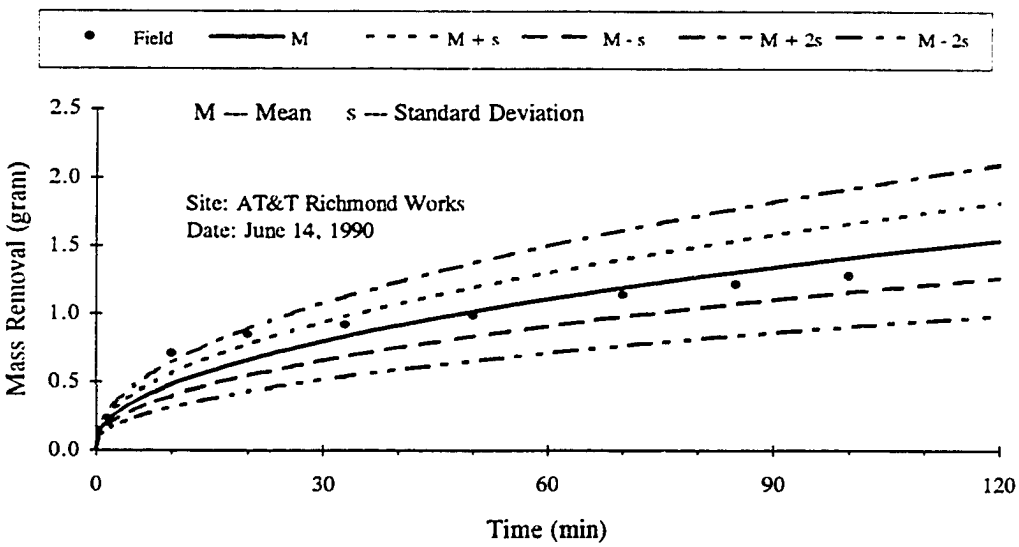

Figure 6.5 A Comparison of Mass Removal between Field Measurement and Analytic Solution (TCA)

Reproduced with permission of the copyright owner. Further reproduction prohibited without permission.

A tabular summary of the input data used for model perdition presented in Figure 6.2 and 6.3 is contained in Appendix. The appendix also contains a sample calculation of one value of mean concentration as determined by the analytical model.

6.2 Tinker Air Force Base Site

6.2.1 Site Description

Tinker Air Force Base (AFB) is located in the southeast portion of the Oklahoma City Metropolitan Area. It encompasses 4,277 acres and contains approximately 500 buildings. Presently, it serves as a worldwide repair depot for a variety of aircraft, weapons, and engines. These activities require the use of large quantities of solvents and fuels, which in the past were often stored in underground storage tanks. During the period of 1972 to 1990, investigation revealed that extensive leakage and spills had occurred in the vicinity of the underground tanks. The compounds trichloroethylene (TCE) and toluene were among those encountered as soil contaminants. A detailed description of site characteristics and operation is given by HSMRC (1994), and Figure 6.6 gives a general site plan of the Southwest Tank Area.

The site is underlain by the Garber Sandstone and Wellington formations which extend to a combined total depth of 800 to 1000 feet. They are Permian in age, and are comprised of a system of interbedded sandstones, siltstones, and shales deposited in deltiac and alluvial environments. The lithology of the formation is complex, and bed thicknesses vary greatly over short distances. The thickness of individual beds may range up to 20 to 40 feet, but a vast majority of beds do not exceed several feet in thickness.

Reproduced with permission of the copyright owner. Further reproduction prohibited without permission.

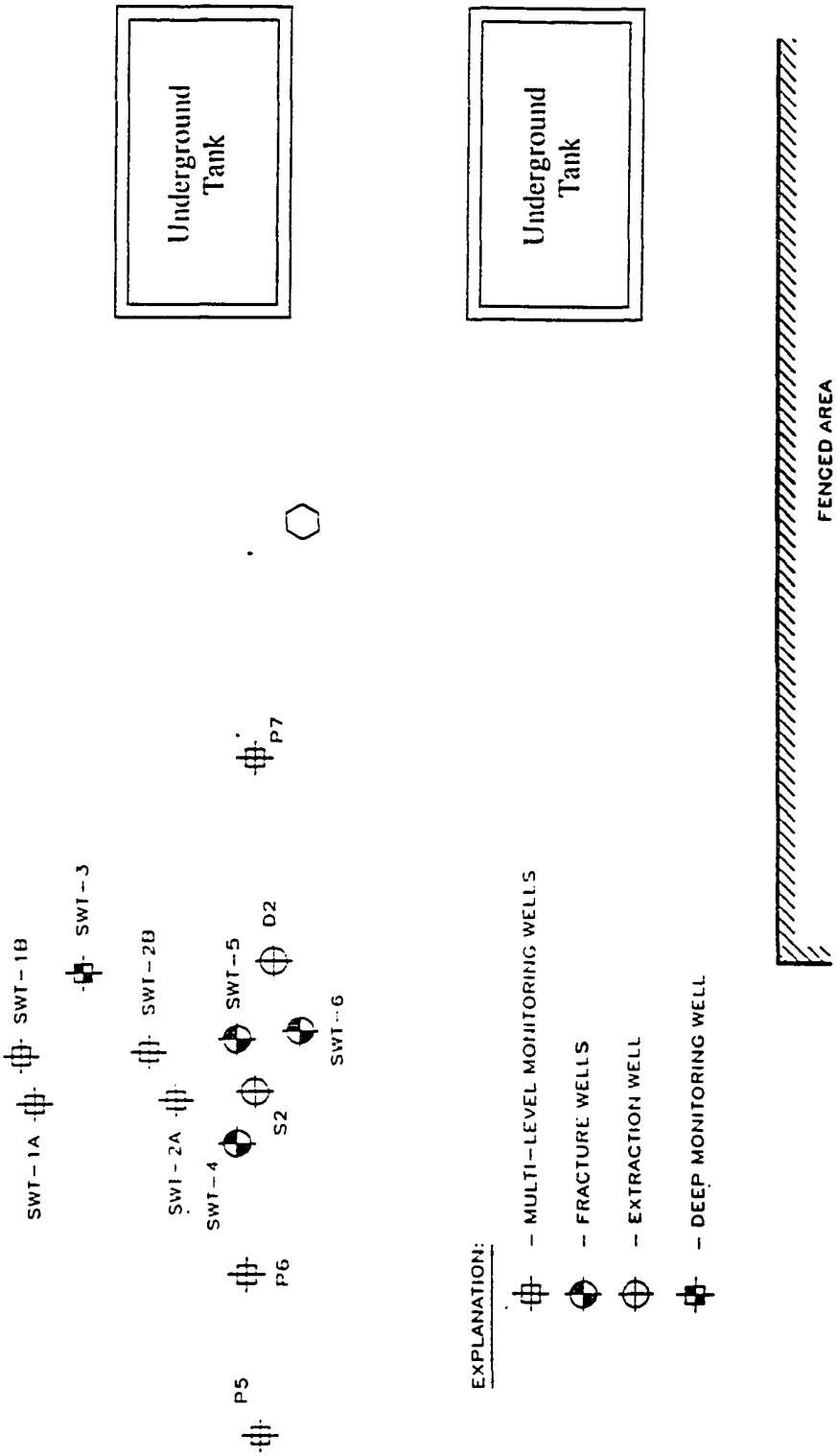

Figure 6.6 Tinker AFB Southwest Tank Site

Reproduced with permission of the copyright owner. Further reproduction prohibited without permission.

The upper 10 feet of soil at the site consists primarily of weathered red clays of the Garber-Wellington Formation containing interbedded silty clay and silt. Clay backfill materials and sandy gravels were found at some locations to a depth of 15 feet. Below the upper clay unit, lithology grades into a sandy unit, which is comprised of clay, pebbly zones, siltstone and silty sand interbedded with fine to coarse grained reddish-brown sand. Cementation of sands begins at about 20 feet below ground surface and increases with depth.

The focus of the pneumatic fracturing demonstration at Tinker AFB was the recovery of fuels and solvents which had leaked into the subsurface from several underground storage tanks. For the purposes of model validation, effluent data from the southwest tank area were chosen. At this location, a vapor extraction system was operated to evaluate the effects of pneumatic fracturing. During the vacuum extraction tests, vapor samples were collected from the effluent in tedlar bags and analyzed with a gas chromatograph. Samples were prepared by using the purge and trap method and analyzed by using a Hewlett Packard 5890a gas chromatograph equipped with dual ECD and FID detectors.

The model comparisons for the present study were limited to the compounds Trichloroethylene (TCE) and Toluene since these data were considered to be the most reliable.

6.2.2 Application of the Analytical Solution

Post-fracture vacuum extraction was conducted at two wells (Well D2 and Well S2) at locations shown in Figure 6.6. The data from Well S2 were chosen for comparison with the model since it was judged closest to the condition of the analytical model, i.e., relatively homogenous condition with moderate levels of contamination.

Reproduced with permission of the copyright owner. Further reproduction prohibited without permission.

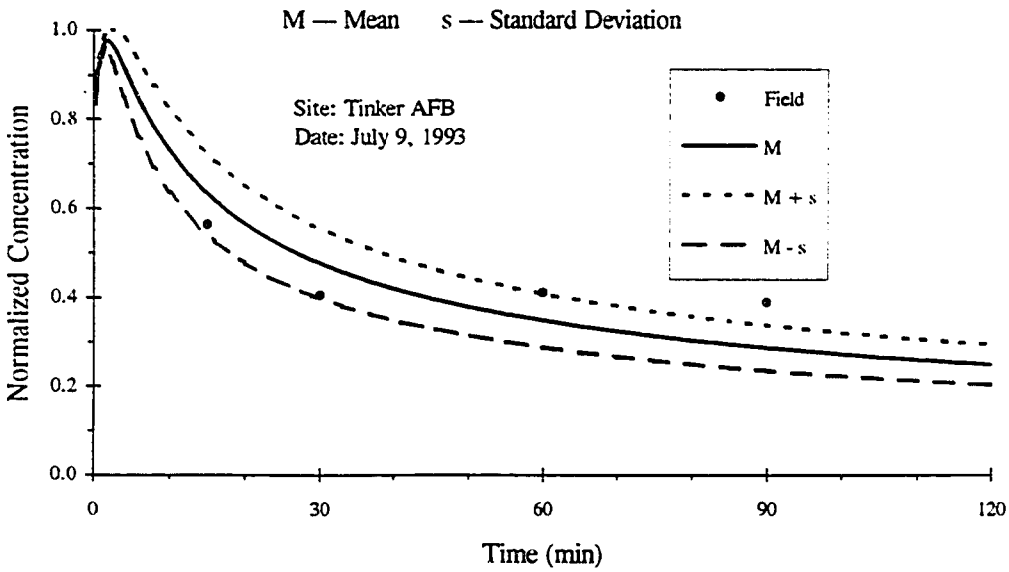

Figure 6.7 A Comparison of Effluent Concentrations between Field Measurement and Analytical Solution (TCE)

Figures 6.7 and 6.8 provide comparisons of effluent concentrations for TCE and Toluene between the field measurements and the analytical solutions. Since the first concentration measurement was taken 15 minutes after the beginning of the test, data for the first two stages of concentration behavior are not available. However, all four field points in the third stage of extraction show reasonable agreement with the analytical solution. A comparison of the data from Tinker AFB (Figures 6.7 and 6.8) and AT&T Richmond Works (Figures 6.2 and 6.3) shows decidedly different effluent concentration behaviors. This serves to demonstrate the adaptability of the model.

Mass removal curves for TCE and Toluene are illustrated in Figures 6.9 and 6.10, respectively. As indicated, most field measurements fall within the first confidence level of the model.

Reproduced with permission of the copyright owner. Further reproduction prohibited without permission.

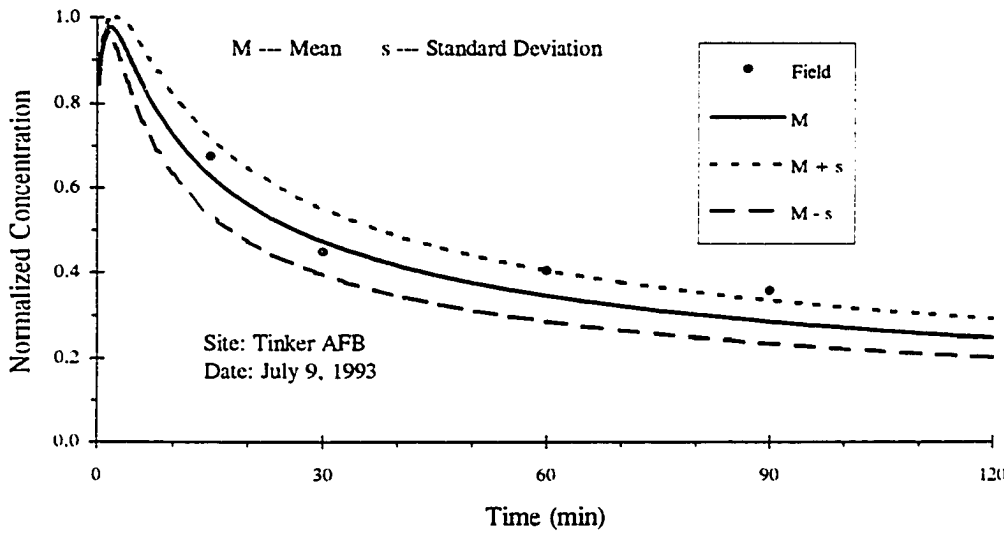

Figure 6.8 A Comparison of Effluent Concentrations between Field Measurement and Analytical Solution (Toluene)

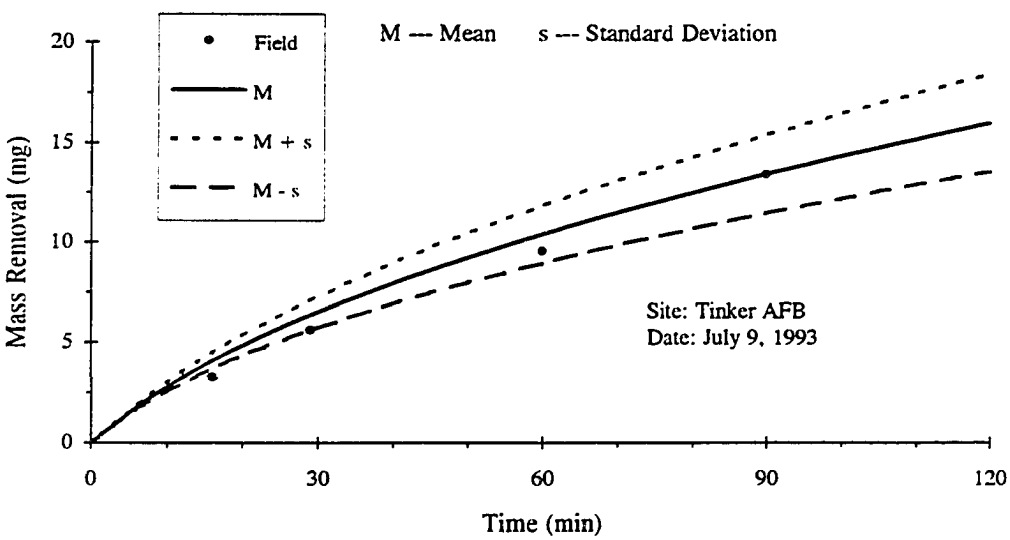

Figure 6.9 A Comparison of Mass Removal between Field Measurement and Analytical Solution (TCE)

Reproduced with permission of the copyright owner. Further reproduction prohibited without permission.

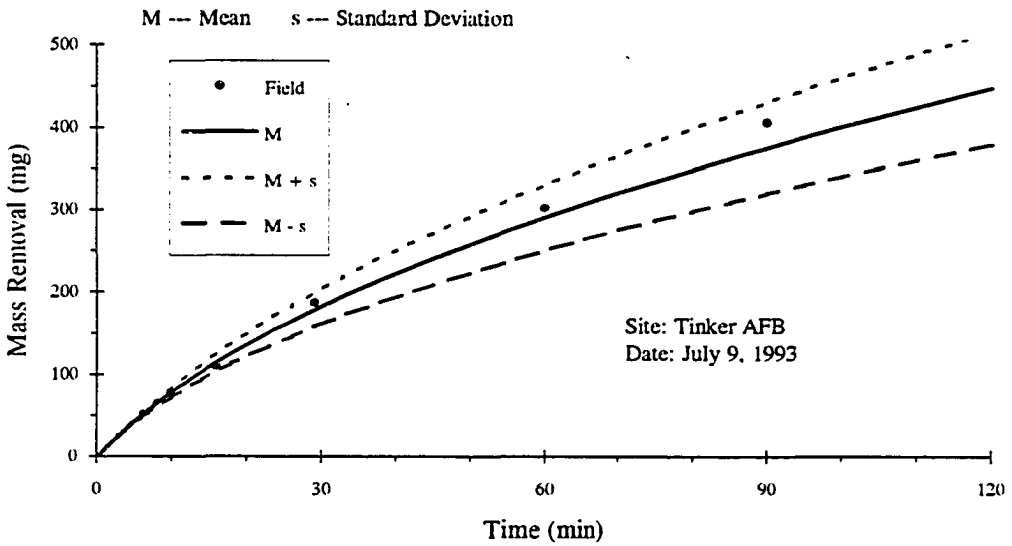

Figure 6.10 A Comparison of Mass Removal between Field Measurement and Analytical Solution (Toluene)

A tabular summary of the input data used for model prediction presented in Figure 6.7 and 6.8 is contained in Appendix. The appendix also contains a sample calculation of one value of mean concentration as determined by the analytical model.

6.3 Laboratory Experiment

A number of laboratory experiments were previously conducted to simulate pneumatic fracturing at a bench scale. These experiments were carried out in plexiglass vats filled with contaminated soil (see Figure 2.3) and are described in detail by Papanicolaou (1989) and Shah (1991). These vat experiments provided numerous measurements of contaminant removal rate for both fractured and unfractured soils (e.g., Figure 2.4). It was decided to compare these laboratory data with the analytical solutions developed in Chapter 3 for the purposes of model validation.

Reproduced with permission of the copyright owner. Further reproduction prohibited without permission.

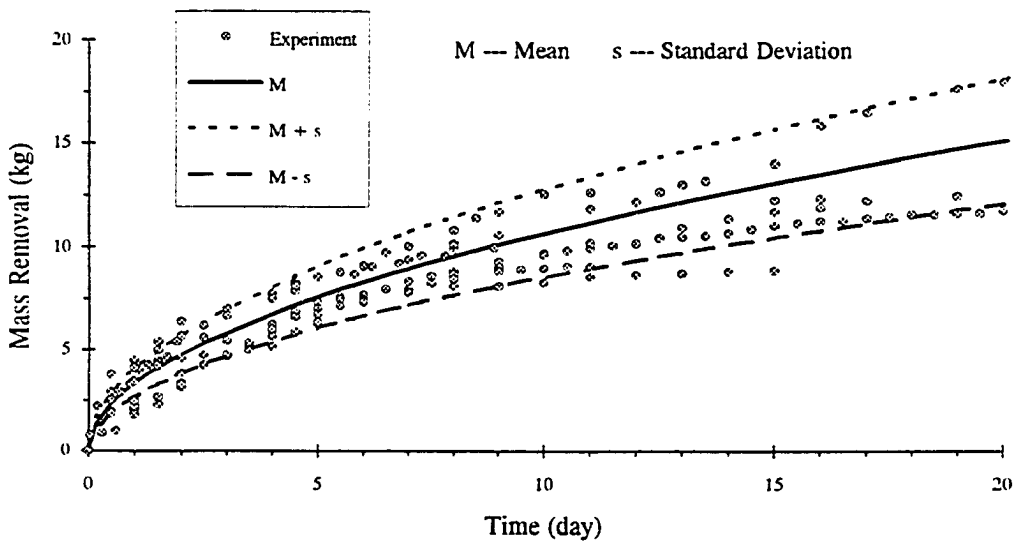

Figure 6.11 A Comparison of Mass Removal between Laboratory Experimental Data and Analytical Solution

Figure 6.11 compares the results of the laboratory experiments with the analytical simulation for mass removal. In general, the agreement appears quite satisfactory, with most of the laboratory experimental data points falling within the first confidence level. Some of the experimental scatter is certainly attributable to the wall effects, and the obvious differences in geometry between the laboratory experiments and those assumed in the model. Also, some of the experiments utilized plain water as a surrogate contaminant, which deviates from the basic model assumption of a volatile organic compound. It is further noted that certain input data required for the model were not recorded for some of the early laboratory experiments (e.g., flow rate), and had to be estimated. In view of the above uncertainties, the agreement between the laboratory data and the model is considered satisfactory.

Reproduced with permission of the copyright owner. Further reproduction prohibited without permission.

6.4 Remarks

In general, the analytical model appears to predict effluent behavior from both field demonstrations reasonably well. Among the two field case studies, the AT&T Richmond Works site provided the most complete validation, since data were measured every two minutes over a period of approximate one and a half hours. Data from Tinker AFB site were more limited, but still proved useful for model validation.

The laboratory data from previous vat experiment also showed general agreement with the analytical model. These data were considerably more scattered, however, which is attributed to geometric differences and variations in experimental procedure.

Reproduced with permission of the copyright owner. Further reproduction prohibited without permission.

CHAPTER 7

CONCLUSIONS AND RECOMMENDATIONS

7.1 Conclusions

The pneumatic fracturing process has proven to be an effective enhancing technology for in situ remediation based on a number of field demonstrations, as well as laboratory experiments. This study has focused on the mathematical description of contaminant removal for the pneumatic fracturing process. Based on the analysis presented in the previous chapters, the principal conclusions are summarized as follows:

1. A mathematical model based on the dual porosity approach has been developed to simulate the process of contaminant removal from pneumatically induced fractures, including both two dimensional and axial symmetric cases. The two dimensional approach can be applied for cases of trench or horizontal well extraction, while the axial symmetrical analysis can be used for radial extraction from a vertical borehole. The model consists of two partial differential equations: one diffusion equation for the porous medium [Equation (3.7) or (3.77)] and one diffusion-convection equation for the discrete fracture [Equation (3.19) or (3.86)]. The initial and boundary conditions for the model equations have been determined based on operational considerations for a soil vapor extraction system. These two equations are linked together by the conditions at the interface of the porous medium and the discrete fracture, and, thus, must be solved simultaneously.

2. Analytical solutions for both the two dimensional and axial symmetrical cases were obtained through the Laplace transform technique. These explicit

Reproduced with permission of the copyright owner. Further reproduction prohibited without permission.

solutions are expressed in terms of exponential and error functions (see Equations (3.69), (3.70), (3.128), and (3.129)), and can be conveniently used by engineers and scientists in the field.

3. Four physical parameters are utilized in the model including tortuosity, retardation factor, fracture aperture, and flow rate. Fracture aperture and flow rate are obtained from field measurements of the pneumatic fracturing process, while tortuosity and retardation factor are estimated from available information in the current literature. Guidelines are provided for determination of all four parameters.

4. A statistical analysis of mass removal is conducted to evaluate its sensitivity to variations in the four principal parameters mentioned above. Five sets of tortuosities and retardation factors with normal distributions are used in the evaluation. The influence of tortuosity on mass removal is similar to that of retardation factor. Based on numerical calculations, a linear relationship of normalized standard deviations between mass removal and tortuosity or retardation factor is obtained for these numerical case studies (see Figure 5.5 and 5.10). The normalized standard deviation of mass removal is substantially less (approximately 65%) than that for either tortuosity or retardation factor. The sensitivity of mass removal to fracture aperture is minimal, although it affects mass removal indirectly through extraction flow rate. The sensitivity of mass removal to flow rate depends on flow range. Mass removal is sensitive to small flow rates (e.g., less than 10 liter/min), but insensitive to large flow rates (e.g., greater than 40 liter/min).

5. Comparisons of the mathematical model with field data were carried out for two field projects involving pneumatic fracturing and soil vapor extraction at contaminated sites. Good correlation was obtained between model predictions and

Reproduced with permission of the copyright owner. Further reproduction prohibited without permission.

the field data. A comparison of the model with results from previous laboratory experiments also indicated satisfactory agreement, although some scatter of the laboratory data was observed, and was attributed mainly to geometric differences between the model and the laboratory apparatus.

6. Engineering applications of this model to site remediation are feasible since the model provides a quantitative analysis of mass removal with respect to time. The model can be used to evaluate remediation efficiency and predict treatment times, which are important aspects of engineering planning.

7.2 Recommendations

While the pneumatic fracturing process is proving to be an effective technology for contaminant removal from different geological formations, it is still considered to be an emerging technology. More work is necessary to expand its applications and to improve the understanding of its underlying mechanisms. The following specific recommendations are presented:

1. In the application of pneumatic fracturing process, it is often necessary to fracture at different depths in the same borehole. Therefore, consideration of fracture characteristics and transport phenomena in a multi-fracture case should be investigated. Since an analytical solution for transport in a multi-fracture system would be very difficult to achieve, a numerical approach should be considered for such situations.

2. An analytical model in conjunction with sorption kinetics and chemical-soil interactions should be developed, since sorption kinetics plays an important role in long term remediation processes.

3. Validation of the present model should continue as additional field data becomes available. Particular attention should be given to long term extraction

Reproduced with permission of the copyright owner. Further reproduction prohibited without permission.

data from sites where pneumatic fracturing has been applied for periods of several weeks or months.

4. The present mathematical model and solution should be incorporated into a computer code and program for engineering design purposes.

Reproduced with permission of the copyright owner. Further reproduction prohibited without permission.

APPENDIX

SAMPLE CALCULATION

The values of each of the parameters used in the three case studies presented in Chapter 6 are listed in Table A.1. A sample calculation of applying the model in predicting effluent concentration from soil vapor extraction data is presented in detail below for the case of AT&T Richmond Works site with methylene chloride.

The normalized effluent concentration given by Equation (3.126) is expressed in the form of both exponential and error functions which can be obtained in the standard mathematical handbook (e.g., Abramowitz and Stegun, 1972). To calculate the mean value of C_3/C_o, the tortuosity with the assigned probability distribution (see Figure 5.1) is used. Thus, each of the 11 tortuosities from 0.1 to 0.7 is used for Equation (3.126). For the foilowing given input parameters

$$n = 0.55, \quad n_a = 0.24, \quad D_2 = 1.1 \times 10^{-6} \text{ m}^2 / \text{sec}, \quad R = 20, \quad b = 2.5 \times 10^{-3} \text{ m},$$

$$Q_3 = 30 \text{ liter} / \text{min} = 5 \times 10^{-4} \text{ m}^3 / \text{sec}, \quad r = 0.4 \text{ m}, \quad t = 150 \text{ sec}$$

one can proceed the calculation by substituting these values into Equation (3.126). Hence,

$$\frac{C_3}{C_o} = \text{erf}\left[\frac{0.24 \times 3.14\sqrt{1.1 \times 10^{-6} \times 20}}{5 \times 10^{-4}} \times 0.4^2\left(150 - \frac{2 \times 3.14 \times 2.5 \times 10^{-3}}{5 \times 10^{-4}} \times 0.4^2\right)^{-\frac{1}{2}}\right]$$

$$-\exp\left[\frac{0.24^2 \times 1.1 \times 10^{-6} \times 20 \times 150}{\left(2.5 \times 10^{-3}\right)^2}\right] \times \left[\text{erfc}\left(\frac{0.24 \times \sqrt{1.1 \times 10^{-6} \times 20 \times 150}}{2.5 \times 10^{-3}}\right)\right]$$

Reproduced with permission of the copyright owner. Further reproduction prohibited without permission.

Reproduced with permission of the copyright owner. Further reproduction prohibited without permission.

Table A.1 Parameters Used in Case Studies (Chapter 6)

Site	AT & T Richmond Works		Tinker AFB		Laboratory Experiment
Chemical	Methylene Chloride (CH_2Cl_2)	1,1,1,-Trichloroethane ($C_2H_3Cl_3$)	Trichloroethylene (C_2HCl_3)	Toluene ($C_6H_5CH_3$)	Ethanol / Water (CH_3CH_2OH) (H_2O)
Porosity	0.55	0.55	0.55	0.55	0.6
Air-filled Porosity	0.24	0.24	0.24	0.24	0.42
Tortuosity*	0.40	0.40	0.40	0.40	0.70
Diffusion Coefficient in air (cm^2/s)	0.11	0.11	0.083	0.088	0.23
Diffusion Coefficient* in soil (cm^2/s)	0.04	0.04	0.033	0.035	0.16
Retardation Factor*	20	11	42	47	1200
Flow Rate (liter/min)	30	30	68	68	70
Half Aperture (mm)	2.5	2.5	2.5	2.5	2.5

* Given data are mean values

$$+\exp\left(\frac{0.24^2 \times 1.1 \times 10^{-6} \times 20 \times 150}{(2.5 \times 10^{-3})^2}\right)$$

$$\times\operatorname{erfc}\left[\frac{0.24 \times 3.14\sqrt{1.1 \times 10^{-6} \times 20}}{5 \times 10^{-4}} \times 0.4^2\left(150 - \frac{2 \times 3.14 \times 2.5 \times 10^{-3}}{5 \times 10^{-4}} \times 0.4^2\right)^{-\frac{1}{2}}\right.$$

$$\left.+\frac{0.24 \times \sqrt{1.1 \times 10^{-6} \times 20}}{2.5 \times 10^{-3}} \times \left(150 - \frac{2 \times 3.14 \times 2.5 \times 10^{-3}}{5 \times 10^{-4}} \times 0.4^2\right)^{-\frac{1}{2}}\right]$$

$= 0.095 - 0.103 + 0.102$

$= 0.094$

Having obtained the value of C_3/C_o as indicated, the next step is to calculate the mean value of C_3/C_o and the standard deviation. First, applying the same set of parameter values except that tortuosity changes from 0.1 to the other ten values listed in Table A.2, the normalized effluent concentrations can be obtained as shown in Table A.2 in a similar manner. Then, the mean value of C_3/C_o can be obtained by the following calculation:

$$\frac{\overline{C_3}}{C_o} = 0.028 \times 0.094 + 0.041 \times 0.123 + 0.076 \times 0.145 + 0.118 \times 0.163$$
$$+ 0.154 \times 0.179 + 0.168 \times 0.194 + 0.154 \times 0.208 + 0.118 \times 0.221$$
$$+ 0.076 \times 0.233 + 0.041 \times 0.244 + 0.028 \times 0.255$$
$$= 0.191$$

The standard deviation, δ, can now be calculated as follows:

$$\delta = 0.028 \times (0.191 - 0.094)^2 + 0.041 \times (0.191 - 0.123)^2 + 0.076 \times (0.191 - 0.145)^2$$
$$+ 0.118 \times (0.191 - 0.163)^2 + 0.154 \times (0.191 - 0.179)^2 + 0.168 \times (0.191 - 0.194)^2$$
$$+ 0.154 \times (0.191 - 0.208)^2 + 0.118 \times (0.191 - 0.221)^2 + 0.076 \times (0.191 - 0.233)^2$$

Reproduced with permission of the copyright owner. Further reproduction prohibited without permission.

$$+0.076\times(0.191-0.233)^2+0.041\times(0.191-0.244)^2+0.028\times(0.191-0.255)^2$$

$$=0.035$$

Table A.2 Sample Calculation for Mean Concentration

Probability	Tortuosity τ	Diffusion Coefficient D_2 (m^2 / s)	$\frac{C_3}{C_o}$
0.028	0.10	1.1×10^{-6}	0.094
0.041	0.16	1.8×10^{-6}	0.123
0.076	0.22	2.4×10^{-6}	0.145
0.118	0.28	3.1×10^{-6}	0.163
0.154	0.34	3.7×10^{-6}	0.179
0.168	0.40	4.4×10^{-6}	0.194
0.154	0.46	5.1×10^{-6}	0.208
0.118	0.52	5.7×10^{-6}	0.221
0.076	0.58	6.4×10^{-6}	0.233
0.041	0.64	7.0×10^{-6}	0.244
0.028	0.70	7.7×10^{-6}	0.255

Reproduced with permission of the copyright owner. Further reproduction prohibited without permission.

REFERENCES

Abramowitz, M and Stegun, I. A. (1972). *Handbook of Mathematical Functions.* Dover Publications, New York, N. Y.

Barenblatt, G. I., Entov, V. M., and Ryzhik, V. M. (1990). *Theory of Fluid Flows Through Natural Rocks.* Kluwer Academic Publishers, Boston, M. A.

Barenblatt, G. I., Zheltov, Iu. P., and Kochina, I. N. (1960). "Basic Concepts in the Theory of Seepage of Homogeneous Liquids in fissured Rocks (Strata)." PMM, 24(5), 1287-1303.

Beckktt, G. D., and Huntley, D. (1994). "Characterization of Flow Parameters Controlling Soil Vapor Extraction." Groundwater, 22(2), 239-247.

Bear, J. (1993). "Modeling Flow and Contaminant Transport in Fractured Rocks." *Flow and Contaminant Transport in Fractured Rock.* Academic Press, Inc., New York, N. Y., 1-37.

Bear, J. (1972). Dynamics of Fluids in Porous Media. American Elsevier Publishing Company, Inc., New York, Chapter 10.

Bedient, P. B., Rifai, H. S., and Newell, C. J. (1994). *Ground Water Contamination.* PTR Prentice Hall, Englewood Cliffs, N. J.

Bird, R. B., Stewart, W. E., and Lightfoot, E. N. (1960). *Transport Phenomena.* John Wiley & Sons, Inc., New York, N. Y. Part III.

Blake, G. R., and Page, J. B. (1948). "Direct Measurement of Gaseous Diffusion in Soils." Soil Science Society Proceedings, 13, 37-42.

Bowman, R. S. (1989). "Manipulation of the Vadose Zone to Enhance Toxic Organic Chemical Removal." *Toxic Organic Chemicals in Porous Media.* Springer-Verlag, New York, N. Y., 275-287.

Braester, C., and Thunvik, R. (1983). "An Analysis of the Conditions of Gas Migration from a Low-level Radioactive Waste Repository." SKB Technical Report, No. 83-21, Swedish Nuclear Fuel and Waste Management Co., Stockholm.

Brown, M. H. (1980). *Laying Waste.* Pantheon Books, New York, N. Y.

Reproduced with permission of the copyright owner. Further reproduction prohibited without permission.

Buckingham, E. (1904). "Contributions to Our Knowledge of the Aeration of Soils." Bulletin No. 25, U.S. Department of Agriculture, Bureau of Soils, Washington, D. C.

Carman, P. C. (1956). *Flow of Gases through Porous Media*, London Butterworth's Scientific Publications, London.

Chen, C. S., and Woodside, G. D. (1988). "Analytical Solutions for Aquifer Decontamination by Pumping." Water Resources Research, 24(8), 1329-1338.

Chen, C. S. (1986). "Solutions for Radionuclide Transport from an Injection Well into a Single Fracture in a Porous Formation." Water Resources Research, 22(4), 508-518.

Chen, C. S. (1985). "Analytical and Approximate Solutions to Radial Dispersion from an Injection Well to a Geological Unit with Simultaneous Diffusion into Adjacent Strata." Water Resources Research, 21(8), 1069-1076.

Currie, J. A. (1960a). "Gaseous Diffusion in Porous Media, Part 1. - A Non-steady State Method." British Journal of Applied Physics, 11, 314-317.

Currie, J. A. (1960b). "Gaseous Diffusion in Porous Media, Part 2. - Dry Granular Material." British Journal of Applied Physics, 11, 318-324.

Currie, J. A. (1961). "Gaseous Diffusion in Porous Media, Part 3. - Wet Granular Material." British Journal of Applied Physics, 12, 275-281.

Dragum, J. (1988). *The Soil Chemistry of Hazardous Materials*. Hazardous Materials Control Research Institute, Silver Spring, M. D.

Dullien, F. A. L. (1991). *Porous Media: Fluid Transport and Pore Structure*. Academic Press, New York, N. Y.

Dupont, R. R. (1993). "Fundamentals of Bioventing Applied to Fuel Contaminated Sites." Environmental Progress, 12(1), 45-53.

Erdelyi, A, Magnus, W., Oberhettinger, F., and Tricomi. F. G. (1954). *Tables of Integral Transforms*. McGraw-Hill, New York, N. Y.

Fitzgerald, C. D. (1993). "Integration of Pneumatic Fracturing to Enhance In Situ Bioremediation." M.S. Thesis, Department of Civil and Environmental Engineering, New Jersey Institute of Technology, Newark, N. J.

Freeze, R. A., and Cherry, J. A. (1979). *Groundwater*, Prentice-Hall, Inc., Englewood Cliffs, N. J.

Reproduced with permission of the copyright owner. Further reproduction prohibited without permission.

Fryar, A. E., and Domenico, P. A. (1989). "Analytical Inverse Modeling of Regional-Scale Tritium Waste Migration." Journal of Contaminant Hydrology, 4, 113-125.

Gelhar, L. W., Gutjahr, A. L., and Naff, R. L. (1979). "Stochastic Analysis of Macrodispersion in a Stratified Aquifer." Water Resources Research, 15(6), 1387-1397.

Germain, D., and Frind, E. O. (1989). "Modeling Contaminant Migration in Fracture Networks: Effects of Matrix Diffusion." *Contaminant Transport in Groundwater*. Rotterdam, 267-274.

Grasso, D. (1993). *Hazardous Waste Site Remediation Source Control*. CRC Press, Inc., New York, N. Y.

Greenkorn, R. A. (1983). *Flow Phenomena in Porous Media*. Marcel Dekker, Inc., New York, N. Y.

Harris, C., Want, W. L., and Ward, M. A. (1987). *Hazardous Waste*. Quorum Books, New York, N. Y.

Hemond, H. F., and Fechner, E. J. (1994). *Chemical Fate and Transport in the Environment*. Academic Press, New York, N. Y.

Hodge, D. S., and Devinny, J. S. (1995). "Modeling Removal of Air Contaminants by Biofiltration." Journal of Environmental Engineering, 121(1), 21-32.

Hoffman, D., and Daniels, W. (1984). "Assessment of the Potential for Radionuclide Migration from a Nuclear Explosion Cavity." *Groundwater Contamination*. National Academy Press, Washington, D. C., 1-35.

Hsieh, P. A., Neuman, S. P., Stiles, G. K., and Simpson, E. S. (1985). "Field Determination of Three-dimensional Hydraulic Conductivity Tensor of Anisotropic Media, 2, Methodology and Application to Fractured Rock." Water Resources Research, 21(11), 1667-1676.

HSMRC (Hazardous Substance Management Research Center). (1994a). "Pneumatic Fracturing Demonstration, Tinker Air Force Base, Oklahoma City, Oklahoma." Research Report Prepared for US Department of Energy, United States Air Force, and US Environmental Protection Agency, Newark, N. J.

HSMRC (Hazardous Substance Management Research Center). (1994b). "Integration of Pneumatic Fracturing and ISV Technologies: DOE Hanford

Reproduced with permission of the copyright owner. Further reproduction prohibited without permission.

Facility." Research Report Prepared for Battelle Memorial Institute, Pacific Northwest Laboratory, Newark, N. J.

Hutzler, Neil J., Murphy, B. E., and Gierke, J. S. (1989). "Review of Soil Vapor Extraction System Technology." June 1989 Workshop Proceedings: Soil Vapor Extraction Technology Assessment by Camp Dresser & Mekee Inc., Boston, M. A., 52-61.

Karickhoff, S. W., Brown, D. S., and Scott, T. A. (1979). "Sorption of Hydrophobic Poiiutants on Natural Sediments." Water Res., 13, 241-248.

King, T. C. (1993). "Mechanism of Pneumatic Fracturing." M.S. Thesis, Department of Civil and Environmental Engineering, New Jersey Institute of Technology, Newark, N. J.

Küpper, J. A., Schwartz, F. W. and Ssteffler, P. M. (1995a). "A Comparison of Fracture Mixing Models, 1. A Transfer Function Approach to Mass Transport Modeling." journal of Contaminant Hydrology, 18, 1-32.

Küpper, J. A., Schwartz, F. W. and Ssteffler, P. M. (1995b). "A Comparison of Fracture Mixing Models, 2. Analysis of Simulation Trials." journal of Contaminant Hydrology, 18, 33-58.

Lai, S-H, Tiedje, J. M., and Erickson, A. E. (1976). "In Situ Measurement of Gas Diffusion Coefficient in Soil." Journal of Soil Science Society America, 40, 3-6.

Latta, G. E. (1983). "Transform Methods." Chapter 11, *Handbook of Applied Mathematics*, Edited by Pearson, Carl E., Van Nostrand Reinhold Company, New York, N. Y.

Long, J. C. S., Remer, J. S., Wilson, C. R., and Witherspoon, P. A. (1982). "Porous Media Equivalent for Networks of Discontinuous Fractures." Water Resources Research, 18(3), 645-658.

Long, J. C. S., and Witherspoon, P. A. (1985). "The Relationship of the Degree of Interconnection to Permeability of Fractured Networks." Journal of Geophysics Research, 90 (B4), 3087-3098.

McCann, M., P., Danko, B, J. and Guerriero, M. (1994). "Remediation of a VOC-Contaminated Superfund Site Using Soil Vapor Extraction, Groundwater Extraction, and Treatment: A Case Study." Environmental progress, 13(3), 22-30.

Reproduced with permission of the copyright owner. Further reproduction prohibited without permission.

McCarthy, K. A., and Johnson, R. L. (1993). "Transport of Volatile Organic Compounds Across the Capillary Fringe." Water Resources Research, 29(6), 1675-1683.

McWhorter, D. B. (1990). "Unsteady Radial Flow of Gas in the Vadose Zone." Journal of Contaminant Hydrology, 5, 297-314.

Mercer, J. W., Skipp, D. C., and Giffin, D. (1990). "Basics of Pump-and-Treat Ground Water Remediation Technology." EPA-600/8-90/003.

Mills, C. H. (1995). "Bioremediation Comes of Age." Civil Engineering, ASCE, May, 80-81.

Murdoch, L. C. (1992a). "Hydraulic Fracturing of Soil during Laboratory Experiments, Part 1. Methods and Observations." Geotechnique, 43(2), 255-265.

Murdoch, L. C. (1992b). "Hydraulic Fracturing of Soil during Laboratory Experiments, Part 2. Propagation." Geotechnique, 43(2), 267-276.

Murdoch, L. C. (1992c). "Hydraulic Fracturing of Soil during Laboratory Experiments, Part 3. Theoretical Analysis." Geotechnique, 43(2), 277-287.

Nautiyal, D. (1994). "Fluid Flow Modeling for Pneumatically Fracture Formations." M.S. Thesis, Department of Civil and Environmental Engineering, New Jersey Institute of Technology, Newark, N. J.

Nielson, K. K., Rich, D. C., and Rogers, V. C. (1982). "Comparison of Radon Diffusion Coefficients Measured by Transient-Diffusion and Steady-State Laboratory Methods." U. S. Nuclear Regulatory Commission Report NUREG/CR-2875.

Nielson, K. K., Rogers, V. C., and Gee, G. W. (1984). "Diffusion of Radon through Soils: a Pore Distribution Model." Journal of Soil Science Society America, 48, 482-487.

Papanicolaou, P. (1989). "Laboratory Model Studies of Pneumatic Fracturing of Soils to Remove Volatile Organic Compounds." M.S. Thesis, Department of Civil and Environmental Engineering, New Jersey Institute of Technology, Newark, N. J.

Parker, B. L., Gillham, R. W., and Cherry, J. A. (1994). "Diffusive Disappearance of Immiscible Phase Organic Liquids in Fractured Geologic Media, Ground Water. 4, 37-58.

Reproduced with permission of the copyright owner. Further reproduction prohibited without permission.

Pearson, C. E. (1983). "Partial Differential Equations of Second and Higher Order" Chapter 9, *Handbook of Applied Mathematics*. Van Nostrand Reinhold Company, New York, N. Y.

Penman, H. L. (1940a). "Gas and Vapour Movements in the Soil, I, the Diffusion of Vapours through Porous Solids." J. Agric. Sci., 30, 437-462.

Penman, H. L. (1940b). "Gas and Vapour Movements in the Soil, II, the Diffusion of Carbon Dioxide through Porous Solids." J. Agric. Sci., 30, 570-581.

Philip, J. R. (1988). "The Fluid Mechanics of Fracture and other Junctions." Water Resources Research, 24(2), 239-246.

Pruess, K., and Wang, J. S. Y. (1987). "Numerical Modeling of Isothermal and Nonisothermal Flow in Unsaturated Fractured Rock - A Review." *Flow and Transport Through Unsaturated Fractured Rock*. American Geophysical Union, Washington, D. C., 11-21.

Rasmuson, A. (1985). "Analysis of Hydrodynamic Dispersion in Discrete Fracture Networks Using the Method of Moments." Water Resources Research, 21(11), 1677-1683.

Raven, K. G., Novakowski, K. S., and Lapcevic, P. A. (1988). "Interpretation of field Tracer Tests of a Single Fracture Using a Transient Solute Storage Model." Water Resources Research, 24(12), 2019-2032.

Ross, B., and Lu, N. (1994). "Efficiency of Air Inlet Wells in Vapor Extraction Systems." Water Resources Research, 30(2), 581-584.

Scheidegger, A. D. (1974). *The Physics of Flow through Porous Media*. University of Toronto Press, Toronto, Ont, Canada.

Schuring, J. R., and Chan, P. C. (1992). "Removal of Contaminants from the Vadose Zone by Pneumatic Fracturing." Research Report Submitted to USGS, Department of Interior, USGS Award 14-08-0001-G1739.

Schuring, J. R., Jurka, V., and Chan, P. C. (1991/92). "Pneumatic Fracturing to Remove VOCs." Remediation Journal, 51-68.

Schwartz, F. W., and Smith, L. (1988). "A Continuum Approach for Modeling Mass Transport in Fractured Media." Water Resources Research, 24(8), 1360-1372.

Shackeford, C. D. (1991). "Laboratory Diffusion Testing for Waste Disposal -- A Review." Journal of Contaminant Hydrology, 7, 177-217.

Reproduced with permission of the copyright owner. Further reproduction prohibited without permission.

Shah, N. P. (1991). "Study of Pneumatic Fracturing to Enhance Vapor Extraction of the Vadose Zone." M.S. Thesis, Department of Civil and Environmental Engineering, New Jersey Institute of Technology, Newark, N. J.

Silker, W. B., and Kalkwarf, D. R. (1983). "Radon Diffusion in Candidate Soils for Covering Uranium Mill Tailings." U. S. Nuclear Regulatory Commission Report NUREG/CR-2924.

Smith, L., and Schwartz, F. W. (1984). "Mass Transport, an Analysis of the Influence of Fracture Geometry on Mass Transport in Fractured Media." Water Resources Research, 20(9), 1241-1252.

Streltsova, T. D. (1988). *Well Testing in Heterogeneous Formations*. John Wiley & sons, New York, N. Y.

Sudicky, E. A., and McLaren, R. G. (1992). "The Laplace Transform Galerkin Technique for Large-scale Simulation of Mass Transport in Discretely Fractured Porous Formations." Water Resources Research, 28(2), 499-514.

Szatkowski, A., Imhoff, P. T. and Miller, C. T. (1994). "Development of a Correlation for Aqueous-Vapor Phase Mass Transfer in Porous Media." Journal of Contaminant Hydrology, 18, 85-106.

Tang, D. H., and Babu, D. K. (1979). "Analytical Solution of a Velocity Dependent Dispersion Problem." Water Resources Research, 15(6), 1471-1478.

Tang, D. H., Frind, E. O., and Sudicky, E. A. (1981). "Contaminant Transport in Fractured Porous Media: Analytical Solution for a Single Fracture." Water Resources Research, 17(3), 555-564.

Taylor, S. A. (1949). "Oxygen Diffusion in Porous Media as a Measure of Soil Aeration." Soil Science Society Proceedings, 14, 55-61.

Tofani, G., and Horath, F. (1990). "Continuous Tiltmeter Monitoring to Identify Ground Deformation Mechanisms." Geotechnical News, 8(2), 1-4.

Travis, C. C., and Macinnis, J. M. (1992). "Vapor Extraction of Organics from Subsurface Soils, Is It Effective?" Environ. Sci. & Technol., 26(10), 1885-1887.

US Environmental Protection Agency. (1980). "Everybody's Problem: Hazardous Waste." EPA-600/8-80-042d.

US Environmental Protection Agency. (1991). "Engineering Bulletin -- In Situ Soil Flushing." EPA/540/2-91/021.

Reproduced with permission of the copyright owner. Further reproduction prohibited without permission.

US Environmental Protection Agency. (1993a). "Hydraulic Fracturing of Contaminated Soil." EPA/540/MR-93/505.

US Environmental Protection Agency. (1993b). "Remediation Technologies Screening Matrix and Reference Guide." EPA 542-B-93-005.

US Environmental Protection Agency. (1993c). "Accutech Pneumatic Fracturing Extraction and Hot Gas Injection, Phase I." EPA/540/AR-93/509.

US Environmental Protection Agency. (1994a). "In Situ Vitrification." EPA 540/MR-94/520.

US Environmental Protection Agency. (1994b). "In Situ Vitrification Technology." EPA 540/R-94/520a.

US Environmental Protection Agency. (1995a). "Integrated Pneumatic Fracturing and Bioremediation for the In-situ Treatment of Contaminated Soil." EPA Cooperative Agreement Number CR 818207-01-0.

US Environmental Protection Agency. (1995b). "Subsurface Volatilization and Ventilation System." EPA/540/MR-94/529.

US Patent No. 5,032,042 dated July 16, (1991). "Method and Apparatus for Eliminating Non-Naturally Occurring Subsurface, Liquid Toxic Contaminants from Soil." by J. R. Schuring, P. C. Chan, J. W. Liskowitz, P. Papanicolaou, and C. T. Bruening.

Wagner, K., Boter, K., Claff, R., Evans, M., Henry, S., Hodge, V., Mahmud, S., Sarno, D., Scopino, E., and Spooner, P. (1986). *Remedial Action Technology for Waste Disposal Sites*, Noyes Data Corporation, Park Ridge, N. J.

Youngquist, G. R. (1979). "Diffusion and Flow of Gases in Porous Solids." Industrial and Engineering Chemistry, 10, 58-69.

Zuber, A., and Motyka, J. (1994). "Matrix Porosity as the Most Important Parameter of Fissured Rocks for Solute Transport at Large Scales." Journal of Hydrology, 158, 19-46.

Reproduced with permission of the copyright owner. Further reproduction prohibited without permission.